

THESIS
2
2004
56625087

LIBRARY Michigan State University

This is to certify that the thesis entitled

NON-LINEAR DYNAMICS OF A FRICTIONALLY EXCITED CANTILEVER BEAM

presented by

Jeffrey Larkin Quinby

has been accepted towards fulfillment of the requirements for the

M.S. degree in Mechanical Engineering

Major Professor's Signature

9/24/03

Date

PLACE IN RETURN BOX to remove this checkout from your record. TO AVOID FINES return on or before date due. MAY BE RECALLED with earlier due date if requested.

DATE DUE	DATE DUE	DATE DUE

6/01 c:/CIRC/DateDue.p65-p.15

NON-LINEAR DYNAMICS OF A FRICTIONALLY EXCITED CANTILEVER BEAM

By

Jeffrey Larkin Quinby

A THESIS

Submitted to
Michigan State University
In partial fulfillment of the requirements
For the degree of

MASTER OF SCIENCE

Department of Mechanical Engineering

2003

ABSTRACT

NON-LINEAR DYNAMICS OF A FRICTIONALLY EXCITED CANTILEVER BEAM

BY

Jeffrey Larkin Quinby

The main motivation of this thesis is to study a phenomenon of extremely low frequency responses to periodically excited structural oscillators, and to observe this and other non-linear dynamic phenomena in an experiment. The tip of a cantilevered beam in an experiment exhibited extreme low frequency (on the order of 1/20 to 1/100 of the driving frequency) as well as chaotic and quasi-periodic responses under different forcing frequencies. Performing a frequency sweep experiment, regions of dynamic activity were identified. Then, to examine these regions more closely, fixed frequencies that belonged to the regions were selected. Data gathered by a strain gages attached to the cantilever beam were examined in the Poincaré section. This in turn allowed for graphic representations of the dynamics occurring in the oscillating beam. The Poincaré section data was further processed into torus-angle return maps and Poincaré section of Poincaré section data to help characterize the dynamic responses of the system. The FFT was also taken using the original data as well as the Poincaré section data. These methods of examining the gathered data confirmed the types of responses observed in the beam.

For Paul Texeira Jr. (1978-2001)

ACKNOWLEDGMENTS

This work was conducted with the support of the Michigan State University

College of Engineering and the department of Mechanical Engineering as well as support
from the National Science Foundation grant No. CMS-0099603. This research was
conducted due to the support of Dr. Brian Feeny and the faculty of the System Dynamic
and Vibrations Laboratory at Michigan State University. I would also like to thank all of
my fellow colleagues for the help they have given me over the past three years.

TABLE OF CONTENS

L	LIST OF TABLES	
LIST OF FIGURES		viii
1	Introduction	1
	1.1 Motivation	1
	1.2 Background on Low-Frequency Behavior	2
	1.2.1 High-to-Low Frequency Energy Transfer	2
	1.2.2 Ultra-subharmonic Responses	4
	1.2.3 Frequency Demultiplication	4
	1.2.4 Dither	6
	1.2.5 Beating	6
	1.2.6 Other Studies	7
	1.3 Background on Frictionally Excited Systems	8
	1.4 Overview of Thesis	9
2	Description of the Experiment	10
	2.1 Background	10
	2.2 Experimental Setup	11
	2.3 System Characteristics	14
	2.4 Friction Measurement	17
	2.5 Method of Poincaré Sections	22
3	Frequency Sweeps	26
	3.1 Frequency Data Sweeps	26
	3.2 Subharmonic Order in each Region	30
	3.2.1 Region I	32
	3.2.2 Region II	34
	3.2.3 Region Hybrid, III & IV	36
	3.2.4 Region V	39
	3.2.5 Region VI	41
	3.3 Summery	46
4	Fixed Frequency	48
	4.1 Fixed frequency Examination	48
	4.1.1 Region I (8 & 9.8 Hz)	49
	4.1.2 Region II (21.9, 22.1 & 22.3 Hz)	59
	4.1.3 Region III & Hybrid (25.7 Hz)	73
	4.1.4 Region VI (43.8, 44.4, 45.2 & 45.6 Hz)	78
	4.1.5 Analysis of 37.9 Hz	87

BIBLIOGRAPHY		101
APPENDIX		96
5	Conclusion	91
	4.2 Torus Doubling	88

LIST OF TABLES

4.1	FNN data of 8 and 9.8 Hz	57
4.2	FNN data of 21.9, 22.1, and 22.3 Hz	69
4.3	FNN data of 25.7 Hz	77
4.4	FNN data of 44.4, 45.2, and 45.6 Hz	83

LIST OF FIGURES

1.1	A hand sketch of a figure taken from Van Der Pol & Van Der Mark 1927 <i>Nature</i> paper [13].	5
2.1	Experimental set up	12
2.2	Diagram of experimental setup	12
2.3	Rotated view of sections A-A and B-B	13
2.4	FFT response to the unloaded cantilever	16
2.5	FFT response of the loaded cantilever	16
2.6	FFT response of the impulse test of vertical motion of the loaded beam	17
2.7	Kappagantu's friction measurement setup	19
2.8	Kappagantu's sample time-series of displacement, velocity, friction force & effective normal load	20
2.9	Kappagantu's friction-displacement relation	21
2.10	Kappagantu's friction-velocity relation	21
2.11	Phase representation of the Poincaré plot	22
2.12	An example of a data and the sequence of strain gage volts taken form the Poincaré section	23
2.13	An example of actual data from the Poincaré section	24
3.1	Frequency up sweep data showing the Poincaré, the DC drift and the Poincaré minus the DC drift	28
3.2	Frequency down sweep data showing the Poincaré, the DC drift and the Poincaré minus the DC drift	29
3.3	Frequency up sweep of region I and the subharmonic orders of the response	33
3.4	Frequency down sweep of region I and the subharmonic orders	33

3.5	Frequency up sweep of region II and the subharmonic orders	35
3.6	Frequency down sweep of region II and the subharmonic orders	35
3.7	Frequency up sweep of the Hybrid region and the subharmonic orders	37
3.8	Frequency up sweep of the Hybrid region sub 1 and the subharmonic orders	37
3.9	Frequency down sweep of region III and the subharmonic orders	38
3.10	Frequency up sweep of the Hybrid region sub 2 and the subharmonic orders	38
3.11	Frequency down sweep of region IV and the subharmonic orders	39
3.12	Frequency up sweep of region V and the subharmonic orders	40
3.13	Frequency down sweep of region V and the subharmonic orders	40
3.14	Frequency up sweep of region VI and the subharmonic order	41
3.15	Frequency down sweep of region VI and the subharmonic order	42
3.16	Frequency up sweep region VI sub 1 and the subharmonic order	42
3.17	Frequency up sweep region VI sub 2 and the subharmonic order	43
3.18	Frequency down sweep of region VI sub 1 and the subharmonic order	43
3.19	Frequency down sweep of region VI sub 2 and the subharmonic order	44
3.20	Apparent demultiplication of region VI sub 2	46
4.1	Poincaré section delay map of 8 Hz	51
4.2	Poincaré section delay map of 9.8 Hz	51
4.3	Delay map of the Poincaré section of the Poincaré section delay map at 8 Hz	52
4.4	Torus angle model	53
4.5	Torus angle dynamics of 8 Hz	54

4.6	Torus angle dynamics of 9.8 Hz	54
4.7	FFT and the Poincaré FFT of 8 Hz	58
4.8	FFT and FFT of the Poincaré section of 9.8 Hz	58
4.9	Poincaré section delay map of 21.9 Hz	60
4.10	Poincaré section of the Poincaré section of 21.9 Hz plotted against its index	61
4.11	Sample of the Poincaré section data at 21.9 Hz plotted against its index	61
4.12	Poincaré section of the Poincaré section of 22.1 Hz plotted against its index	63
4.13	Delay map of the Poincaré section of 22.1 Hz of data segment 1	64
4.14	Delay map of the Poincaré section of 22.1 Hz of data segment 2	64
4.15	Poincaré section of 22.3 Hz with a delay of 1	65
4.16	Torus angle dynamics of 22.1 Hz of sub region 2	67
4.17	Torus angle dynamics of 22.3 Hz	67
4.18	Sample of the Poincaré section data at 22.3 Hz plotted against its index	68
4.19	FFT and the Poincaré FFT of 21.9 Hz	70
4.20	FFT of 22.1 Hz segments 1 & 2	72
4.21	FFT and the Poincaré FFT of 22.3 Hz	72
4.22	Poincaré section of the Poincaré section for 25.7 Hz and its two sub regions	73
4.23	Delay map of the Poincaré section of 25.7 Hz	74
4.24	Torus angle dynamics at 25.7 Hz of sub 1	75
4.25	Torus angle dynamics at 25.7 Hz of sub 2	76
4.26	FFT of 22.1 Hz Sub 1 & Sub 2	78
4.27	Poincaré section of 44.4 Hz with a delay of 1	79

4.28	Poincaré section of 45.2 Hz with a delay of 5	80
4.29	Poincaré section of 45.6 Hz with a delay of 3	80
4.30	Torus angle dynamics of 44.4 Hz	82
4.31	Torus angle dynamics of 45.2 Hz	82
4.32	Torus angle dynamics of 45.6 Hz	83
4.33	FFT and the Poincaré FFT of 44.4 Hz	85
4.34	FFT and the Poincaré FFT of 45.2 Hz	86
4.35	FFT and the Poincaré FFT of 45.6 Hz	87
4.36	The FFT and sample time trace of 37.9 Hz	88
4.37	Poincaré section of the Poincaré section of 45.6 Hz plotted against its Index	89
4.38	Example of torus doubling with increasing excitation frequency	90
A.1	Poincaré section of the Poincaré section of 8 Hz plotted against its index	96
A.2	Poincaré section of the Poincaré section delay map of 9.8 Hz	97
A.3	Correlation dimension and derivative of 8 and 9.8 Hz	98
A.4	Delay Map of the Poincaré section of the Poincaré section of 21.9 Hz with Delay of 1	99
A.5	Correlation number and their derivatives vs. log(r) for 21.9, 22.1 and 22.3 Hz	100
A.6	Correlation number and their derivative vs. log(r) for 44.4, 45.2 and 45.6 Hz	101

Chapter 1

Introduction

This thesis presents a study of a cantilevered beam undergoing frictional excitation. Under different forcing frequencies the tip of the cantilevered beam appeared to exhibit extreme subharmonic as well as chaotic and quasi-periodic responses. This phenomenon was referred to in the doctoral thesis of Ramana V Kappagantu [1]. However, the subharmonic phenomenon was noted but was not of primary interest in his thesis. In this work, we follow-up those initial observations with more detailed observations of the responses of the same experiment. We look at very low-order subharmonic responses, and characterize the dynamics of these and other responses.

1.1 Motivation

The main motivation of this thesis is to study a phenomenon of extremely low frequency responses to periodically excited structural oscillators, and to observe this phenomenon in an experiment. Subharmonics are defined as response frequencies that are smaller than the primary forcing frequency. In some works subharmonics are a periodic response that can be thought of in terms of a Fourier series with fundamental frequency ω . If Ω is the forcing frequency, then ω/Ω defines the *order* of the subharmonic response. Typical subharmonic orders are 1/2, 1/3, or 1/4. In this work, we observe subharmonic responses with much lower orders, in addition to typical subharmonic responses. Because we are interested in the denominator we will use the inverse of the definition. In this thesis the *subharmonic order* will be defined as Ω/ω . It

should be clarified that what we are after is not a subharmonic-resonance periodic response of frequency ω , rather we are looking for a dominate frequency in which the response is chaotic or quasi-periodic.

1.2 Background on Low-Frequency Behavior

The phenomena that are present in this thesis deal with low frequency behaviors. In the following sections examples of different types of low frequency responses will be given. These examples have been characterized into the following four groupings: high-to-low frequency energy transfer, ultra sub harmonic, frequency demultiplication, and dither.

1.2.1 High-to-Low Frequency Energy Transfer

The concept of an energy transfer from high-to-low frequency modes was the focus of a lot of research in the mid 90's. Some of the groundwork was laid in the summer of 1988 at a conference at the Virginia Polytechnic Institute and State

University. Haddow & Hasan [2] gave a talk that dealt with the experimental results of a base excited cantilever beam. They noticed that if the beam was excited at a relatively high resonance it would react in the expected mode shape. But as time elapsed it appeared that energy would 'cascade' from the higher modes down to the lower modes.

What ultimately came about was a combination of first-mode steady-state response at the lowest modal frequency, plus the resonated mode.

This type of phenomena became of great interest to Ali Hasan Nayfeh who is an accomplished scholar in the field nonlinear dynamics. In the early 90's A. H. Nayfeh was second author to his son S. A. Nayfeh in two journal papers that discussed an energy transfer from high- to low-frequency modes in a flexible structure [3,4]. The first paper, which was published in 1993, gave an analytical study of a nonlinear two-degree-of-freedom system with widely spaced modes being excited by a simple-harmonic. The results from this analytical study, which largely used the method of averaging, gave valuable insight when the jump was made to an experiment of a multi-degree-of-freedom system in their second paper. The experiment that the father and son team investigated in their second paper was a cantilever beam undergoing base excitation. Their experimental analysis revealed how nonlinear coupling between linear modes provided an avenue for the energy cascade.

In 1995 Nayfeh & Mook [5] wrote a similar journal paper, which concluded that a low amplitude high frequency excitation can generate a large amplitude low frequency response at a modal frequency. In the same year Nayfeh & Chin [6] discussed a parametrically excited system with a comparable outcome in a paper for *Nonlinear Dynamics*. Over the next couple of years Oh & Nayfeh [7, 8] worked on resonance and modal interactions in composite cantilever plates. Once again the energy transfer between high and low frequency modes had an effect on the dynamic system. In 1996 Anderson, Nayfeh & Balachandran [9] published work on the coupling between high-frequency and low-frequency modes. Their findings showed that interaction between the first mode and the third and fourth modes of their cantilever beam resulted in a transfer of energy from a high-frequency excitation to a low-frequency mode.

The signature for this phenomenon is an input at a frequency near a higher modal frequency, and a steady-state response with a low-mode component at the corresponding lower modal frequency. This is relevant because in our research the dynamic response of our beam seems to following a similar trend, but with an added twist. A high forcing frequency with low amplitude is producing a low frequency large amplitude response. However, the low frequency may be lower then the lowest modal frequency.

1.2.2 Ultra-subharmonic Responses

An "ultra-subharmonic" response is defined as a subharmonic response of a fractional order [10]. Nayfeh & Mook's book *Nonlinear Oscillations* [10] suggests that ultra-subharmonic resonances exist if the constant m is even in the following relation: $\Omega_2 = m\Omega_1$ and $\omega_0 \approx 1/2(\Omega_2 \pm \Omega_1)$, where Ω_1 & Ω_2 are forcing frequencies and ω_0 is the natural frequency. In 1994 Qriouet & Mira [11] took the Duffing-Rayleigh equation and subjected it to an external periodic driving force. According to the authors "this first elementary study" produced complex fractional harmonics that forced them to limit their numerical approach to low frequency periodic solutions. Four years later Yagasaki [12] theoretically described ultra-subharmonic resonance motion using a third-order averaging technique.

1.2.3 Frequency Demultiplication

In 1927 Van Der Pol & Van Der Mark [13] designed an electrical system that when a sinusoidal forcing frequency is applied the output is has a response that is whole

submultiples of the applied sinusoid. The response frequency becomes a fraction of the initial applied frequency, i.e. $\omega/2$, $\omega/3$, $\omega/4$ up to $\omega/40$. The system would only oscillate with "discrete frequencies" or submultiple frequencies. In the experiment, as the capacitance of the circuit was changed the response frequency remained constant until the capacitance was large enough to cause a jump in the frequency, creating a bifurcation diagram, showing that the response followed steps of submultiple frequencies with respect to the capacitance parameter. The demultiplying frequencies followed a minor scale and "strongly reminds one of the tunes of a bagpipes."

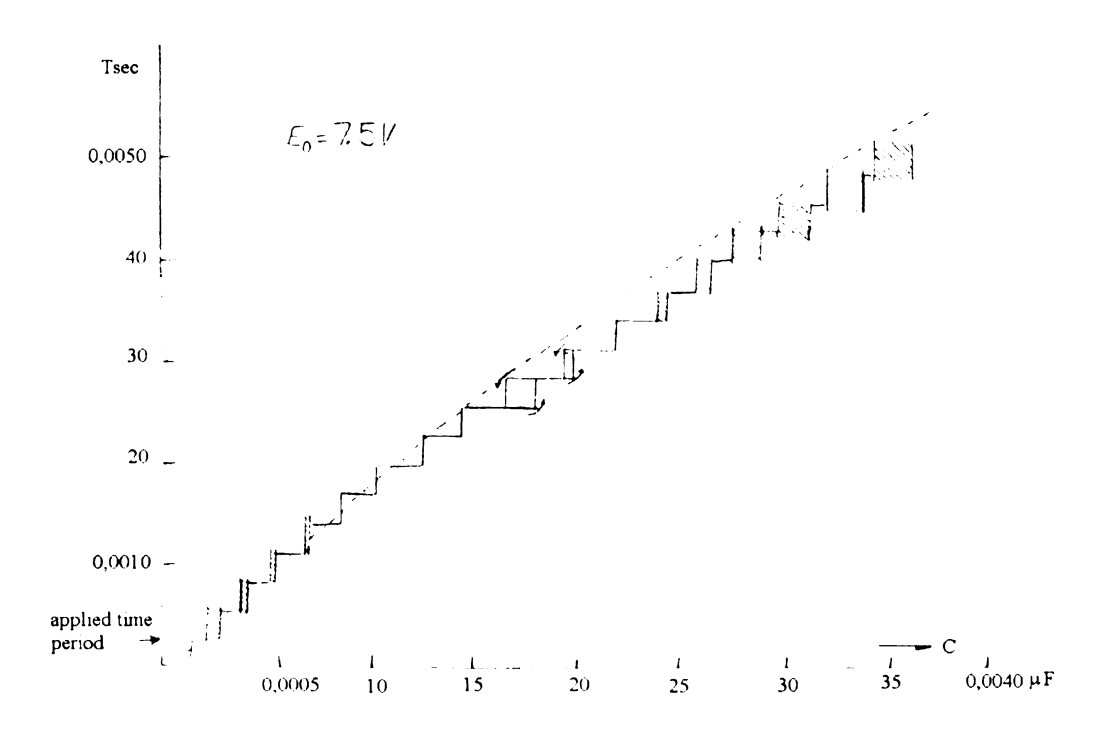


Figure 1.1: A hand sketch of a figure taken from Van Der Pol & Van Der Mark 1927 *Nature* paper [13].

1.2.4 Dither

"Dither" is the application of a high-frequency excitation (much higher than the system's characteristic frequency) to a system with the hopes of affecting the low-frequency behavior of the system. Various oscillatory systems with poor response behavior can be restored by dither. Examples of this are quenching limit cycle behavior [14], stabilizing an equilibrium (inverted pendulum) [15], and improving friction behavior [16]. Dithering excitation makes a system compliant to averaging because its frequency is much higher then the characteristic frequency of the system. This creates two time scales, one slow scale coupled with the oscillator itself and one fast scale coupled with the dither. Feeny & Moon [17] investigated this phenomena and its affect on stick-slip chaos in 2000. By applying dither to a low-frequency forced stick-slip friction oscillator they found that the chaos that was typically intrinsic to the system was extinguished.

This alleviation of stick-slip chaos by using dither seems to be ironic because the experimental research done for this thesis appeared to have the opposite effect. We will see that "dither" was applied to our frictionally excited system, which in turn created a low-frequency chaotic or quasi-periodic stick-slip response.

1.2.5 Beating

Linear and non-linear systems can exhibit beating if responses have two similar frequency components, ω_1 and ω_2 . The result is a low frequency amplitude variation at the frequency $\omega_b = (\omega_2 - \omega_1)/2$. An FFT of the beating signal will show spikes at ω_1

and ω_2 , not ω_b . Non-linear effects can give rise to spikes that are some type of linear combination of the two frequencies, like $\omega_c = 2\omega_2 - \omega_1$.

1.2.6 Other Studies

Some other studies that can be classified as having low-frequency behavior are presented here. Miranda & Thomsen [18] set up a simple model for predicting vibration induced sliding of a mass, which was able to slide along a beam under going base excitation. The results of the model retained features of a real system, which would allow the model to be used in research in using vibration induced sliding for passive vibration damping. One can also notice in the response graphs that the collar slides along the beam at a very low frequency. Zhang & Tao [19] observed beats between subharmonic and super subharmonic responses in an experiment that dealt with nonlinear vibrations in a thin loudspeaker cone. The results of this experiment showed that the nonlinear vibrations are associated with the bending resonance of the loudspeaker cone.

It is also worth mentioning squeak and squeal. These are characterized by high frequency noises resulting form low frequency, or steady sliding motions. While quite the opposite of subharmonic interest, it may involve large-order frequency ratios between input and output. On the other side, brake grunt, growl, and groan may be characterized by lower-frequency noises. If this results form steady sliding (as in braking) it may not be obvious how to define the "order" of the response harmonics.

1.3 Background on Frictionally Excited Systems

Friction is a complex non-linear property that has been studied extensively. Dry friction gives rise to stick-slip motion. As the term stick-slip suggests, at any give time an object my be sticking to a base object while a short time later the same object may now be sliding along the base object. This time independent change between static and dynamic friction can result in chaotic motions that are extremely interesting to watch. Stick-slip oscillators correspond to velocity-field discontinuities, and low dimensional systems have a fundamental characteristic that allows their dynamic responses to be one-dimensionally mapped [20, 21, 22].

There has been a huge global research effort on friction problems in dynamics. Phenomena studied are friction-induced vibration, friction-induced noise (squeak & squeal), such as with stick slip dynamics, control issues, dynamical friction modeling, and friction damping.

R. A. Ibrahim [23] provided an extensive review on the mechanics of friction, giving the science community a better understanding of this complex force involving sliding surfaces. A system's behavior, if it encountered friction, strongly relies on several factors, including: materials and the geometry of sliding surfaces, surface roughness, sliding velocity, temperature, and normal load. In 1994 B. Armstrong-Hélouvry, P. Dupont & C. Canudas de Wit discussed how friction affects the controls community [24]. Using the results from tribology, lubrication and physics literature and combining it with the findings in the controls community, a set of tools and models were created to incorporate friction with control systems. B. Feeny *et.al.* gave a historical review of the dynamics of systems with friction in 1998 [25] and S. Shaw presented a study on

dynamic response of a system with dry friction [21]. Kappagantu's Ph.D. thesis [1] dealt with the modal reduction of a system undergoing frictional excitation. The experiment for our research is an offshoot of Kappagantu's work.

1.4 Overview of Thesis

In Chapter 2 a description of the experiment will be given. It will include a background on Ramana Kappagantu's Ph.D. thesis; an in-depth look at the experimental set up and system characteristics; a qualitative summary of Kappagantu's friction measurements; and a look at the methods that were used to analyze data gathered during the experiment. In Chapter 3 and Chapter 4 the results of the analysis of the experiment will be given. This will include a discussion on how the system dynamic responses were characterized. Chapter 3 includes dynamics during frequency sweeps and identifies frequency ranges of interesting dynamics are identified. Chapter 4 includes in-depth studies of responses at fixed, selected parameter values. Chapter 5 contains the conclusion, giving a summery of the experimental research conducted and possible research that could be taken on in the future.

Chapter 2

Description of the Experiment

This chapter, as the title suggests, is a description of the experiment. It contains an in-depth look at the physical set up, equipment, materials and contact geometry used in the experiment, as well as the methods used to gather measurement data such as nonlinear response data, frequency response data, modal frequencies and shaker contact frequencies.

2.1 Background

This experiment exhibits a phenomenon that was referred to in the doctoral thesis of Ramana V. Kappagantu. Kappagantu's thesis [1], as his title suggests, dealt with "A method of order reduction in modeling multi-degree-of-freedom and continuous systems with frictional excitation". The tip of his cantilevered beam experiment with frictional excitation appeared to behave in subharmonic as well as chaotic and quasi-periodic response under different forcing frequencies. This phenomenon was noted but was not of primary interest in Kappagantu's thesis.

The research presented in this thesis took the same experimental setup of Kappagantu and looked more closely at this interesting phenomenon. Poincaré methods were used to get a better view of the dynamical system behavior. It was found that the system did in fact have chaotic and quasi-periodic motion with very large order subharmonic frequencies.

2.2 Experimental Setup

The shaker was a PM Vibration Exciter Type 4808 with a Power Amplifier Type 2712, both products by Brüel & Kjær. A Stanford Research Systems Model DS340 15MHz Synthesized Function Generator was used to produce the forcing function. These experimental components were used to force the cantilever beam via friction excitation. This accrues because a rubber nub at the tip of the cantilever beam rests on a contact surface that is being shaken by the B&K shaker.

The cantilever beam was instrumented with strain gages. A 2100 System Stain Gage Conditioner and Amplifier System, by Instruments Division Measurements Group INC., amplified the strain gage data. That data was then sent to the TEAC GX-1 Integrated Recorder, which was used as a data acquisition system. Matlab and Fortan were used to post process the experimental data.

Figure 2.2 is a general diagram of the experimental setup and Figure 2.3 shows a rotated view of the two sections. It is important to understand the coordinate system XYZ in Figures 2.2 and 2.3. X is along the length of the cantilever beam, Y is along the thickness of the beam and Z is along the width/height of the beam. According to this coordinate system the crosswise oscillation is in the Y direction.

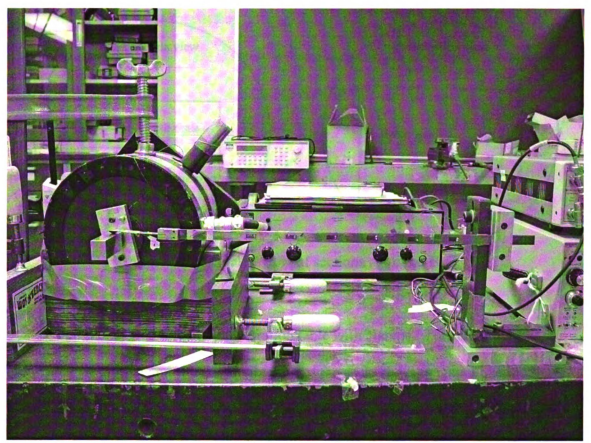


Figure 2.1: Experimental set up.

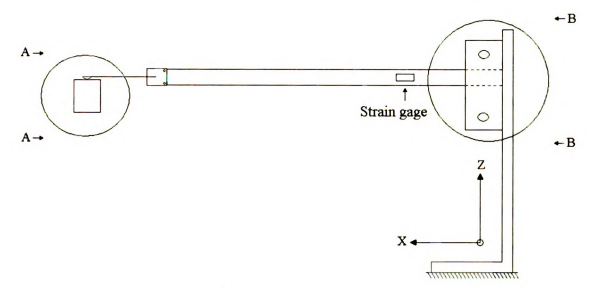


Figure 2.2: Diagram of experimental setup.

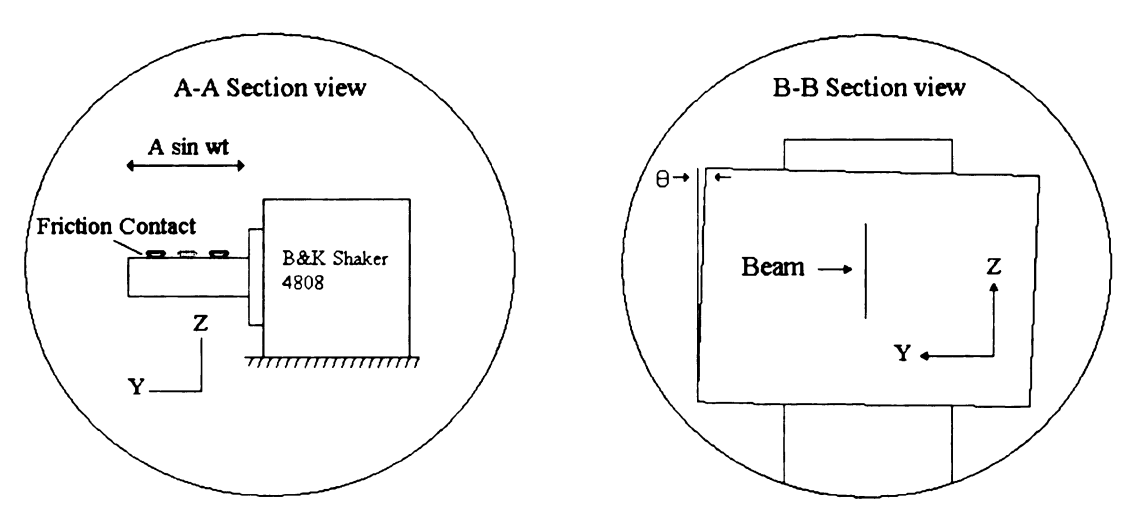


Figure 2.3: Rotated view of sections A-A and B-B.

The shaker was fixed to the vibration table with clamps. This effectively eliminated all normal and rotational vibration of the shaker. Kappagantu had the shaker placed at a slight angle in the Y-Z plane, which made the contact friction between the cantilever beam and the shaker vary depending on the location of the contact. In our experiment this was achieved by rotating the fixed end of the cantilever in the Y-Z plane. This rotation as it turns out this is very important to the behavior of the cantilever. The tilt with the loading beam provided a variation in the normal load of about 0.035 N/cm, where the tip position was estimated in a static displacement, and the load at the midpoint of the surface was 0.63 N. Over the 7 cm span of motion on the surface, the load ranges from 0.466 N to 0.655 N.

The cantilever beam used by Kappagantu was also used in this experiment.

Unlike Kappagantu, who was concerned with modal principles, our experiment aimed at a qualitative description of the dynamics. We used only the strain gage pair closest to the clamped end of the cantilever to produce time series data. Thus, as we are interested in the qualitative nature of the behavior of the cantilever beam, we are using the strain gage

pair as an observer. The cantilever beam was constructed from a piece of mild steel with dimensions of $0.4000 \times 0.0128 \times 0.00086 \text{ m}^3$, elasticity of $E = 128 \times 10^9 \text{ N/m}^2$, and a density of $\rho = 7488 \text{ kg/m}^3$. Another piece of mild steel, with dimensions $0.064 \times 0.0134 \times 0.00056 \text{ m}^3$, elasticity of $E = 126 \times 10^9 \text{ N/m}^2$, and a density of $\rho = 6777 \text{ kg/m}^3$, was attached to the free end of the cantilever beam with its flexural direction rotated 90° to act as a leaf spring. The leaf spring, referred to as a loading beam, had a small rubber nub attached at its free end. The mass of the fixture that connected the cantilever beam to the loading beam was 0.01226 kg. The total length of the cantilever beam and the loading beam setup was 0.464 m. The bending axes of the two beams were perpendicular, meaning the loading beam thickness was along the Z-axis and the width was along the Y-axis while the cantilever thickness is along the Y-axis and the width/height was along the Z-axis. This allowed for forces on the tip of the loading beam to be transmitted to the cantilever.

2.3 System Characteristics

This experiment can be classified as a frictional stick-slip problem. As such, there are two different dynamic states. In the first state the rubber tip sticks to the slider surface, much like a pinned beam. In the second case, the rubber tip slips over the slider surface, such that it deforms like a free beam. A stick-slip response can be seen as an interchange between pinned beam and free beam dynamics. With these two different dynamic cases it is beneficial is to see the Fast Fourier Transform (FFT) of the system pinned and free to locate the model frequencies of the each state.

We examined the linear behavior of both the free and the pinned beam. Loading the tip with a large normal force, such that sliding was not likely to occur, approximated the linear pinned beam case. Figure 2.4 shows the FFT of the unloaded or free floating cantilever and Figure 2.5 shows the FFT of the loaded case, where there was a high normal load between surfaces. The first five modal frequencies for the unloaded case were approximately 2.5, 19.5, 57.5, 112 and 180 Hz. The small peak that can be seen at approximately 37 Hz is believed to be a distortion. The lowest frequencies of the loaded modes were approximately 13.5, 43.5, 93 and 171.5 Hz. It was determined later that it was also important to know the modal frequencies in the vertical (normal) direction because the beam appeared to resonate in the normal direction at several different frequencies. The normal modal frequencies were found by giving the pinned (loaded) beam an impulse along the Z-axis at the fixture between the beam and the loading beam. The output signal taken from the paired strain gages on the loading beam where then FFT by the TEAC. The first normal modal frequency was found to be approximately 47 Hz.

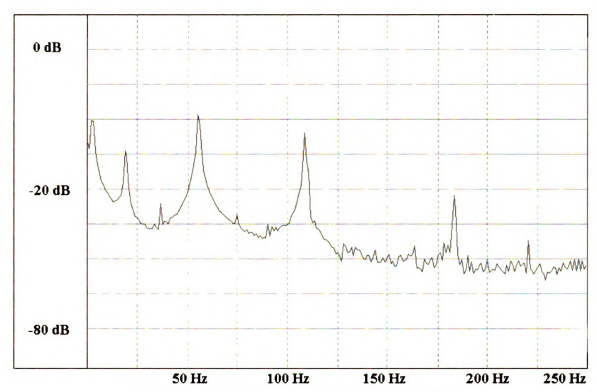


Figure 2.4: FFT response to the unloaded cantilever.

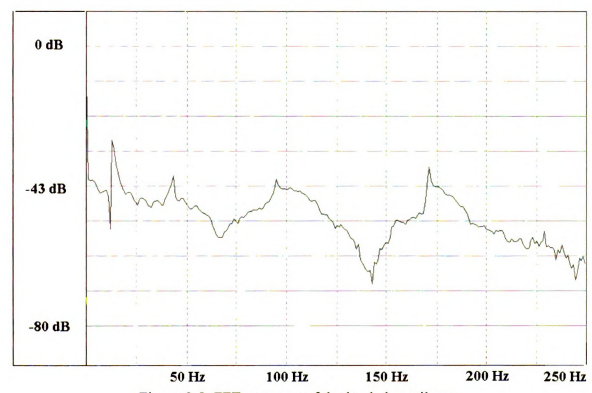


Figure 2.5: FFT response of the loaded cantilever.

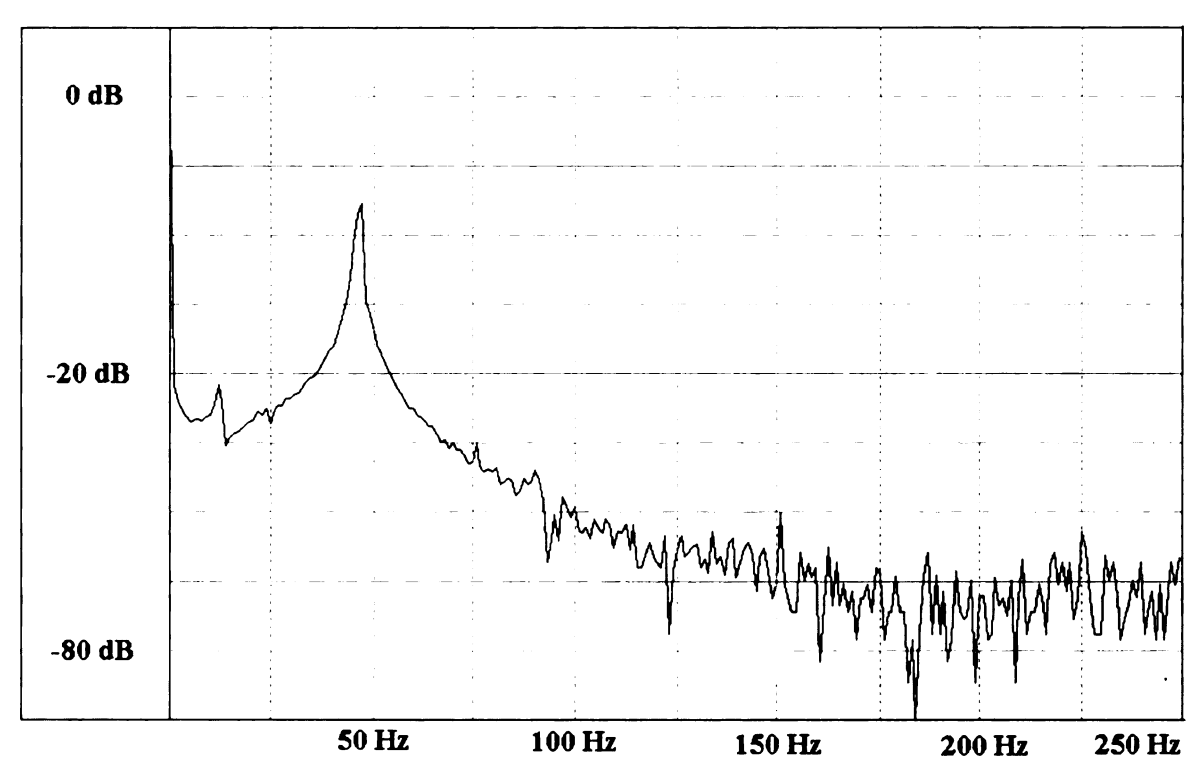


Figure 2.6: FFT response of the impulse test of vertical motion of the loaded beam.

With the modal frequencies we are now interested in finding the forcing frequencies in which the tip dynamics were present and showed appealing characteristics. The signal generator was set to approximately 5Hz and slowly increased to approximately 60Hz during which the tip of the beam was observed for interesting and exciting dynamic behavior. In the end we focused on 11 different frequencies: 8, 9.8, 21.9, 22.1, 22.3, 25.7, 37.9, 43.8, 44.4, 45.2 and 45.6Hz. Each one of these frequencies had similar but distinct tip movements that were fascinating to watch.

2.4 Friction Characteristics

Kappagantu, in his thesis, did an extensive study on the friction characteristics of his cantilever beam and the surface that it rested on. Since our experiment is using the

same beam and a frictional surface made of the same material, the friction characteristics should be similar to the results of Kappagantu. Since we expect the same qualitative friction behavior, and our interest is in a qualitative description of the dynamics, we have not quantified the current friction behavior; rather we summarize Kappagantu's friction measurements.

The Figure 2.7 (which came from Kappagantu's thesis) shows the apparatus used by Kappagantu to investigate friction characteristic for his experiment. This setup used equipment and materials that were very similar to his main experiment and allowed him to gather information about the displacement, velocity, friction force and effective normal load which the cantilever beam would experience during his experiment (Figure 2.8 taken from Kappagantu's thesis shows this). He was also able to see the relationship between the friction force and displacement of the beam (Figure 2.9 taken from Kappagantu's thesis) as well as the relationship between the friction force and the velocity of the beam (Figure 2.10 taken from Kappagantu's thesis).

The hysteresis in the force-velocity curve in Fig. 2.9 is consistent with a compliant contact with negligible mass. Kappagantu measured the contact compliance and crosschecked it with the stick-slip transition velocity. The contact stiffness was estimated to be K_y = -20 kN/m and the coefficient of sliding friction was μ =0.55 [1].

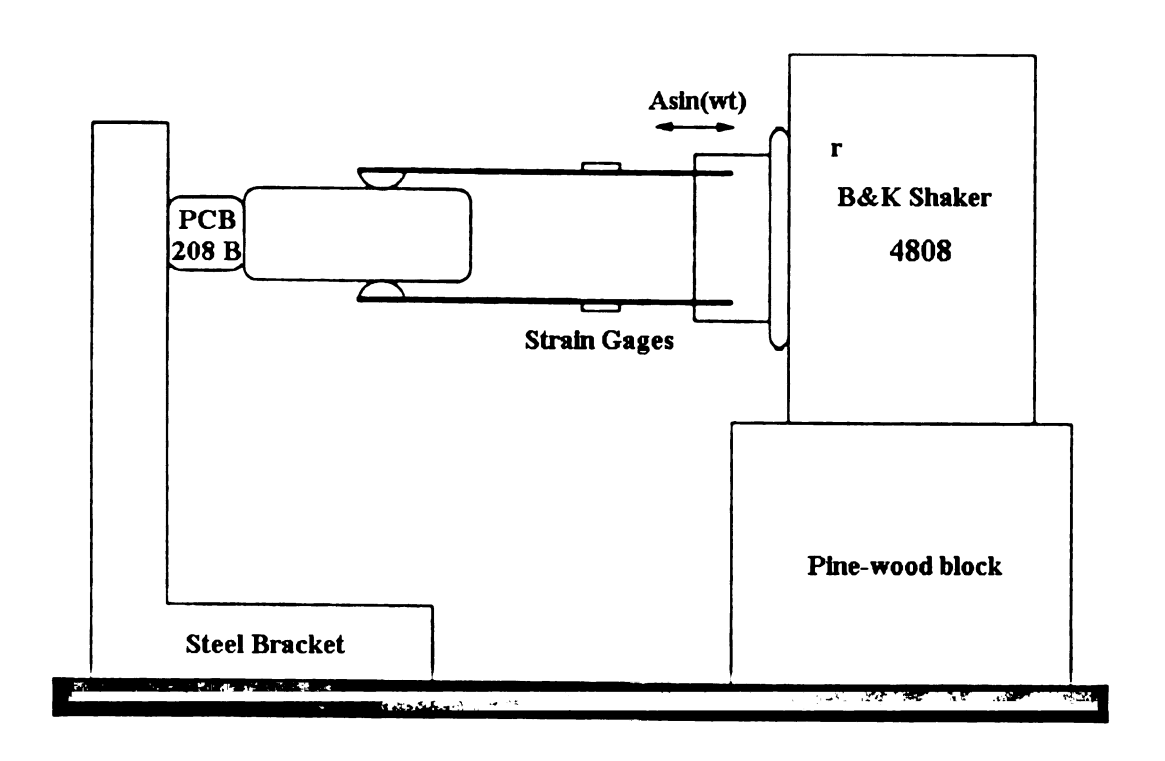


Figure 2.7: Kappagantu's friction measurement setup.

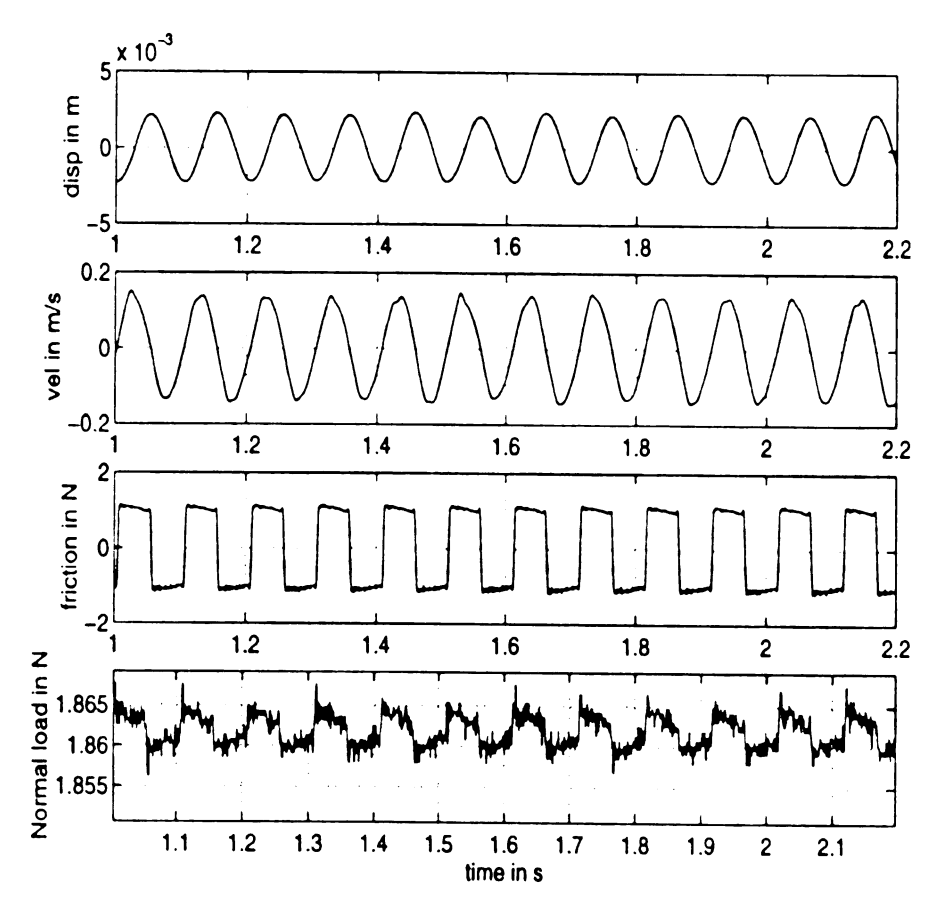


Figure 2.8: Kappagantu's sampled time-series of displacement, velocity, friction force & effective normal load.

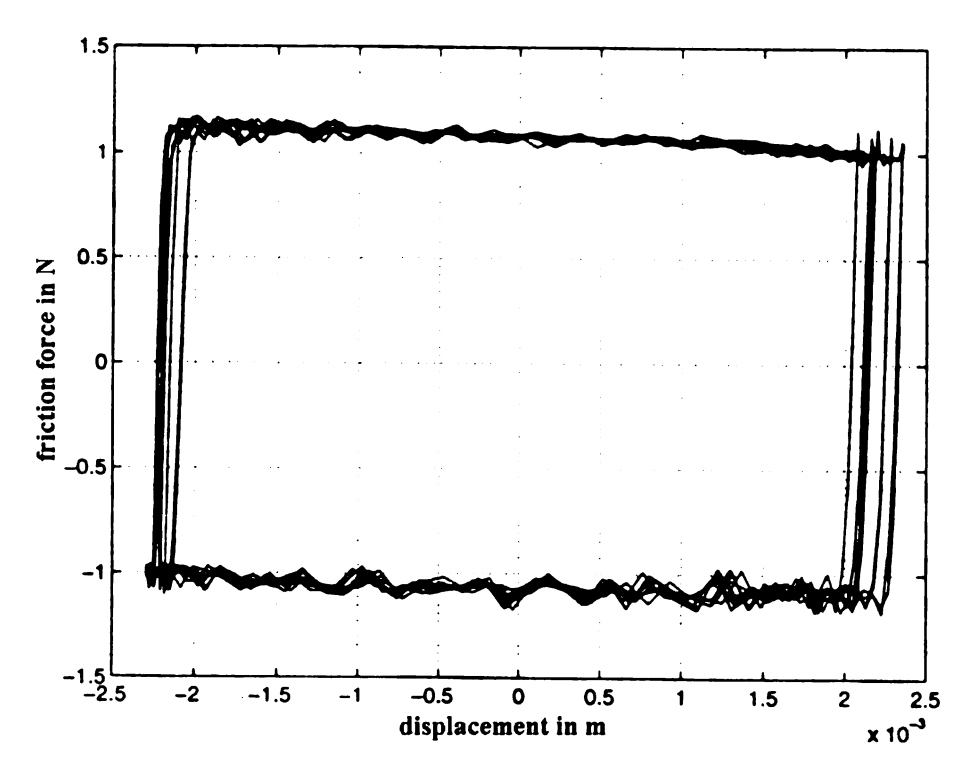


Figure 2.9: Kappagantu's friction-displacement relation.

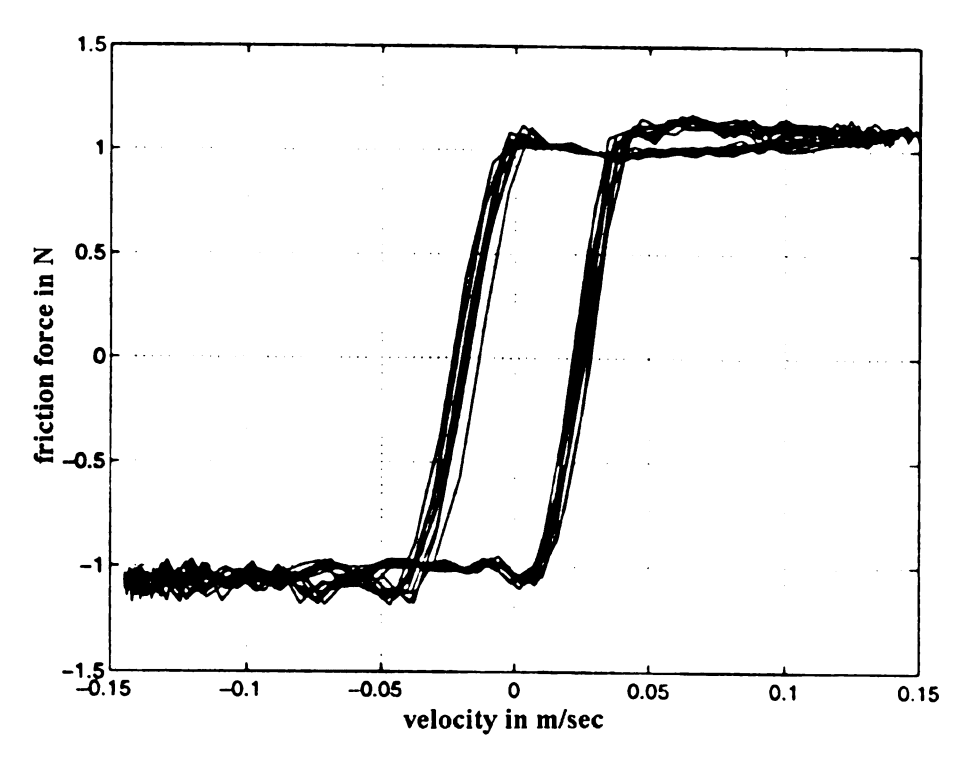


Figure 2.10: Kappagantu's friction-velocity relation.

2.5 Method of Poincaré Sections

Jules Henri Poincaré was a French mathematician who lived from the midnineteenth to the early twentieth century. He is considered by many as the grandfather of topology and qualitative dynamics. His work helped the development of deterministic chaos [26]. With our experiment we used one of Poincaré's techniques to help us view our data.

Since the input f(t) is periodic, if you make ϕ equal to the phase of f(t), you are effectively adding a periodic or cyclic axis to the state space. If the response states are \vec{x} and $\dot{\vec{x}}$, then the Poincaré section is a cross section, Σ , of the 3-D state space. Response trajectories form points as they pierce Σ . As a result, a discrete map represents the continuous flow on Σ . This is depicted in Figure 2.11.

More generally, there are n response states, and so the Poincaré section Σ is n-dimensional. In our work, we extract one component from the n-dimensional Poincaré section, and look at the sampled series of this component.

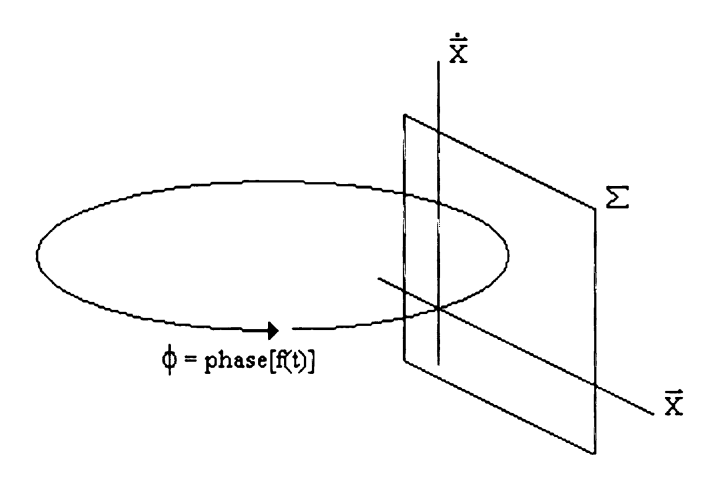


Figure 2.11: Phase representation of the Poincaré plot.

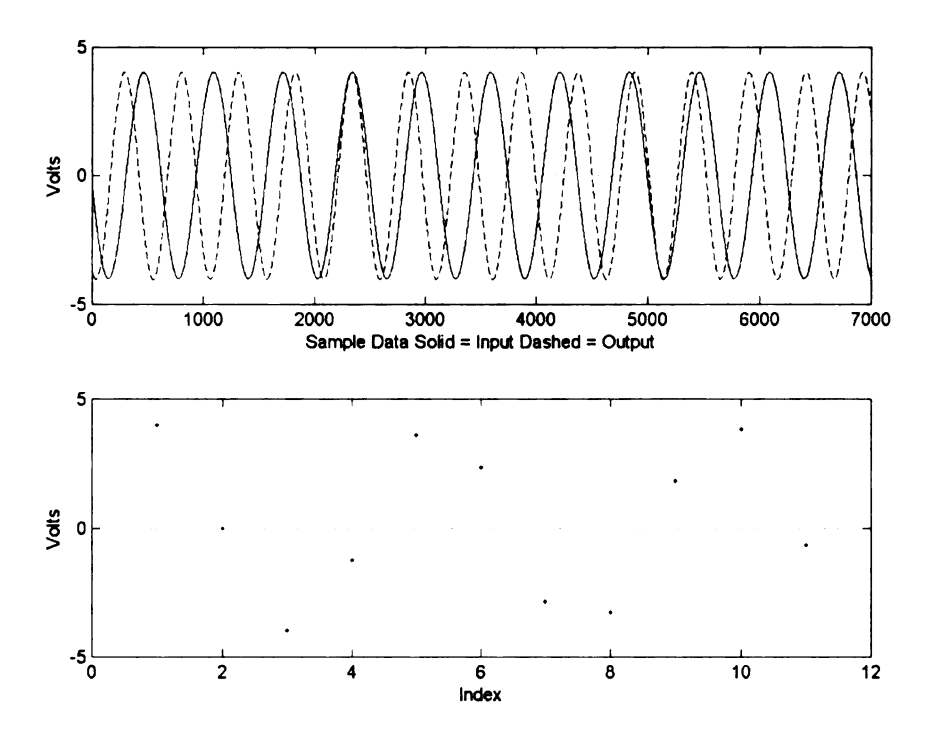


Figure 2.12: An example of a data and the sequence of strain gage volts taken form the Poincaré section.

With the sinusoid from the signal generator used as the input signal and the strain gage response-signal as the output signal, the strain gage signal was mapped at specific moments with respect to the input signal. More specifically, every time the leading edge of the signal generator input (which in all cases was a sine wave at some specified frequency) passed through zero with a positive slope, the corresponding point in the output signal was flagged and saved. This results in the sampling of one coordinate from the Poincaré section. Figure 2.12 shows an example of this; however in this case both signals are sine waves.

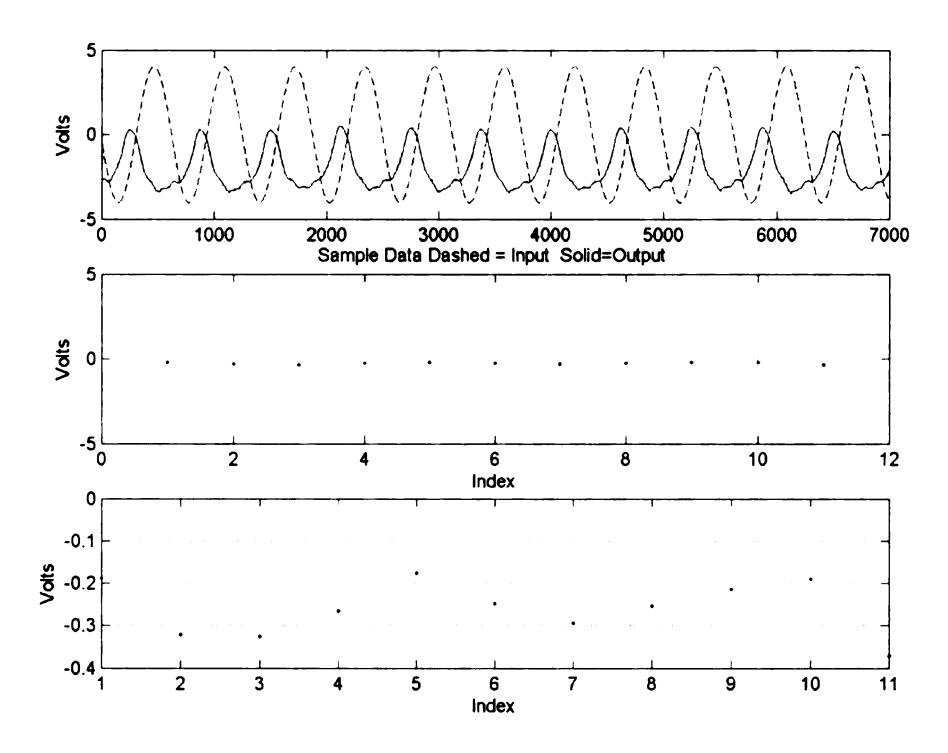


Figure 2.13: An example of actual data from the Poincaré section.

With our data the output signal is not going to be a perfect sine wave like the example given. Rather it is the response signal from the strain gage closest to the base of the cantilever beam.

Figure 2.13 shows a small sample of actual response data and the series of data of a component of the Poincaré section with respect to the forcing phase. This Poincaré data allows us to investigate what type of dynamic motion the cantilever is undergoing. Even from the small sample provided above it can be seen that the Poincaré data allows a pattern that might otherwise be over looked to be seen. The Poincaré data is then mapped as a delay map that allows the observer to see the path the Poincaré data follows in a reconstruction of the Poincaré section. This was a starting point to see what type of analyses should follow. In some cases it was easy to tell that the data behaved as if it was

moving through a torus or a torus doubling. In others however it was difficult to determine the behavior. Visual inspection of the delay map allowed us to see which way our investigation should head regardless of the case examined.

Chapter 3

Frequency Sweeps

This chapter contains the results from frequency sweeps. Up and down sweeps were performed, which consisted of sweeping though frequencies from 8 to 50 Hz and 50 to 8 Hz receptively. The input and output data were collected via a strain gage. The main question was whether there were frequencies where the cantilever beam behavior was relevant to our study. The simple answer to this is a resounding yes. The frequency sweeps identified frequency intervals of interesting dynamics, and helped estimate the order of the response frequencies.

3.1 Frequency Data Sweeps

A frequency sweep window of 8 to 50 Hz was chosen after the casual inspection from 5 to 60 Hz mentioned in section 2.3. It was felt that this window of 42 Hz was convenient because it incorporated all the regions that presented the phenomena we wanted to study. For these sweeps the amplifier gain of the B&K power amplifier was set to approximately 5.5 with the output impedance set to "high". The function generator amplitude was set to 4.00 peak-to-peak voltage. The function generator frequency was increased (or decreased for the down sweep) at approximately 0.01 Hz every 0.31 seconds. The total time of the sweep was just under 22 minutes. Thus, at 8 Hz, there were about 2 1/2 cycles of excitation for each frequency setting in the sweep. If the response had, say, a subharmonic at order 5, then there would only be half of a response cycle occurring before the sweep parameter changed. At the high-frequency end of the

sweep, say 50 Hz, there were about 15 input cycles per 0.01 Hz sweep parameter increment. Still, if the response subharmonic had high order, insufficient response cycles would take place for each sweep parameter value for the system to approach steady-state. As such, the resulting sweep responses do not approach steady state at each parameter setting. Rather, the sweeps really represent transient responses with a slowly varying parameter. (The effect of the slowly varying sweep vs. steady state in a nonlinear system has been examined by Raman, Bajaj, & Davies [27].) Nonetheless, we use these sweeps to give hints at how the responses depend on frequency and what frequency values generate interesting forced responses.

The sampling rate was 5000 Hz. Twenty-two minutes of data amounted to 6.6 million data. To reduce this, we retained the strain responses in the Poincaré section. When the data was extracted from the Poincaré section, the period between extracted Poincaré-sections data was also determined, thereby providing the driving frequency associated with each data point. As a result, we obtained, for our sweep data, strains in the Poincaré section, and driving frequencies.

A response point in the Poincaré section does not have constant drift, amplitude and phase information. It became clear that we could not tell from the frequency sweep data if the large amplitudes being presented were real or just the beam being displaced about a new equilibrium and having small oscillation about this new point. To reduce this problem we created a low-pass filter program in Matlab to draw out the DC drift for the original data sample. The low pass filter was set to 0.25 Hz. The filter was applied using the transfer function, $\frac{1}{s^2 + bs + a^2}$ where $a = 0.25 * 2 * \pi$ (rad/sec), $b = 2\zeta a$ with $\zeta = 0.707$, and s is the Laplace transform variable. The filter was applied to the data

first by integrating the signal as input to the filter, using Matlab's lsim command. This filtered signal was then reversed and applied to the same transfer function using the same Matlab function. The reversal of the data was applied to nearly cancel the filter's phase effects. The double application of this transfer function amounts to a 4^{th} order filter with a cutoff frequency at a. Subtracting this DC drift from the original data effectively allowed one to view the data as if it was oscillating about the same equilibrium the entire time. Figures 3.1 and 3.2 show the up and down frequency sweep data respectively. The nonzero DC components of x indicate an effective quadratic nonlinearity in the system.

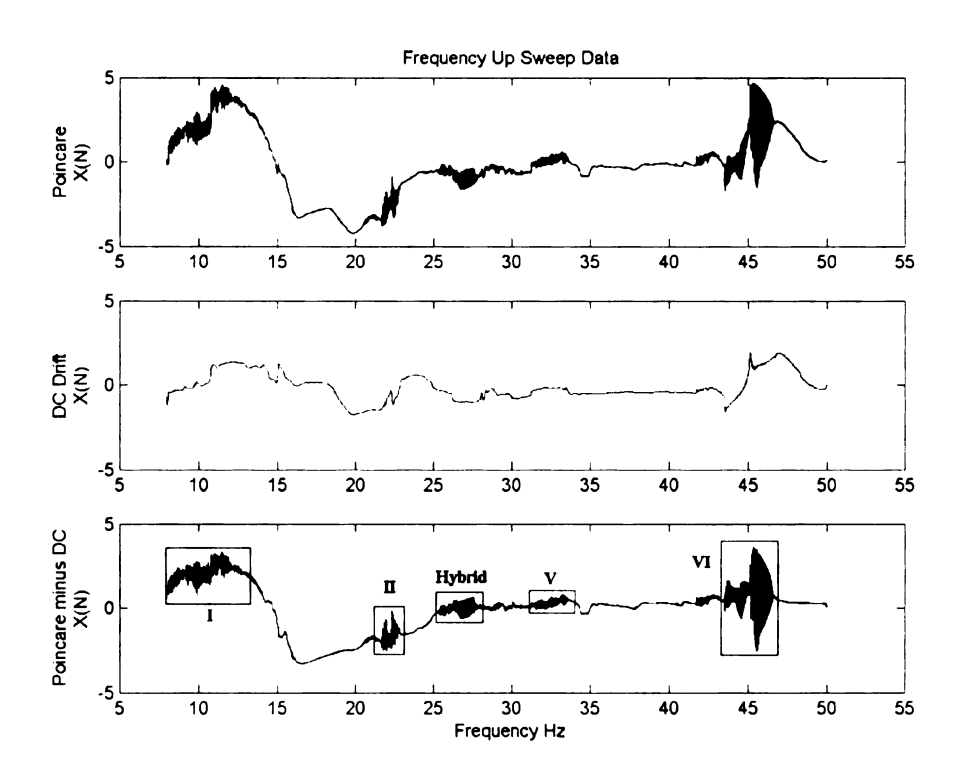


Figure 3.1: Frequency up sweep data showing the Poincaré, the DC drift and the Poincaré minus the DC drift.

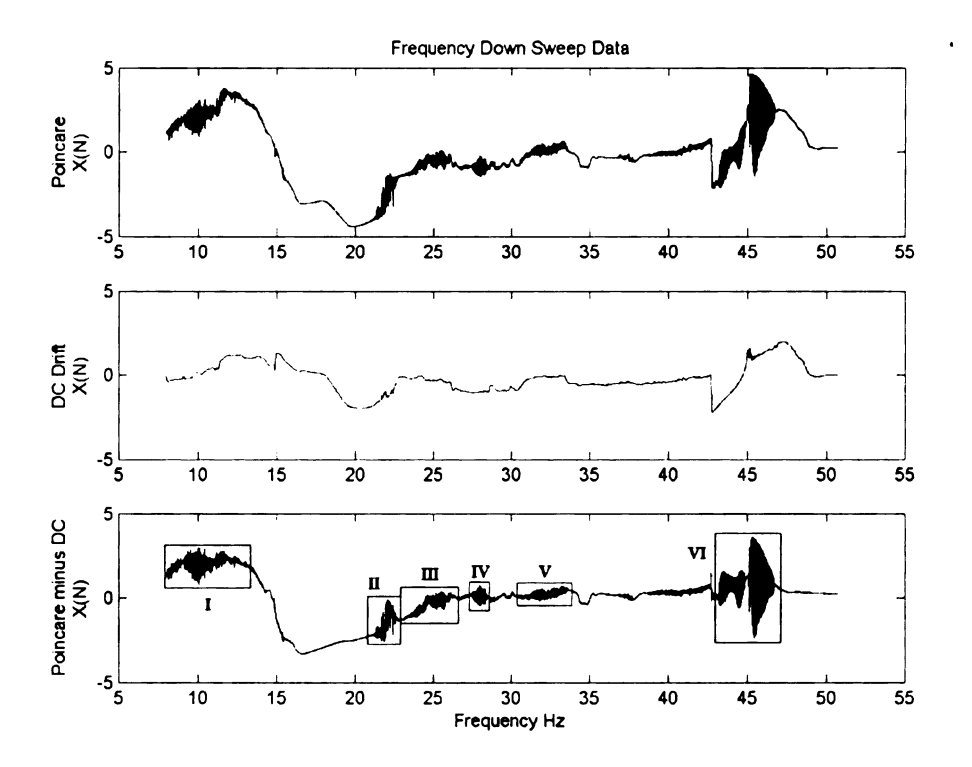


Figure 3.2: Frequency down sweep data showing the Poincaré, the DC drift and the Poincaré minus the DC drift.

The response in the Poincare variable minus dc drift figures are not the actual amplitude that is experienced doing the experiment, but rather Poincaré section samples taken for the experimental data. The data shown is more analogous to the real part of the complex oscillation. An approximate calibration for the dc drift is that one-volt positive or negative is equal to about one centimeter on either side of the strain gage equilibrium. Frequency intervals for which significant oscillations occurred are labeled as Regions *I-VI* in Figures 3.1 and 3.2. It should be remembered that the modal frequencies for the unloaded case were approximately 2.5, 19.5, 57.5, 112, and 180 Hz, and that none of the regions of dynamics drift occurred at these frequencies. The first two loaded model frequencies were approximately 13.5 and 43.5 Hz, which occurred at the edges of regions *I* and *VI* respectively. The normal-degree-of-freedom frequency, which is approximately

47 Hz, lines up with region VI and is mostly likely the reason for the response that occurs. This normal vibration became noticeable in region hybrid and VI. In fact the normal vibration was very large in the first subregion, but became somewhat subdued in the second subregion. The comparison of these two regions will be discussed in more detail in section 3.3. Labeled on both of the Poincaré-minus-DC graphs are regions of oscillatory activity. These regions, though different, do appear to be comparable. Since Figure 3.2, the down sweep, shows the most distinct regions, it was used to number the regions. The "hybrid" region of the Figure 3.1 does not fit into the mold set by Figure 3.2. Rather the "hybrid" region appears to be a combination of regions III and IV from the down sweep, where region III has slide up the frequency scale and region IV has moved down the frequency scale. This could be the case since the initial conditions of the beam will differ between the up and down sweeps making the corresponding responses of the beam analogous but still unique.

3.2 Subharmonic Order in each Region

From the behavior of the beam we felt that it was important to look at the "subharmonic order" of the regions of interest. We accomplished this by taking a region and performing a short-time average FFT calculation on a small window of data. This window of data started at the beginning of the region. Index by index we calculated the average FFT for each window. The end product was a short-time average of the FFT across each window, whence we obtain the average subharmonic at each point of the region.

In this context, what we mean by "subharmonic order" is the ratio Ω/ω , where ω is the dominant frequency in a response that may not be periodic. This reference to a "subharmonic response" may thus be different from the traditional reference to a periodic response of a period which is a multiple of the excitation period. We use the terminology "subharmonic order" since many of our response have a dominant component at a frequency which is lower then the excitation frequency.

In each frequency region, a short-time window length q was chosen to be large enough to capture the lowest frequency expected (from previous inspections of the data), yet small enough to represent a narrow frequency interval. Given q, the frequency window for each short-time FFT was from the sweep parameter window, $[f_{\min}, f_{\max}]$, from which we estimate the average driving frequency as $f_d = (f_{\min} + f_{\max})/2$. Given q and f_d , the approximate time record for a short-time FFT was q/f_d . This defined the frequency resolution (minimum frequency) in the short-time FFT as f_d/q . The maximum frequency of the short-time FFT was based on the Nyquist criterion as $f_d/2$. Hence, a given short-time FFT had a minimum detectable frequency of f_d/q and a maximum detectable frequency of f_d/q . The short-time FFT frequency axis has values f_d/q , $2f_d/q$, $3f_d/q$,..., kf_d/q ,..., $f_d/2$.

In the calculation of the subharmonic order, we found the frequency for which the short-time FFT was a maximum, say $k f_d/q$. Then we computed the *subharmonic order* as $f_d/(k f_d/q) = q/k$, where k can have an integer value from 1 to q/2. The reciprocal of the order would be k/q. Comparing k = 1 and k = 2 corresponds to a factor of two in the order. Signals with aberrant low frequency components (for example due to

transients and changes in dynamic behavior across the window) lead to small k. Because of this, if k = 1, we set the order to zero to omit that case and limit the scale of the order axis in the plots. Thus, the maximum presentable subharmonic order is q/2.

3.2.1 Region I

In this case, q = 50, leading to a maximum presentable subharmonic order of 25, and a frequency window width for the short time FFTs of the up and down sweep of approximately 0.15 and 0.153 Hz respectively. Region I is located approximately between 8 and 13.5 Hz. Figure 3.3 shows the frequency up sweep Poincaré-section strain signal of the region along with its subharmonic order. Figure 3.4 displays the same as Figure 3.3 but is of the down sweep.

Both up and down sweeps are rather consistent in indicating subharmonic orders in ranging from of 3 to 7, depending on the input frequency. Isolated incidents of large subharmonic orders are likely due to shifts in the sweep response, which would be represented as large changes in the course of the short-time signal window, and hence correspond to low frequency components. It is also possible that chaotic responses with broad band FFTs are present, such that the lower frequencies in the FFTs dominate.

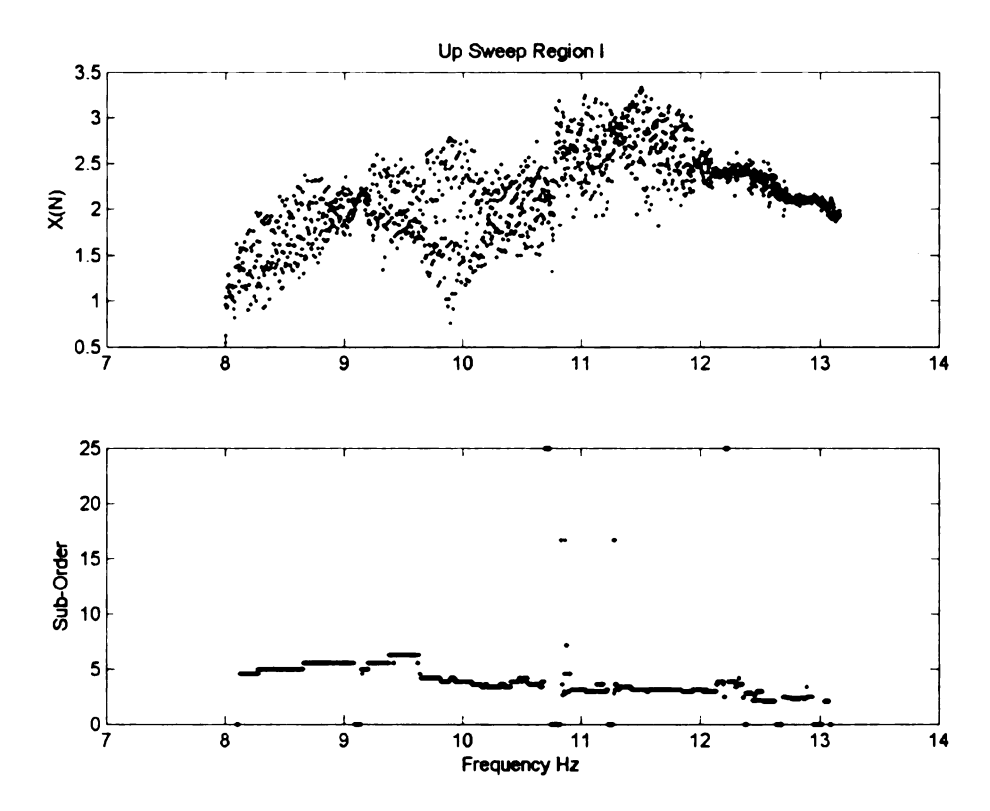


Figure 3.3: Frequency up sweep of region I and the subharmonic orders of the response.

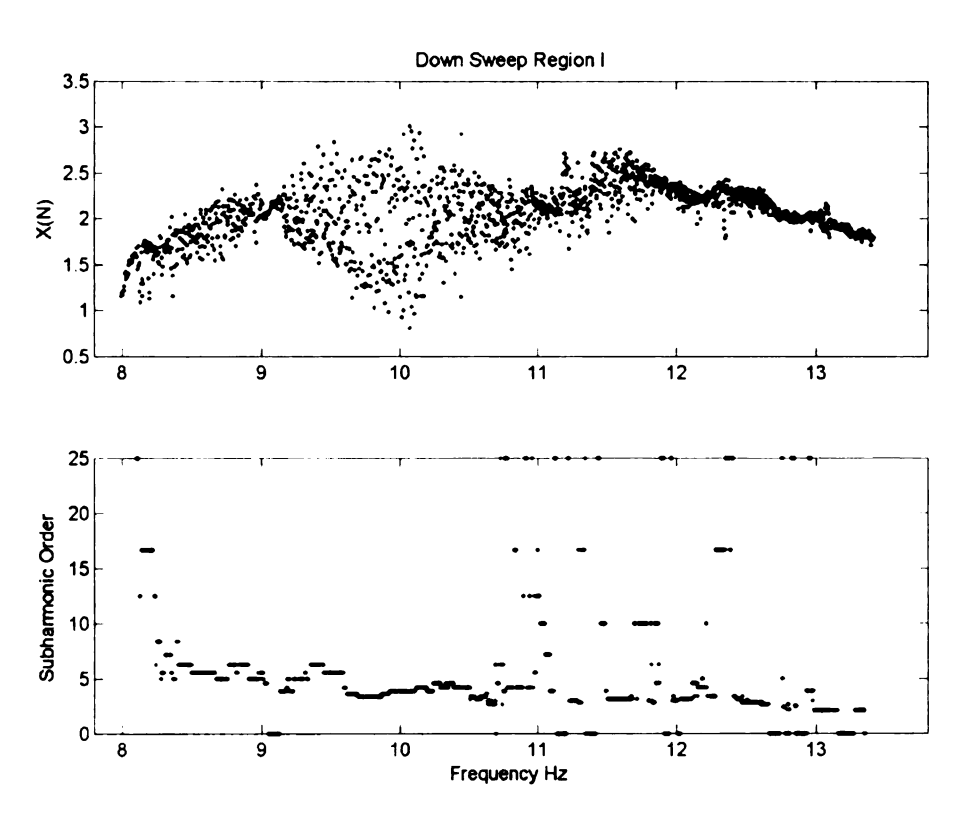


Figure 3.4: Frequency down sweep of region I and the subharmonic orders.

3.2.2 Region II

In this case, q = 200, leading to a maximum detectable subharmonic order of 100, and an average short-time FFT frequency window for the up and down sweep of approximately 0.29 and 0.3 Hz respectively. Region II is located approximately between 20.8 and 23.2 Hz. Figure 3.5 shows the Poincaré section of the up sweep of the region along with its subharmonics and Figure 3.6 shows the Poincaré section of the down sweep of the region along with its subharmonics. Viewing Figure 3.5, the subharmonics jump around like so: 40, 28.5, 50, 67, 5, 40, 18, 33.5 and 40 Hz. To compare, in Figure 3.6 the subharmonic orders are as follows: 25, 28.5, 33.5, 40, 50, 28.5, 25 and 33.5Hz. Here, the isolated "regular-order" subharmonic is not observed (as in the order 5 seen in the upsweep). It is possible that the finite sweep rate glossed over it. Thus, in general the values of the subharmonic orders do differ but a basic pattern stays the same between the up and down sweeps, which implies that the up and down sweeps in fact share a similar dynamic behavior in region II although the absolute response may very slightly. Again, the incidents of zero-subharmonic orders in the plot arise in fact from the maximal subharmonic order, reset to zero for the plot, disregarded as they are likely to indicate low frequency transients during the sweep.

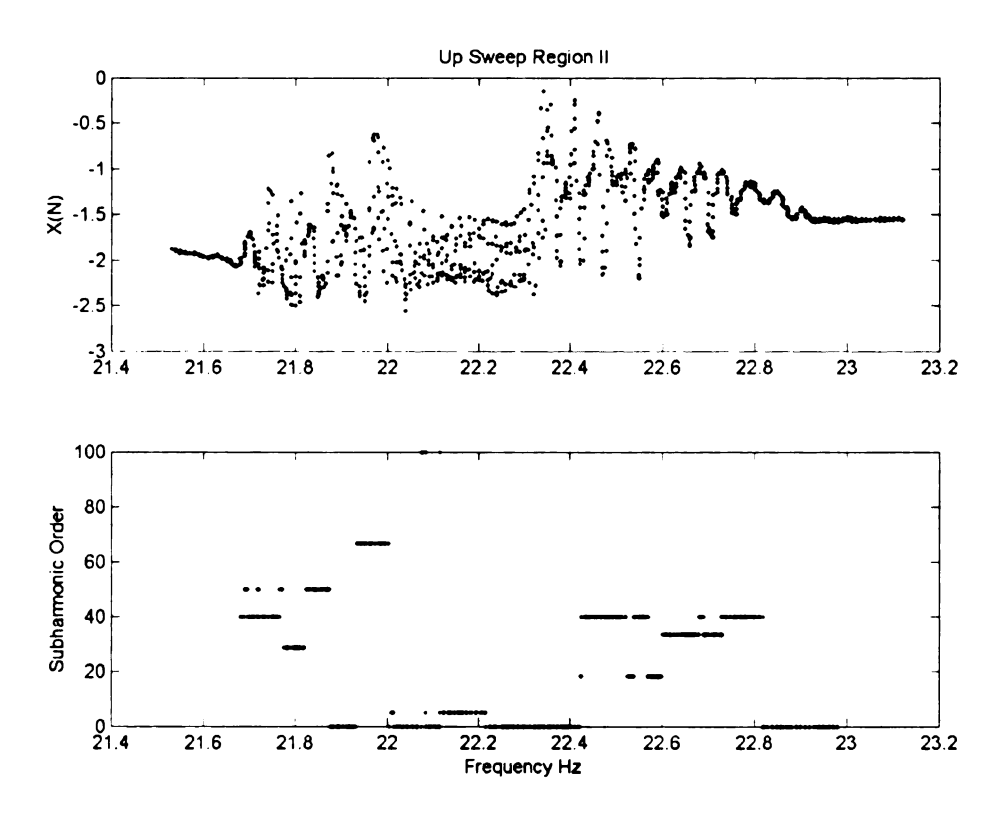


Figure 3.5: Frequency up sweep of region II and the subharmonic orders.

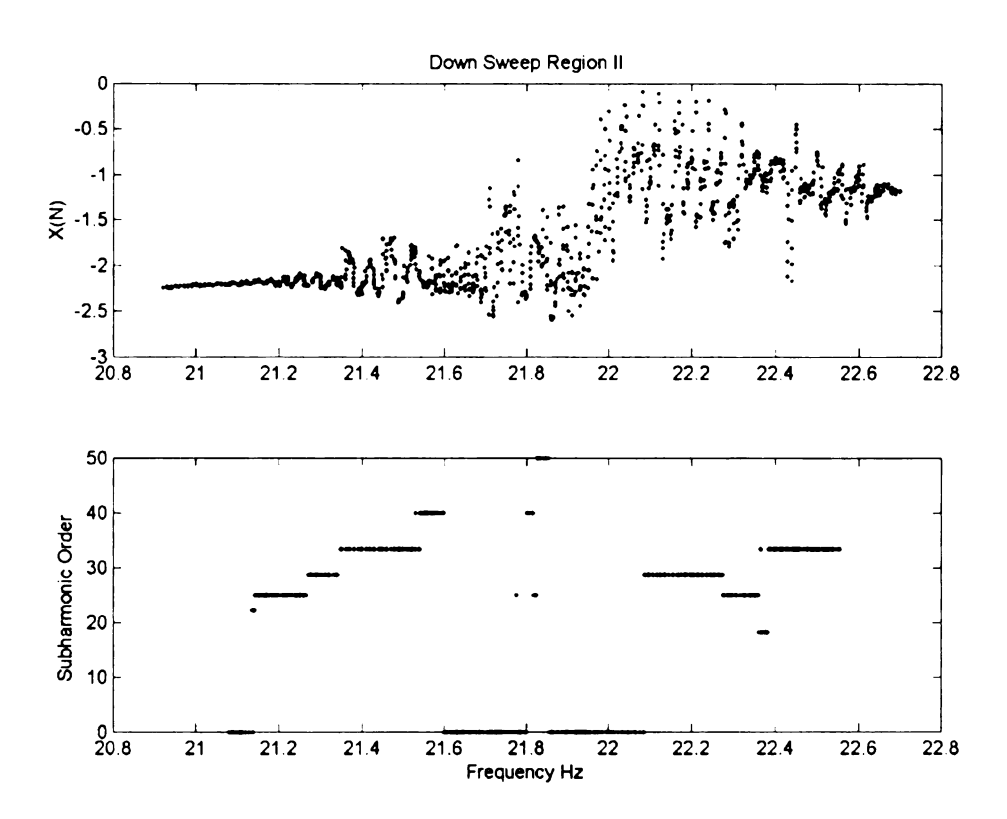


Figure 3.6: Frequency down sweep of region II and the subharmonic orders.

3.2.3 Region Hybrid, III & IV

In this case, q = 200, leading to a maximum presentable subharmonic order of 100, and the average short-time FFT frequency windows for the hybrid, *III*, and *IV* regions are approximately 0.24, 0.26, and 0.23 Hz respectively. The "Hybrid" region is located approximately between 25 and 28.3 Hz. Region *III* and *IV* are located approximately between 22.5 to 26.5 Hz and 27.2 to 28.8 Hz respectively. As mentioned earlier the *Hybrid* region of the frequency up sweep appeared to be a combination of regions *III* and *IV* of the frequency down sweep. By looking more closely at Figure 3.7, which shows the *Hybrid* region, it is unmistakable that there are two regions present. Figure 3.8 and Figure 3.10 separates these distinct regions of the *Hybrid* region into two sub regions. For simplicity Figure 3.9, region *III*, and Figure 3.11, region *IV*, have been placed where they are because of the uncanny similarity to their previous Figures 3.8 and 3.10.

Region *III* is characterized by subharmonic orders in the range of about 10-13. The hybrid region shows subharmonic orders that are consistently around 12-13 for the first segment of the up sweep, then jump to over 20, thereafter decreasing markedly to ten as the parameter increases. A similar trend will be seen again in another region.

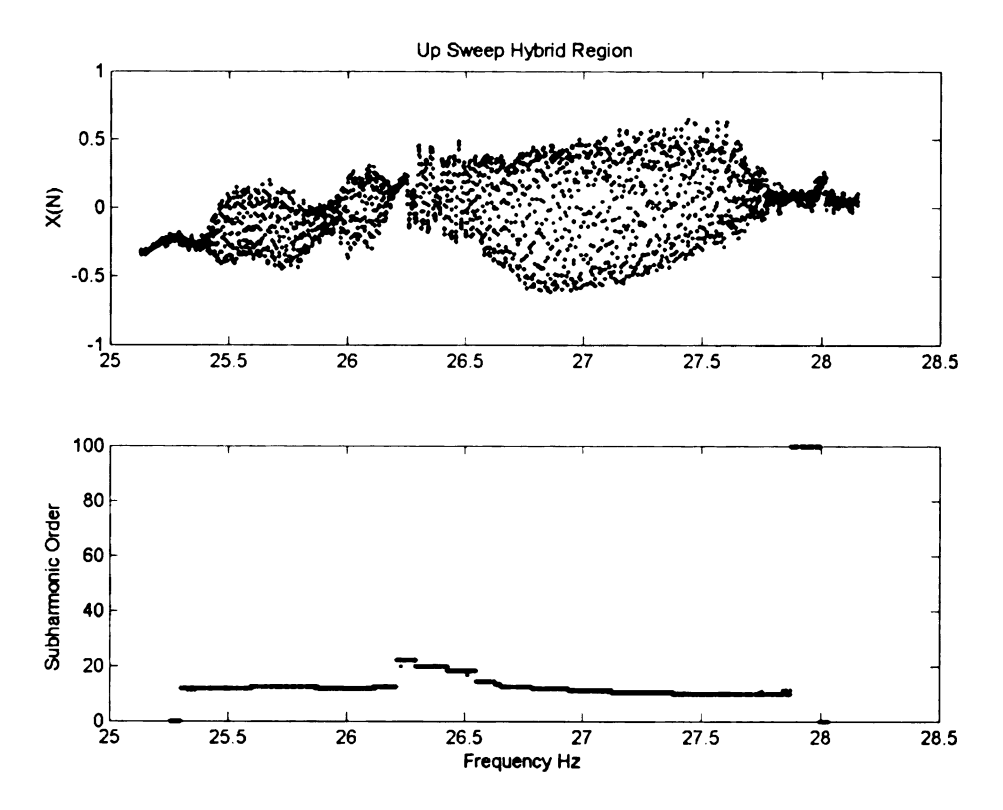


Figure 3.7: Frequency up sweep of the Hybrid region and the subharmonic orders.

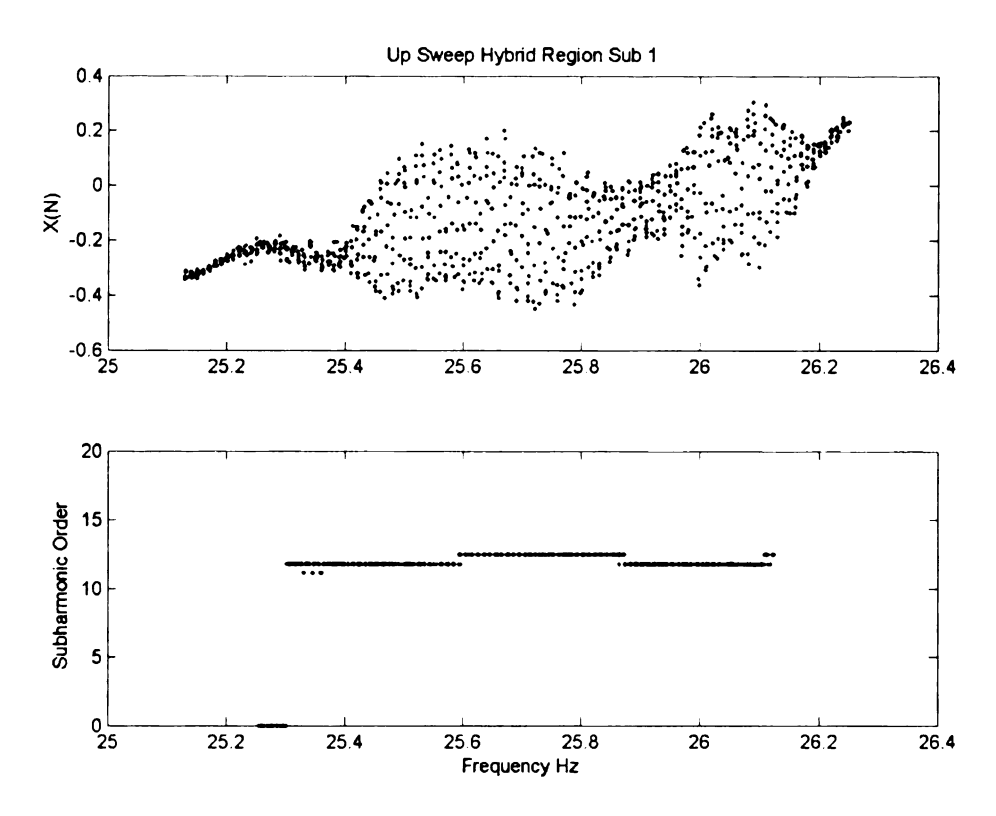


Figure 3.8: Frequency up sweep of the Hybrid region sub 1 and the subharmonic orders.

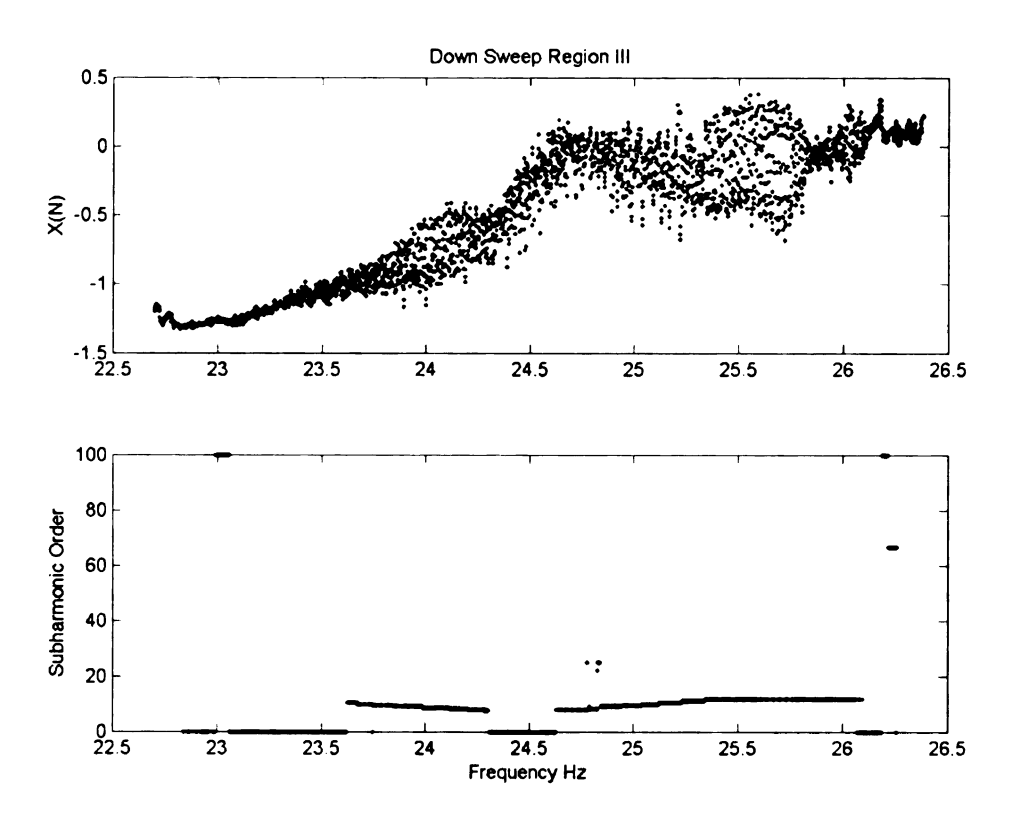


Figure 3.9: Frequency down sweep of region III and the subharmonic orders.

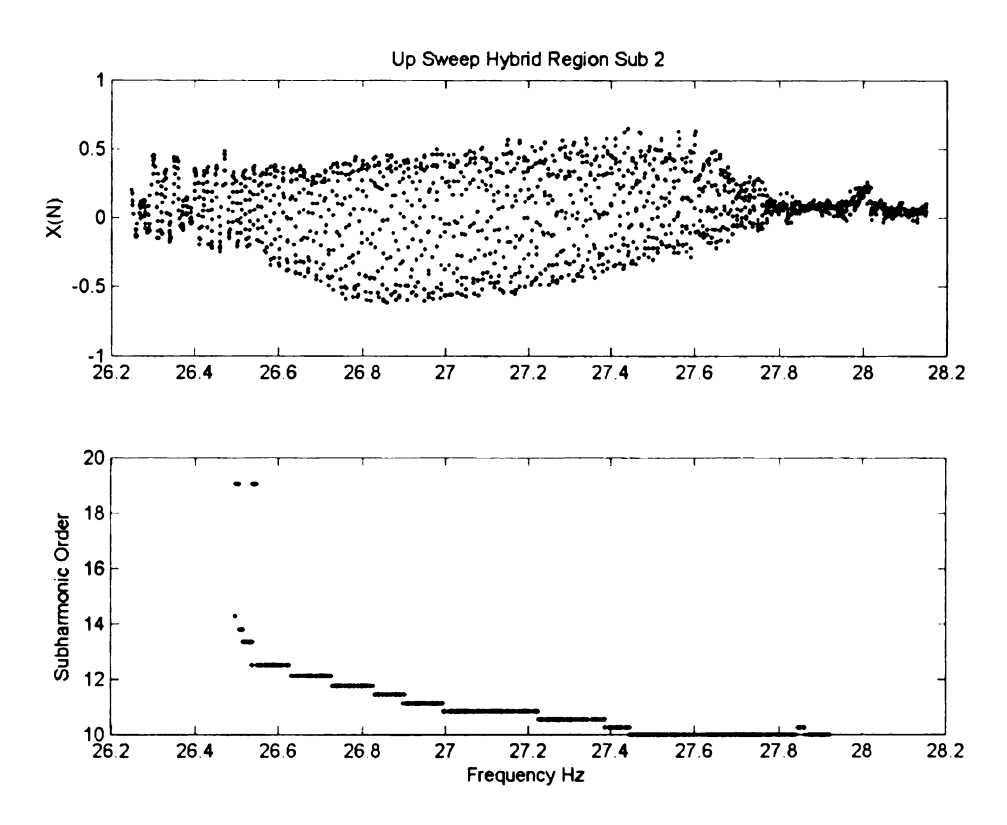


Figure 3.10: Frequency up sweep of the Hybrid region sub 2 and the subharmonic orders.

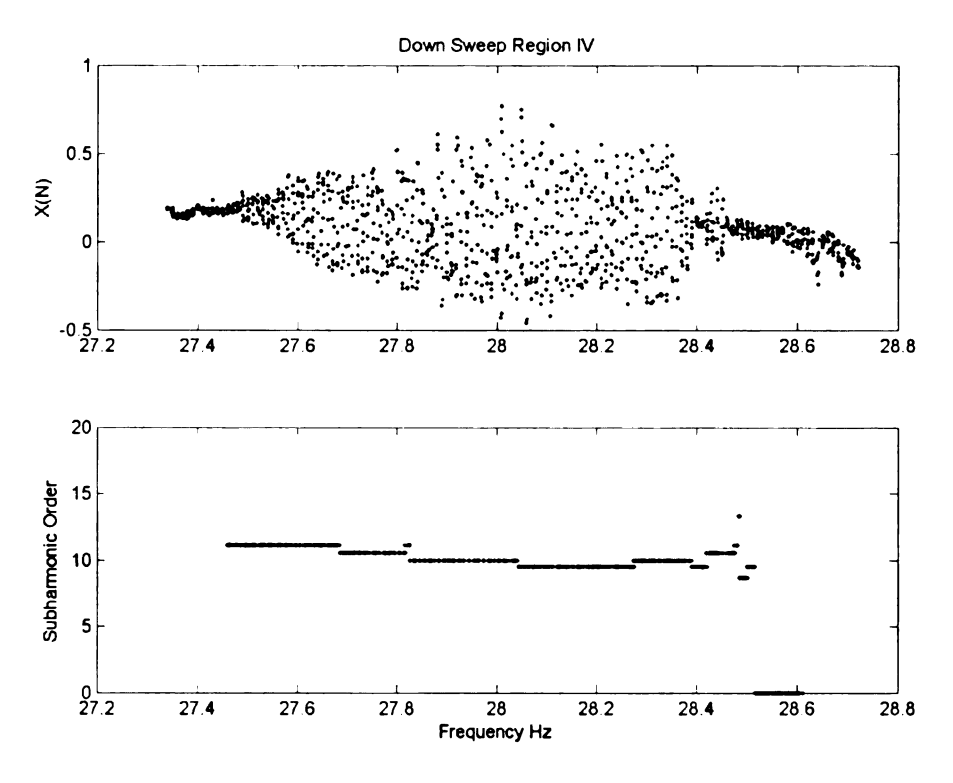


Figure 3.11: Frequency down sweep of region IV and the subharmonic orders.

3.2.4 Region V

Region V is located approximately between 30.2 and 34 Hz. With q=200, the subharmonics of this region feature a general harmonic around 2.2 Hz, though there are short instants where the harmonics jumped to around 20 Hz, but this still did not create a beam response that was interesting in our study. Figure 3.12 and Figure 3.13 in the appendix to see the graphs of the frequency up and down sweeps of region V and their sub-order harmonics.

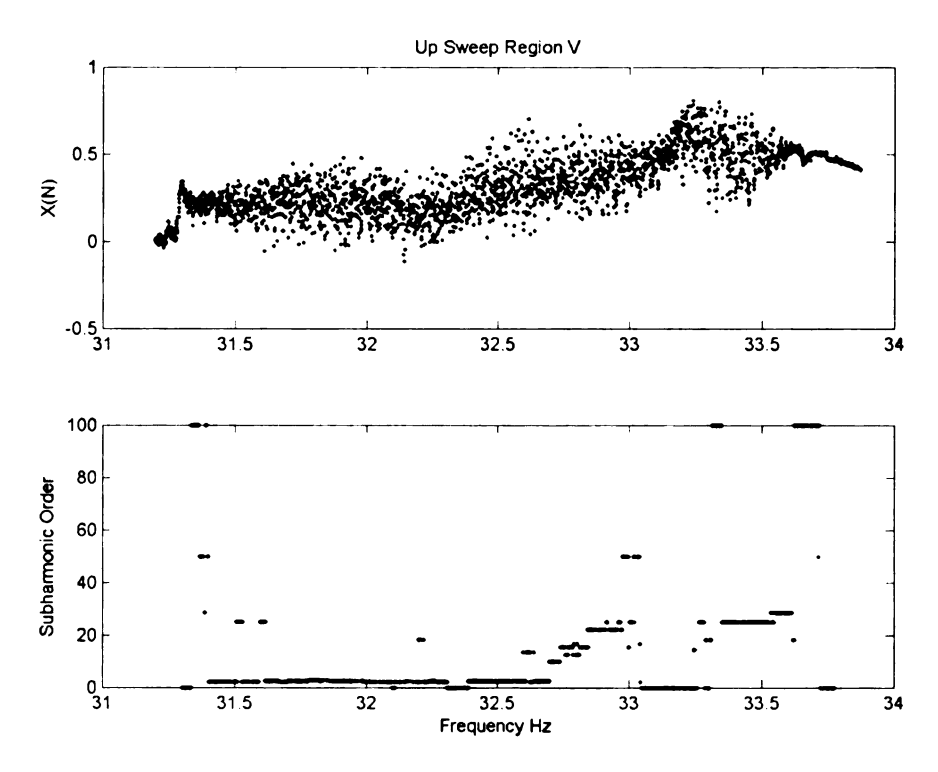


Figure 3.12: Frequency up sweep of region V and the subharmonic orders.

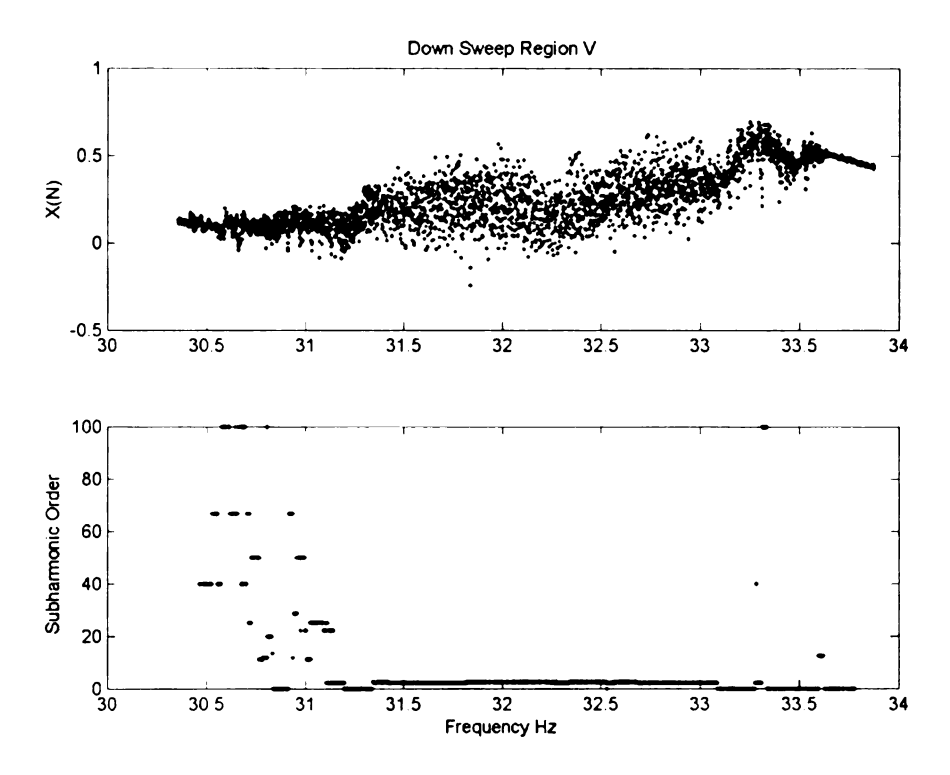


Figure 3.13: Frequency down sweep of region V and the subharmonic orders.

3.2.5 Region VI

In this case, q = 400, leading to a maximum presentable subharmonic order of 200, and short-time FFT frequency windows for the up and down sweeps were 0.28 and 0.284 Hz respectively. Region VI is located approximately between 43 and 47.3 Hz. Figure 3.14 shows the frequency up sweep Poincaré section of region VI along with its subharmonic order and Figure 3.15 shows the down sweep. Upon looking at the frequency up and down sweep graphs of region VI it becomes clear that there are two distinct regions, similar to the Hybrid region. Figure 3.16 to Figure 3.19 show region VI subdivided into to separate regions.

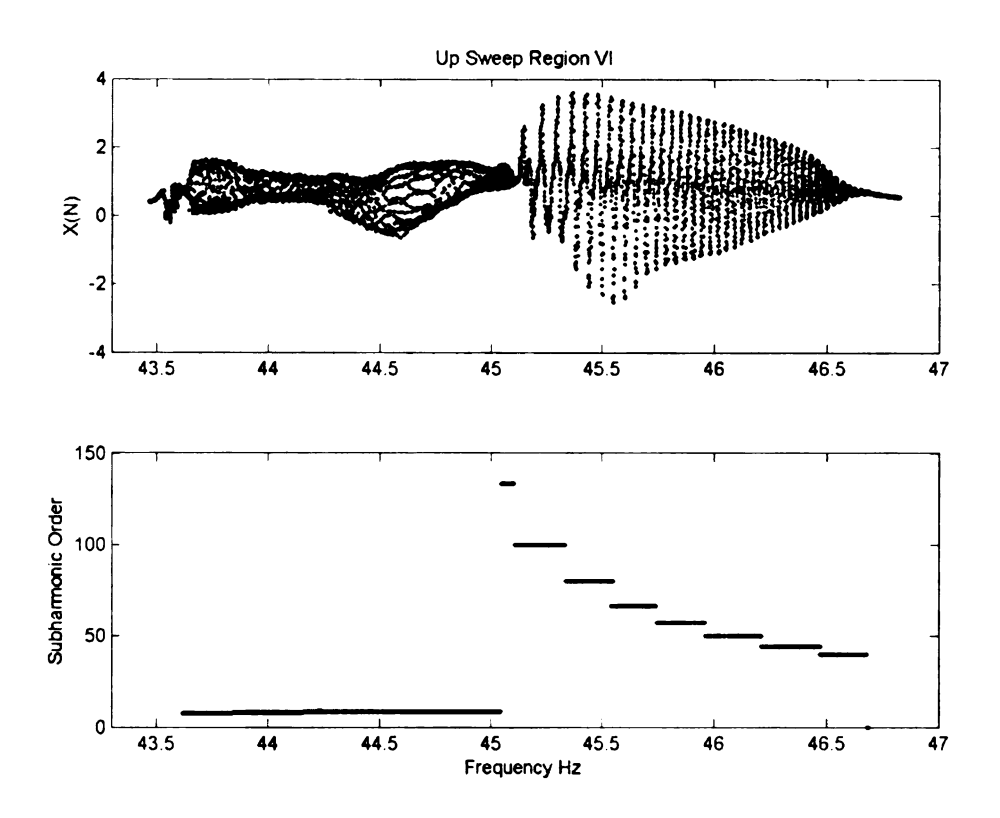


Figure 3.14: Frequency up sweep of region VI and the subharmonic order.

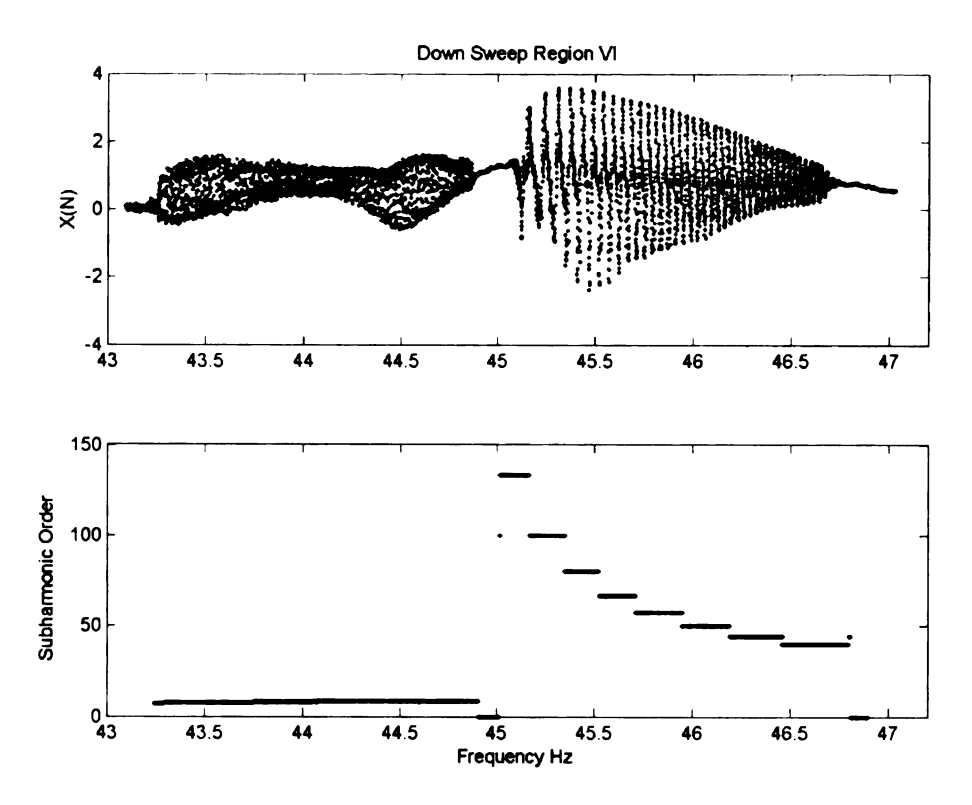


Figure 3.15: Frequency down sweep of region VI and the subharmonic order.

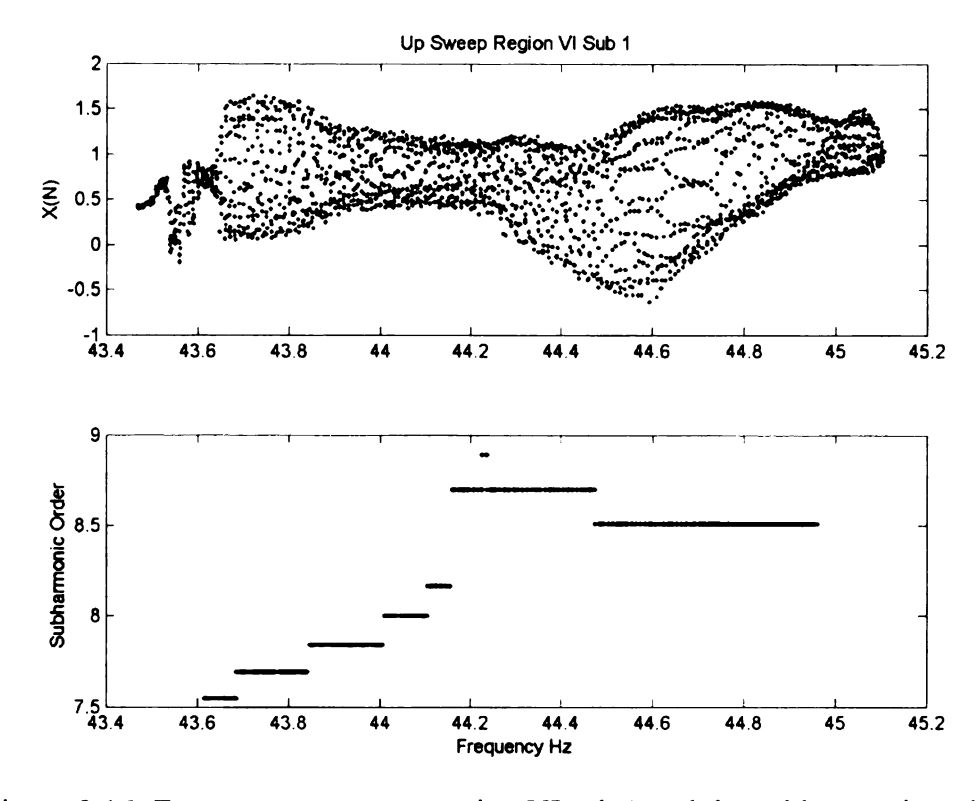


Figure 3.16: Frequency up sweep region VI sub 1 and the subharmonic order.

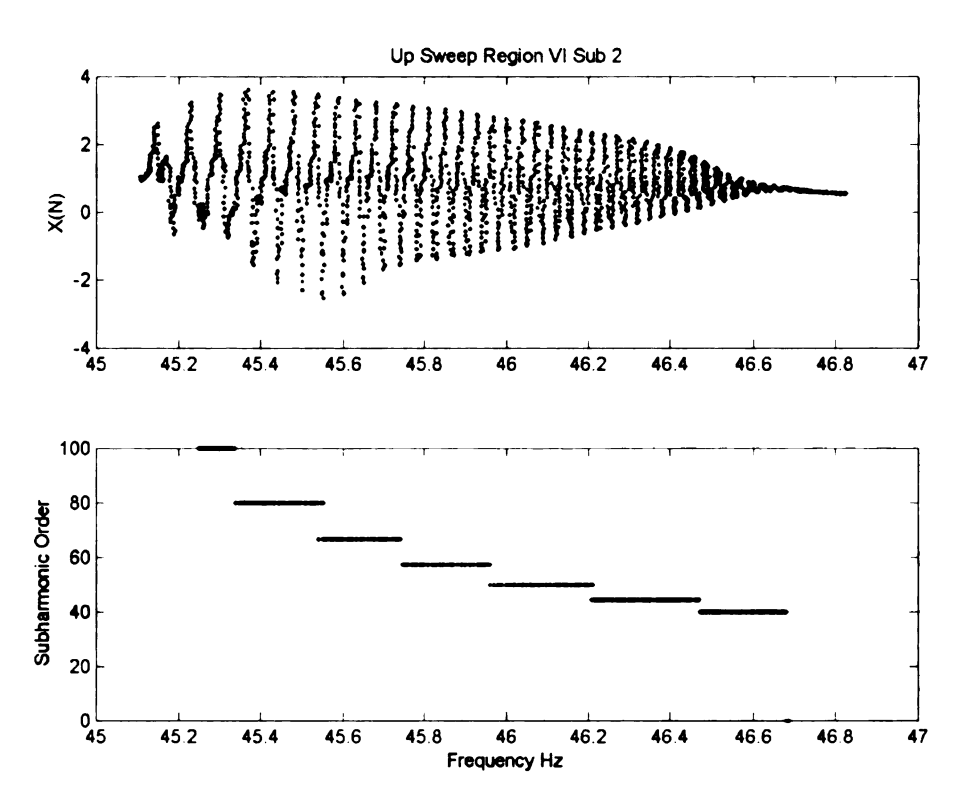


Figure 3.17: Frequency up sweep region VI sub 2 and the subharmonic order.

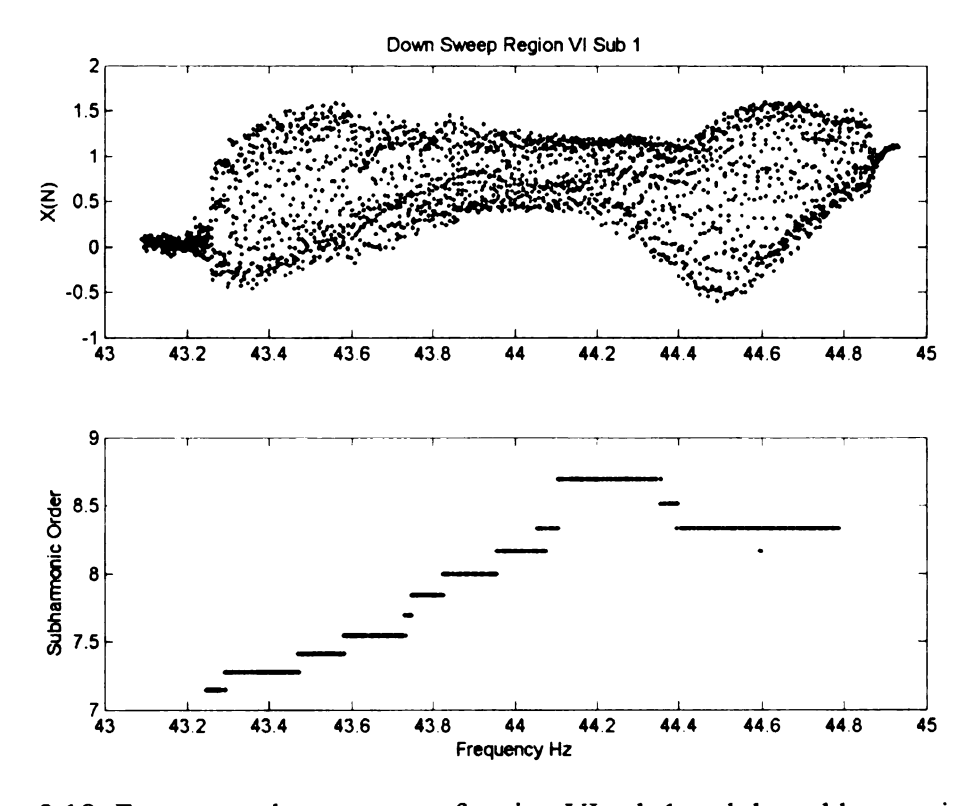


Figure 3.18: Frequency down sweep of region VI sub 1 and the subharmonic order.

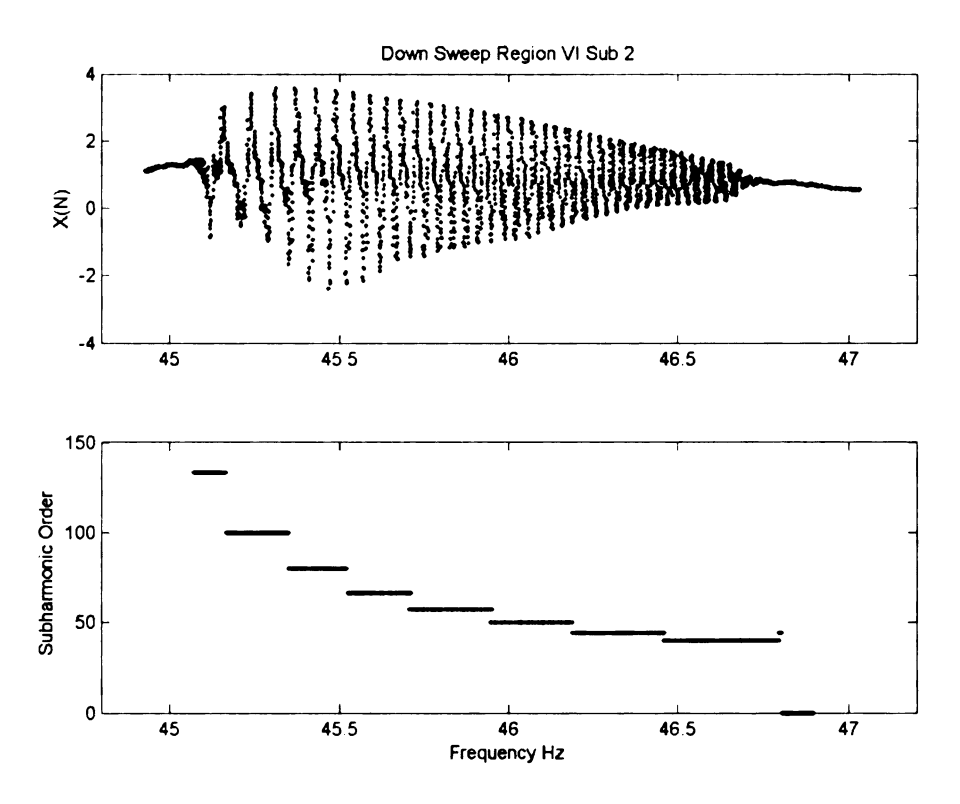


Figure 3.19: Frequency down sweep of region VI sub 2 and the subharmonic order.

In the 43-45 Hz window, we see rather subharmonic orders ranging from about 7 to 9 (Figures 3.16 & 3.18). The 45 to 46.5 Hz window shows a gradual change in subharmonic order, quantized in steps due to our order resolution defined by q/k. Following driving frequency (in either the up or down sweep) downward from 46.5 Hz, for which the subharmonic order is about 40, the subharmonic order increases, actually according to a smooth curve to a remarkably high value (well over 100) before the system bifurcates into the "order-10" subharmonic region.

This gradual change in subharmonic orders is predominately represented by quasi-periodic dynamics, as the order is likely typically irrational. The "order-10"

subi dyn irra beh sub of

> int the

Ма

subharmonic region is also quantized, and typically represented by quasi-periodic dynamics.

Our graph measures subharmonic orders up to 130, as a quantization of some irrational order, during a test with a slow sweep rate. It is interesting to fathom the behavior for true steady-state dynamics as a function of driving frequency.

If we plot the reciprocal of the subharmonic order, i.e. f/f_{driver} , for regions VI sub 2, we get plots, like Figure 3.20, which resemble the frequency demultiplication plots of Van Der Pol and Van Der Mark [13]. It is not the same behavior. Our steps are due to frequency resolution in the short-time FFT plots. The steps of Van Der Pol and Van Der Mark were observed as discrete subharmonic responses, sustained for a parameter interval, and the bifurcating to the next subharmonic, often with accompanying noise at the bifurcation.

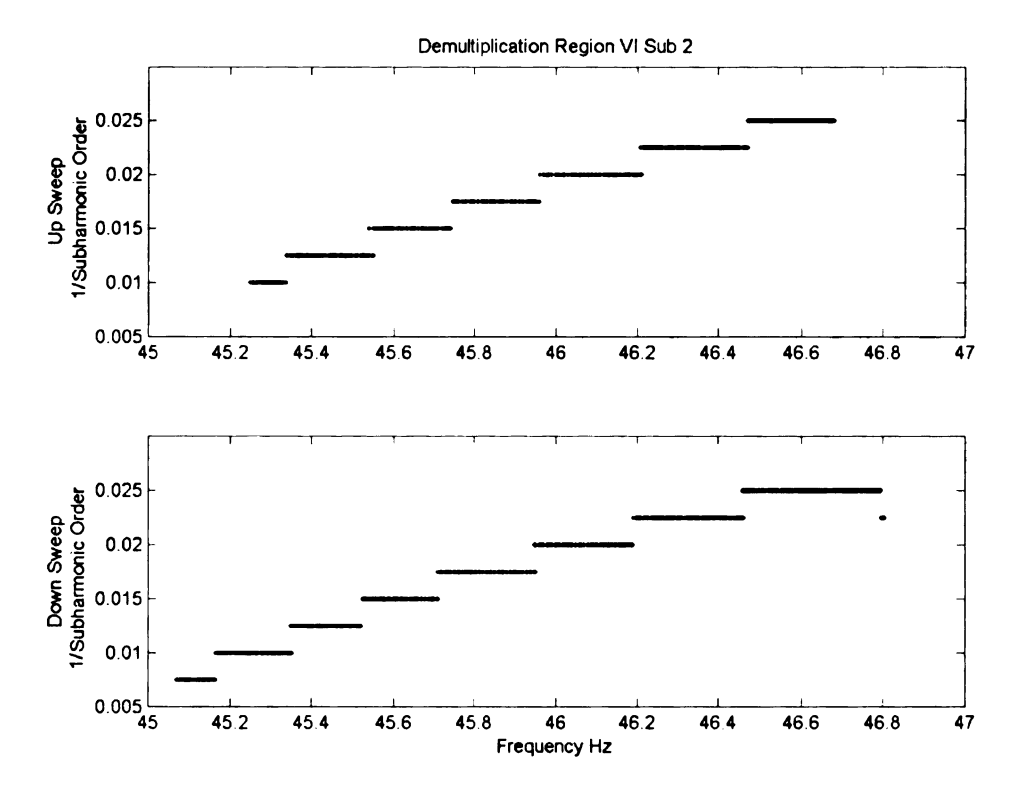


Figure 3.20: Apparent demultiplication of region VI sub 2.

3.3 Summary

The similarity between the *hybrid* region and region *VI* are almost unmistakable. By comparing Figure 3.7 with Figure 3.14 or 3.15 you can see a bifurcation between two zones of the subharmonic responses. With the region *VI* having magnified subharmonic orders compared to the *hybrid* region. Region *VI* involved vibrations in the normal degree of freedom, and it occurs close to the normal modal frequency of 47 Hz. The *hybrid* region also was affected by normal vibration and it occurred close to 47/2 Hz.

From this information we can interpret that the normal degree of freedom plays a roll in the dynamics, in one case (VI) the 47 Hz normal degree of freedom is resonated directly, and in the other case (hybrid) through a superharmonic resonance of order 2

(from $\omega_{normal}/\omega_{driver} \cong 2$). Such a superharmonic resonance of order two requires a quadratic non-linearity, which must already exist by virtue of DC drift figures.

Chapter 4

Fixed-Frequency Responses

In this chapter the frequencies noticed, during the sweeps, to cause the tip of the cantilever beam to under go what appeared to be chaotic or quasi-periodic drift were examined in more detail. As stated in Chapter 2, we focused on 11 different frequencies: 8, 9.8, 21.9, 22.1, 22.3, 25.7, 37.9, 43.8, 44.4, 45.2 and 45.6 Hz. We will group these frequencies with their corresponding regions from Chapter 3. Region *I* holds 8 and 9.8 Hz; region *II* holds 21.9, 22.1, and 22.3 Hz; region *III/Hybrid* holds 25.7 Hz; and region *VI* holds 43.8, 44.4, 45.2, and 45.6 Hz. The only frequency that is not in a region is 37.9 Hz; this frequency was examined not because it caused the chaotic tip drift we wanted to study, rather because its strain gage response signal during the sweep was almost a perfect triangle wave which was a curious quirk.

4.1 Fixed Frequency Examination

Once the fixed frequencies of interest were chosen, a quick estimation of the cantilever tip characteristic drift period was used to estimate the length of the time trace data needed to effectively examine the response behavior of the cantilever beam at the given frequency. In general the higher driving frequencies needed a longer time trace than the lower driving frequencies because they generated lower frequency responses. This time trace data was then post-processed by Matlab to gather data in the Poincaré sections, through which most of the dynamical analyses were performed. Using the Poincaré section condensed the amount of data to be analyzed. A time trace with

millions of data points was reduced to only tens of thousands of Poincaré section data points.

Data from the Poincaré section was viewed in a delay map to provide a reconstruction of the true Poincaré section. The pseudo Poincaré section enabled us to glimpse how the cantilever beam was behaving. This allowed us to come up with other types of analyses, such as taking the Poincaré section of the Poincaré section, or a looking at the torus angle of possible tori, to gather more information about this dynamic phenomenon.

To get a sense of the dimension of the dynamics, we looked at the false nearest neighbors (FNNs) [28] and the fractal (correlation) dimension [29]. The correlation dimension is a measure of the dimension of the attractor (or attracting set), while the FNNs give information on the dimension of the phase space needed to describe the attractor.

We also looked at FFT's of the response signals to understand the frequency content. In performing the FFT's we applied a Hanning window to the data to reduce leakage distortions. We performed the FFT's using the first 10,000 data points of the collected data of each frequency. We omitted data to reduce the sampling rate and thereby fix the Nyquist frequency, and hence the scale of the FFT plot, to a reasonable value (two to five times the driving frequency). In some cases we displayed the FFT of the Poincaré section data to magnify the subharmonic contributions.

4.1.1 Region I (8 & 9.8 Hz)

8 and 9.8 Hz were the forcing frequencies selected from region *I*. The cantilever beam was then forced at the given frequency for an extended amount of time to allow it

to settle into a steady state after which the collection of data was started. Data was collected for 15 minutes at 8 Hz and for 20 minutes at 9.8 Hz. This time trace data was then imported into Matlab and the Poincaré section was taken. Plotting the Poincaré section in a delay map helped in visualization of the data. Figure 4.1 and Figure 4.2 show the delay map with a delay of one index of the Poincaré section samples of 8 and 9.8 Hz respectively. Three iterates of the 8 Hz data travel clockwise in the Poincaré section, moving from spot to spot, occasionally getting trapped in the area of (-0.2, -0.2) for several iterates. The iterates of the 9.8 Hz data also circle clockwise. While the distance from the center of the data (2, 2) increases and decreases, circular motions in the Poincaré sections suggest toroidal dynamics, although in these cases the torus would be fat. Thinking this way, we took the Poincaré section of the Poincaré section and the torus angle to look for dynamical structure. The torus angle was taken about the approximate center of the torus of the delay map of the original Poincaré section.

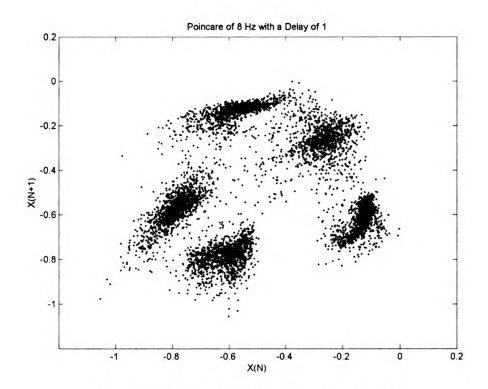


Figure 4.1: Poincaré section delay map of 8 Hz.

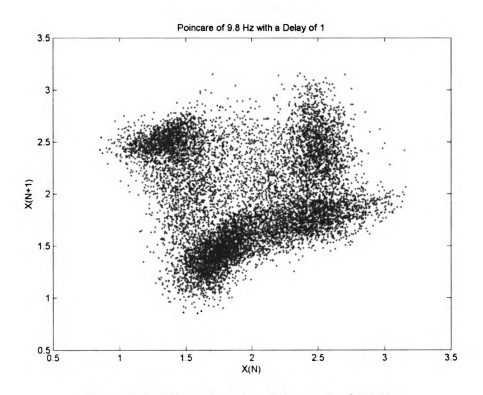


Figure 4.2: Poincaré section delay map of 9.8 Hz.

Figure 4.3 shows the Poincaré section of the Poincaré section for 8 Hz. The Matlab program that performed the Poincaré section of the Poincaré section flagged Poincaré section data that crossed the diagonal from positive to negative, the positive being the bottom right half and thus the negative being the top left half. By viewing the delay map of the 2nd Poincaré section in Figure 4.3 we see that, for the most part, the Poincaré data wraps around the torus, fluctuating at (-0.7, -0.70, but there is also another mini torus the Poincaré periodically visits at (-0.3, -.03). However, Figure 4.3 does not reveal any structure in these toruidal fluctuations, suggesting higher dimensional dynamics between the two components of the torus. Refer to Figure A.1 in the Appendix to see the Poincaré section of the Poincaré section verses its index to see when the mini torus is visited with respect to the larger torus.

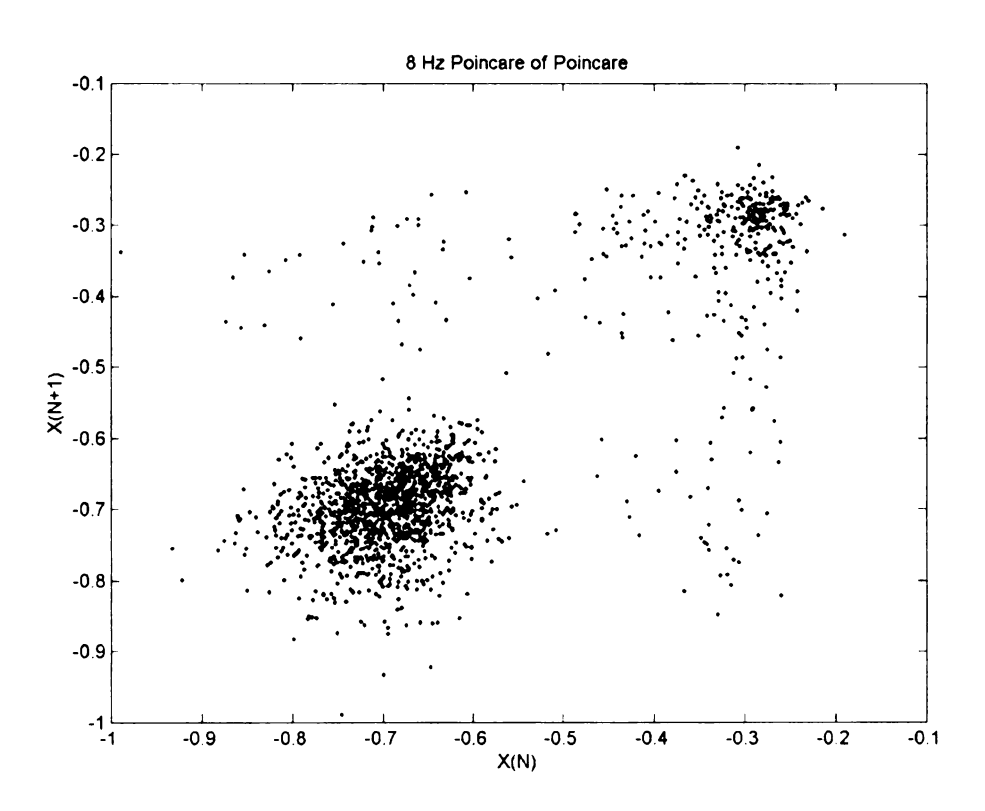


Figure 4.3: Delay map of the Poincaré section of the Poincaré section delay map at 8 Hz.

The Poincaré section of the Poincaré section for 9.8 Hz is unlike the 8 Hz case because this time the Matlab program flagged the Poincaré section data that crossed the diagonal from negative to positive. This was chosen after looking at Figure 4.2 and it was felt that it was a clearer crossing than if we were to go from positive to negative. Figure A.2 in the Appendix shows the outcome, which is that the Poincaré data crosses the diagonal in one continuous area.

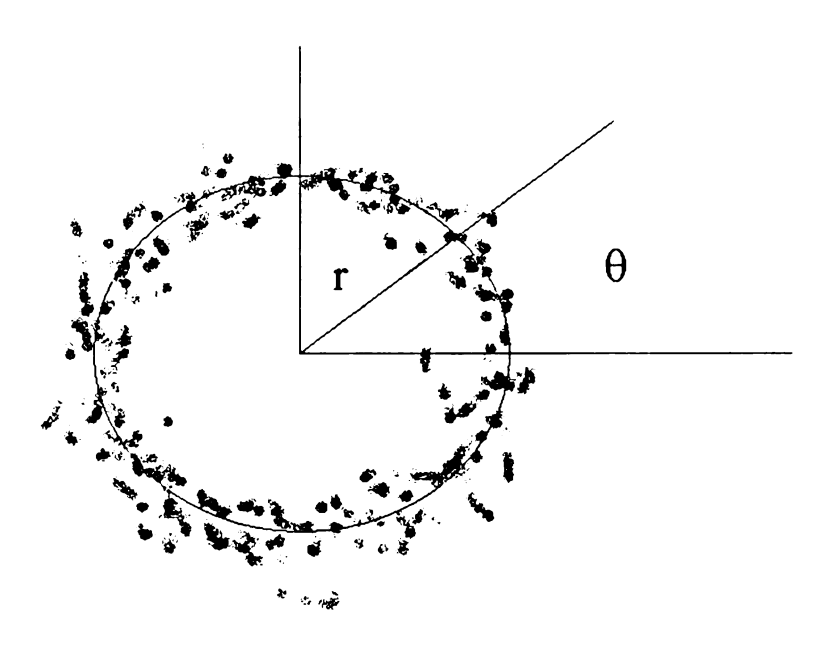


Figure 4.4: Torus angle model.

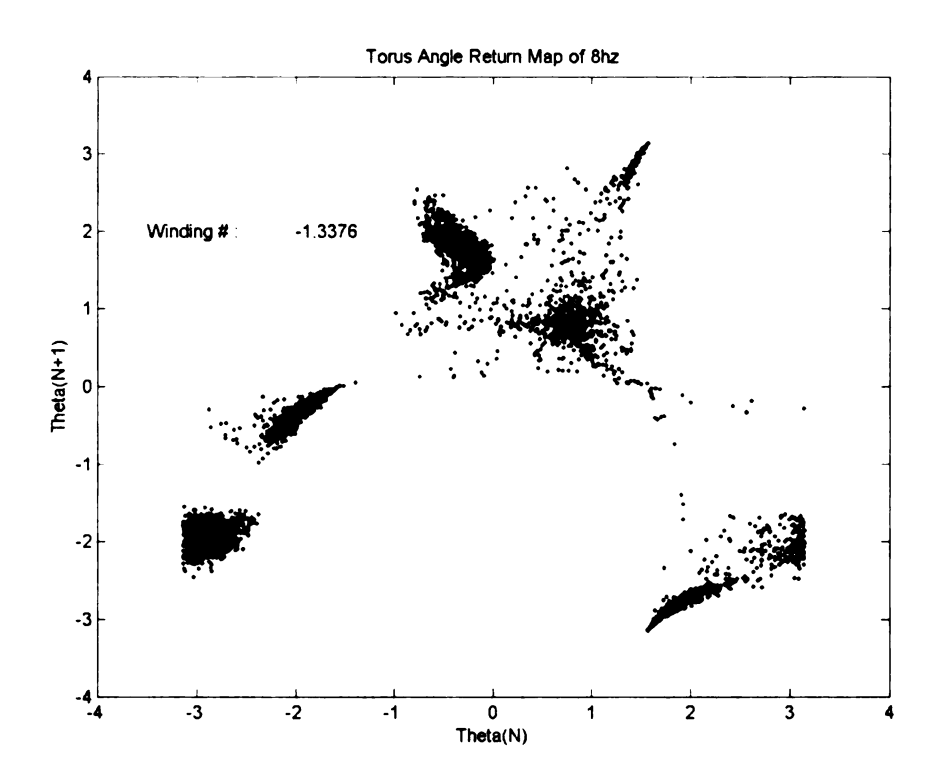


Figure 4.5: Torus angle dynamics of 8 Hz.

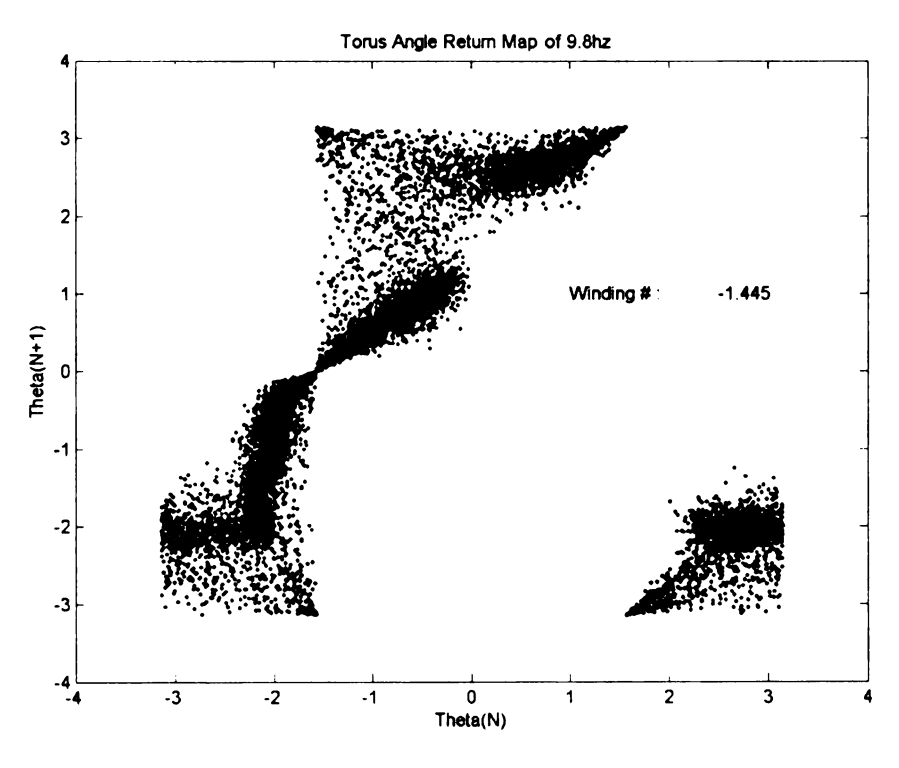


Figure 4.6: Torus angle dynamics of 9.8 Hz.

Figure 4.4 shows a simple schematic model of how the torus angle return map was created from the Poincaré section delay map. Matlab was used to calculate the angle θ in each Poincaré section with respect to a given center. Figure 4.5 and Figure 4.6 show the delay maps of the torus angles, θ , for 8 Hz and 9.8 Hz respectively. At 8 Hz the center coordinates x-bar and y-bar were at -0.5 on Figure 4.1. The x-bar and y-bar, for 9.8 Hz, were 2.1 on Figure 4.2. Figure 4.5 shows that Poincaré section data at an angle of approximately -0.3 rad will map to an angle of approximately -0.2 rad. These data then map to around θ equal to -0.5 rad. Data at θ approximately equal to -0.5 rad mostly map to θ equal to 1-2 rad, but occasionally map to values of θ approximately equal to 0-1 rad. In this region the data is almost trapped, most often mapping back to the same region of θ . This is the "mini torus." Occaisionally they map back to the previous region, but data in the positive end of the 0-1 rad region get cleanly mapped to θ values of +1.5-2.5 rad. These data go to θ approximately equal to π , and wrap to θ equal to negative π , where the process starts over again.

Hence the θ map indicates rather deterministic travel around the main turus, but dynamical interaction which is not a simple 1-D map at the region of the "mini torus."

Figure 4.6 shows, for the 9.8 Hz case, a strong band resembling a circle map, clouded by additional dynamics off the circle map. It suggests that some higher dimensional dynamics occurs with some strong tendency torward circle map, dynamics, yet it does not "settle in" on the circle map. This makes sense, as a thin torus is not apparent in Figure 4.2. The underlying circle map has a near tangency with the indentity diagonal, suggesting intermittency in the dynamics [30].

The figures also give us information on the winding number, which has units of radians per cycle. The winding number for 8 Hz is -1.3376 rads/cyc (or -0.2129 cyc/cyc) and for 9.8 Hz it is -1.445 rads/cyc (or -0.23 cyc/cyc).

After viewing the torus angle figures we see that although there is a definite pattern to the Poincaré section, it appears that the dynamics are only loosely based on a torus. Figure 4.5 show how the Poincaré section jumps from one stage to the next as well as how it might get hung up between two stages. Figure 4.6 appears to fit the classification of a torus little better, but a more of special type of torus known as a fat torus.

The Poincaré sections and torus angle maps show that the dynamics are of higher dimension than 3. It is important to see exactly what dimensions we are dealing with. To do this, a Fortran and a Matlab program were created to find the FNNs (False Nearest Neighbors) [28] and the correlation dimension [29] respectively. Table 4.1 shows the number of FNNs as well as the percent of FFNs to total number of Poincaré section data in each corresponding reconstruction dimension. It is difficult to pinpoint the embedding dimension of the deterministic dynamics, as experimental noise contributes to the FNN counts. If we were to (arbitrarily) prescribe a 1% criterion, it would lead to embedding dimensions of 5 for the 8 Hz data, and 6 for the 9.8 Hz case. The correlation dimension program allows user to view $\log C(r)$ vs. $\log (r)$ (where C(r) is the correlation sum as a function of distance r), choose a scaling region, and find the slope in the scaling region. This slope is an approximation of the fractal (correlation) dimension. The correlation program also allows the user to view an approximation of the derivative of the $\log C(r)$ vs. $\log (r)$. This works as a nice check to see if the fractal dimension is right. Refer to

Figure A.3 in the Appendix to see the correlation data for 8 and 9.8 Hz. It should be said that the correlation dimension slope, d_C , is r dependent, and suggesting that the fractal scaling varies with the size scale. The correlation dimension might be represented by the maximum d_C , or alternatively by the slope of a in the linear region of the $\log C(r)$ vs. $\log(r)$ plot. The FNN and d_C should agree, i.e. the embedding dimension of the FNN, d_E , should have the relationship of $d_C < d_E \le 2d_C + 1$. At any rate the correlation dimension is 3.3275 at 8 Hz and 3.7394 at 9.8 Hz.

	8 Hz		9.8 Hz	
Dimension	FFN	Percent	FFN	Percent
First	7086	98.43%	12144	99.44%
Second	3499	48.60%	8022	65.69%
Third	802	11.14%	2680	21.95%
Fourth	151	2.10%	635	5.20%
Fifth	44	0.61%	197	1.61%
Sixth	16	0.22%	62	0.51%
Seventh	4	0.06%	11	0.09%
Eighth	0	0.00%	0	0.00%
Ninth	0	0.00%	0	0.00%

Table 4.1: FNN data of 8 and 9.8 Hz.

Figure 4.7 and Figure 4.8 show the FFTs as well as the FFTs of the Poincaré sections of 8 Hz and 9.8 respectively. These figures both show the driving frequency as the dominant spike, but the first spikes on both of the FFT graphs occur at 1/4 the driving frequency. This type of subharmonic resonance suggests that the beam's behavior is affected by period doubling [31] at both 8 and 9.8 Hz, although clear period doublings are not apparent in the frequency sweeps of Chapter 3. This may be due to the speed of the sweeps, as discussed in Chapter 3.

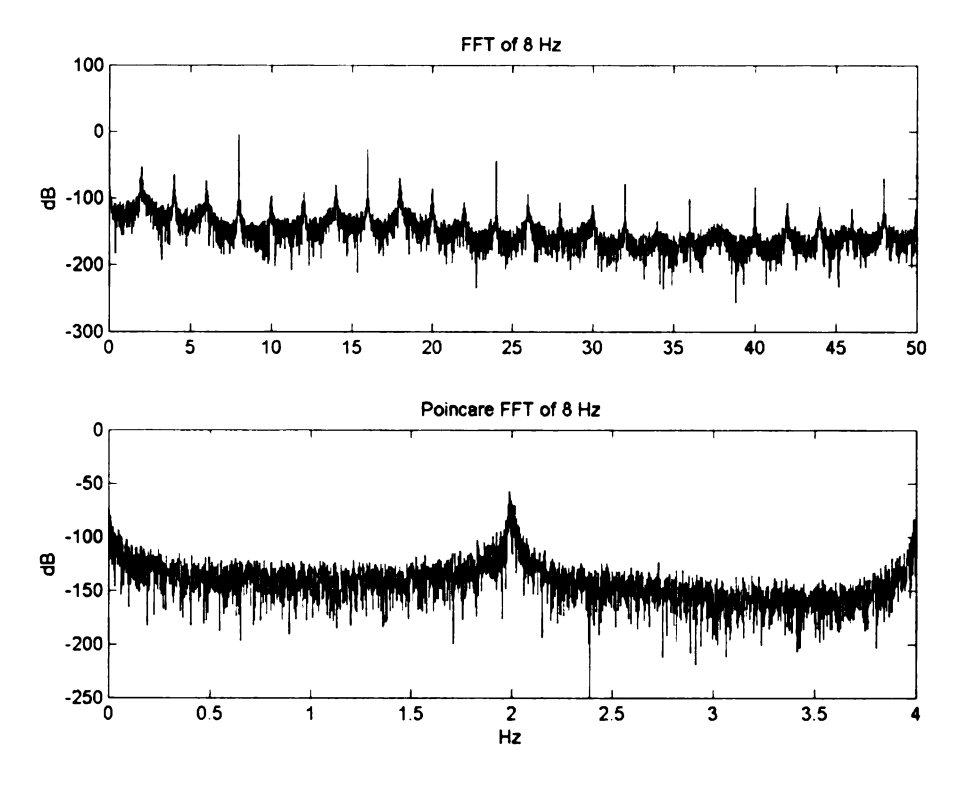


Figure 4.7: FFT and the Poincaré FFT of 8 Hz.

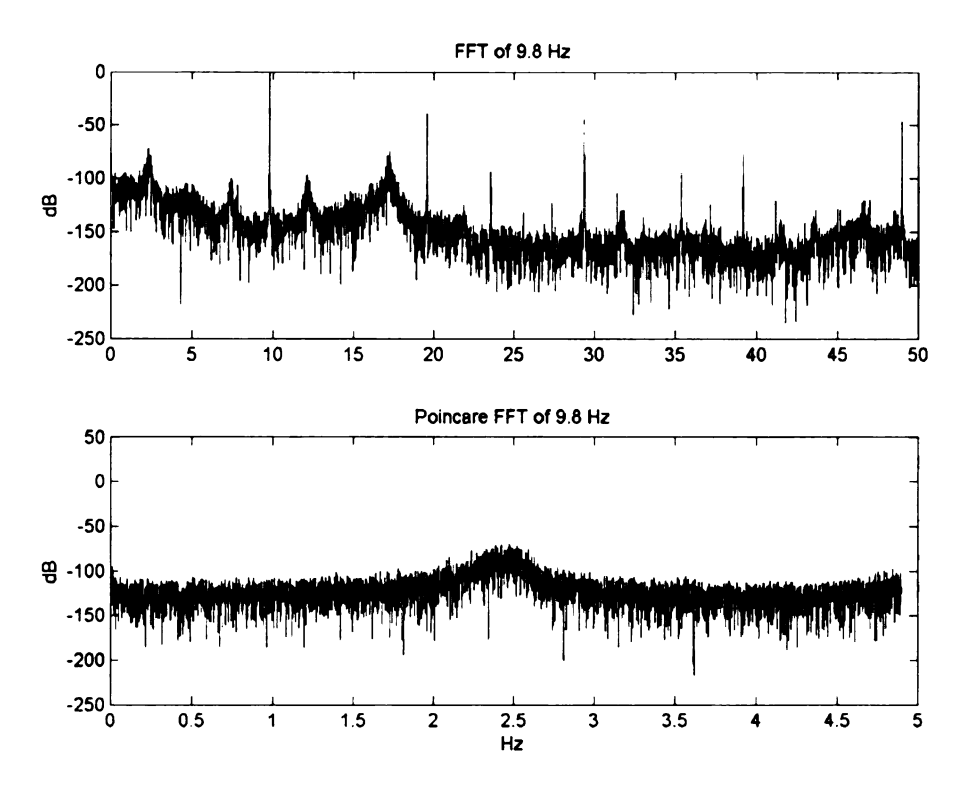


Figure 4.8: FFT and FFT of the Poincaré section of 9.8 Hz.

After viewing the FFT figures and understanding the winding number given from the torus angle dynamic figures, we can see a direct correlation between the subharmonic spike and the winding number. It is also noticeable that the driving frequency divided by the subharmonic spike frequency yields values that are comparable to the subharmonic orders found from the frequency sweep data of Chapter 3.

For the case of 8 Hz, the winding number in cycles per cycles multiplied by the driving frequency produces a subharmonic frequency value of 1.703 Hz (ignoring the minus sign). This in not close to the subharmonic spike frequency of 2 Hz but this may be because of the mini torus winds faster than the larger torus, and does not contribute to the changes in θ , causing this error. Indeed, with the coupling between the "mini torus" and the large torus, using one torus angle may not be representative of the dynamics.

In the case of 9.8 Hz the subharmonic frequency value produced is 2.2534 Hz. This is value is closer to the subharmonic spike frequency. Dividing the driving frequency by the subharmonic frequency will yield the subharmonic order; these values of 4.6976 for 8 Hz and 4.349 for 9.8 Hz correspond closely with the subharmonic orders of region *I* of Chapter 3.

4.1.2 Region II (21.9, 22.1 & 22.3 Hz)

The forcing frequencies selected from region *II* were 21.9, 22.1, and 22.3 Hz. The cantilever beam was then forced at the given frequency for an extended amount of time to allow it to settle into a steady state, after which the collection of data was started. Data was collected for 15 minutes at 21.9 Hz and for 20 minutes at 22.1 and 22.3 Hz. This time trace data was then imported into Matlab and the Poincaré section was taken.

By plotting the Poincaré section in a delay map we were able to observe what path the Poincaré data follows in higher dimension. Figures 4.9 and Figure 4.10 shows the Poincaré section and the Poincaré section of the Poincaré section of 21.9 Hz respectively. In Figure 4.9, the map has an interchange between dynamics around the circular cloud, and the dynamics in the diagonal dark band.

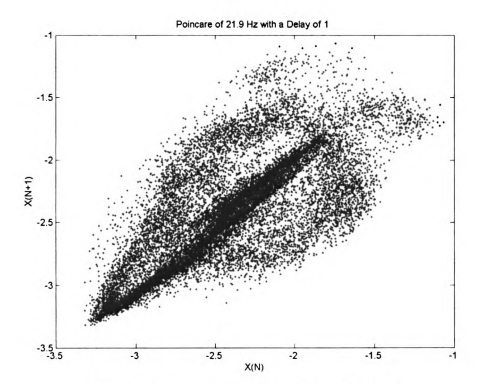


Figure 4.9: Poincaré section delay map of 21.9 Hz.

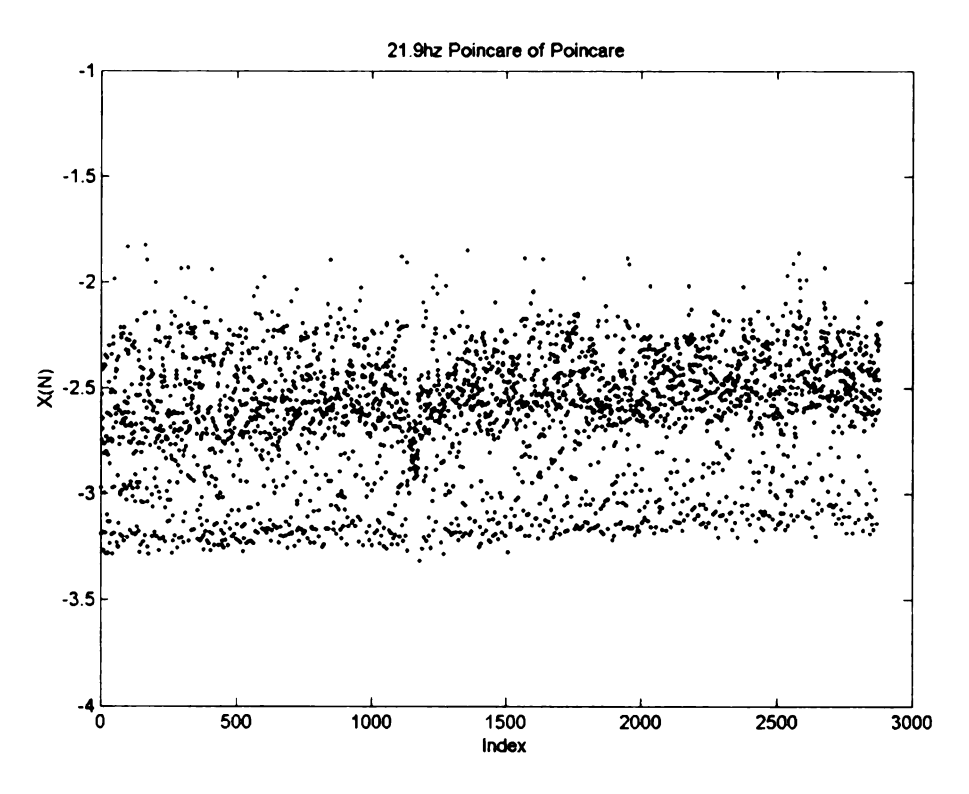


Figure 4.10: Poincaré section of the Poincaré section of 21.9 Hz plotted against its index.

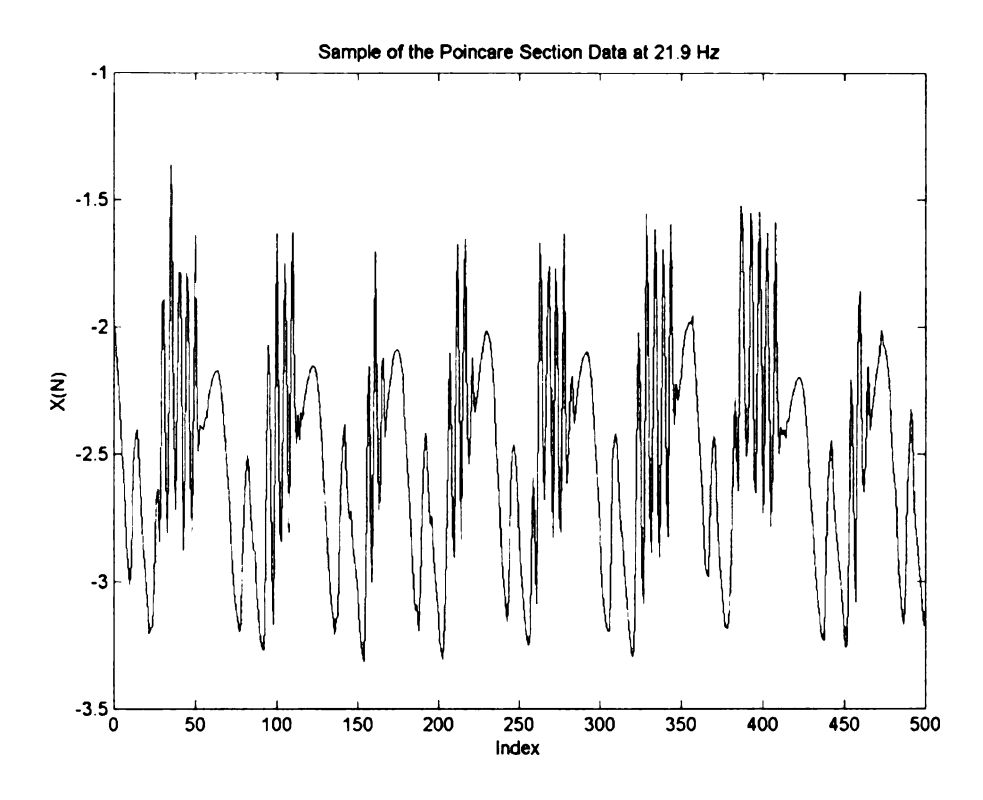


Figure 4.11: Sample of the Poincaré section data at 21.9 Hz plotted against its index.

The delay map of the Poincaré section of the Poincaré section of 21.9 Hz did not give any insight into how Figure 4.9 was behaving; refer to the Appendix Figure A.4 to see the delay map of the cross-section of the Poincaré section of 21.9. Figure 4.10 on the other hand tells us that the Poincaré section of Figure 4.9 represents an attractor, rather than a case were the dynamics of the cantilever beam suddenly change to give us two different responses.

The next frequency to be presented is a case were during the data collection there is a change in the responses and thus two different responses are present. The Matlab program that preformed the cross-section of the Poincaré section of 21.9 Hz flagged Poincaré section data that crossed the diagonal from positive to negative, the positive being the bottom right half and thus the negative being the top left half. Figure 4.11 allows one to see how long the dynamic behavior tends to spend in the slow part ("flat torus") versus how long it spends in the oscillatory part ("round torus").

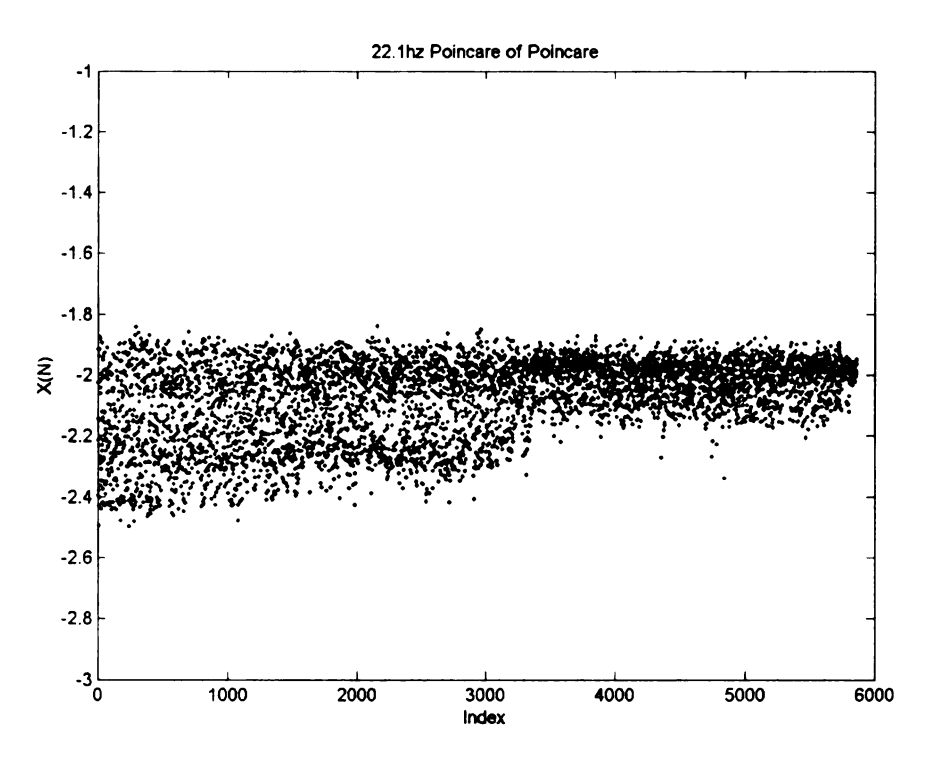


Figure 4.12: Poincaré section of the Poincaré section of 22.1 Hz plotted against its index.

Figure 4.12 shows the Poincaré section of the Poincaré section at a frequency of 22.1 Hz plotted against its index. This figure clearly shows that there are two different segments of the response. It is likely that the slight changes in parameter, such as friction, due to, e.g., temperature and wear, led to a change in the nonlinear system response. As such we have taken the liberty of breaking the response data in to two different sub regions. Below, Figure 4.13 and Figure 4.14 show the Poincaré section delay maps of each region. The figures have the same scale so the reader will be able to see how the data segments would have overlapped and important information would have been missed. Figure 4.14 appears to be a better-defined torus which allows us to use the torus angle program in Matlab to see if in fact it is a torus.

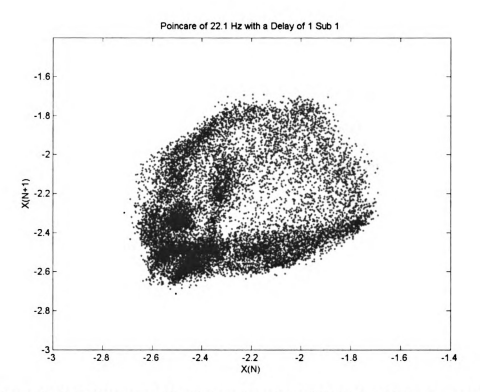


Figure 4.13: Delay map of the Poincaré section of 22.1 Hz of data segment 1.

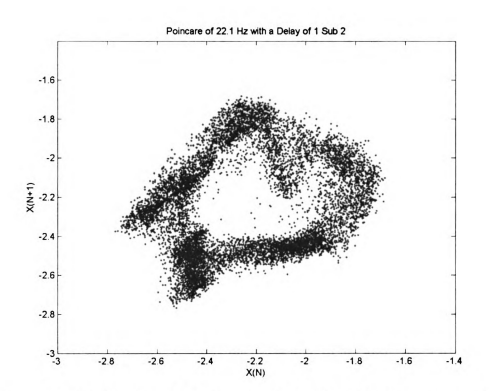


Figure 4.14: Delay map of the Poincaré section of 22.1 Hz of data segment 2.

Figure 4.15 shows the Poincaré section of 22.3 Hz. The dynamics are similar to those of the 21.9 Hz case, in that the map of the data alternates between going around the toroidal loop, and iterating on the diagonal dark band. After viewing this figure we decided that we would be unable to take the Poincaré section of the Poincaré section of the 22.3 Hz data. The problem was that the majority of the data appeared to be along the diagonal axis we wanted to take the cross section along. But as one can see there is still a clear hole in the torus, which allows us to define a center point to use the torus angle program in Matlab.

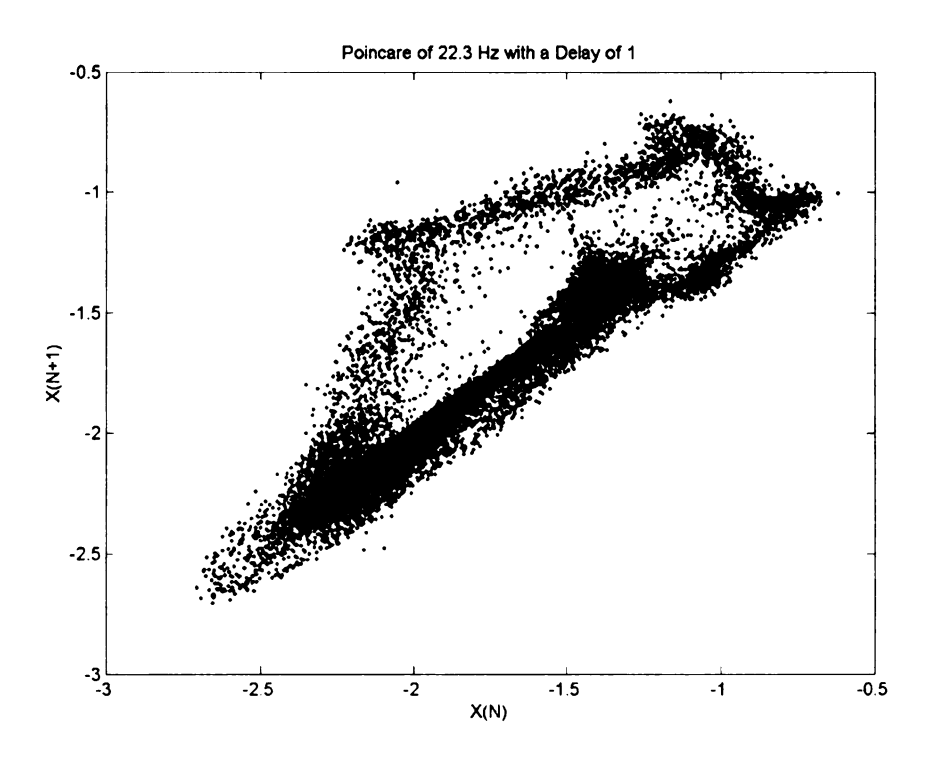


Figure 4.15: Poincaré section of 22.3 Hz with a delay of 1.

Figure 4.16 and Figure 4.17 show the delay map of the torus angle return maps of the Poincaré section of 22.1 Hz data segment 2 and 22.3 Hz respectively. These are more clearly defined, compared to the torus-angle figures in section 2.1.1. The graphs

inform us that the Poincaré sections are in fact toruses, and the dynamics are governed by circle maps. The winding numbers are -1.3367 rads/cyc (-0.2127 cyc/cyc) and -0.24981 rads/cyc (-0.0398 cyc/cyc). The first circle map is monotonic, suggesting quasi-periodic dynamics with some higher dimensional fluctuation. The second circle map has a nearly zero-slope portion, and may therefore be on the brink of chaos by torus wrinkling. The dynamics are similar to those of he 21.9 Hz case, in that the map of the data alternates between going around the toroidal loop and interacting on the diagonal dark band.

Considering a diagonal line along the identity (separating the top left from the bottom right) in the plot there are near tangencies at -2 and -2 suggesting intermittency [30].

The existence of some higher dimensional dynamics (evident in the fatness of the plot) might combine with intermittency to generate chaos. Figure 4.18 shows a sample of the Poincaré section data versus its index, which suggests how long the dynamic behaviors tend to spend in each part of the torus.

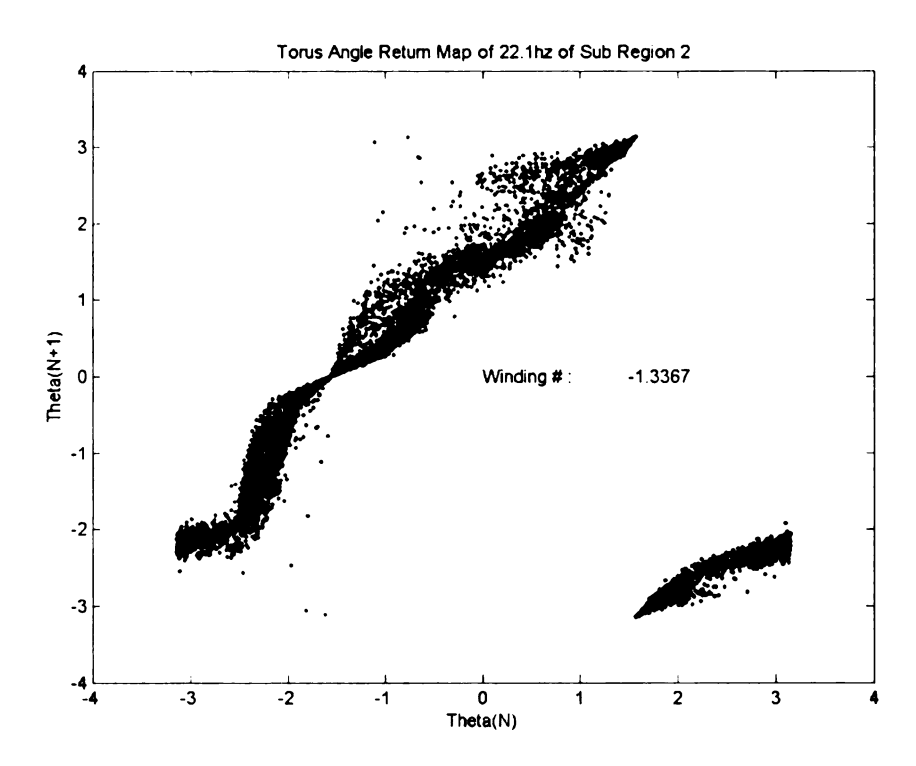


Figure 4.16: Torus angle dynamics of 22.1 Hz of sub region 2.

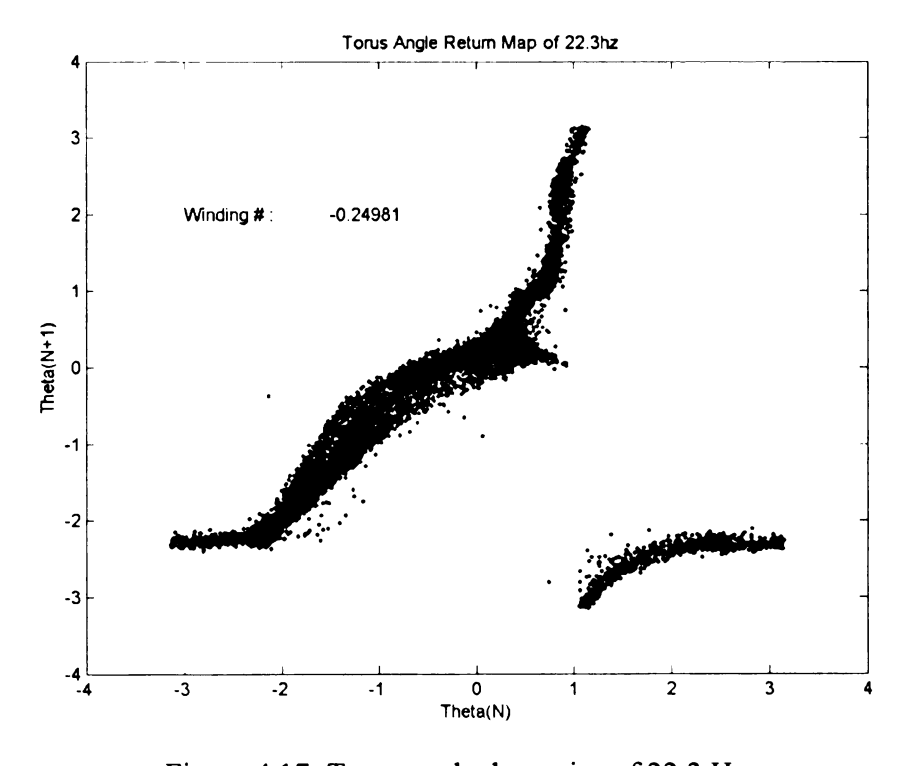


Figure 4.17: Torus angle dynamics of 22.3 Hz.

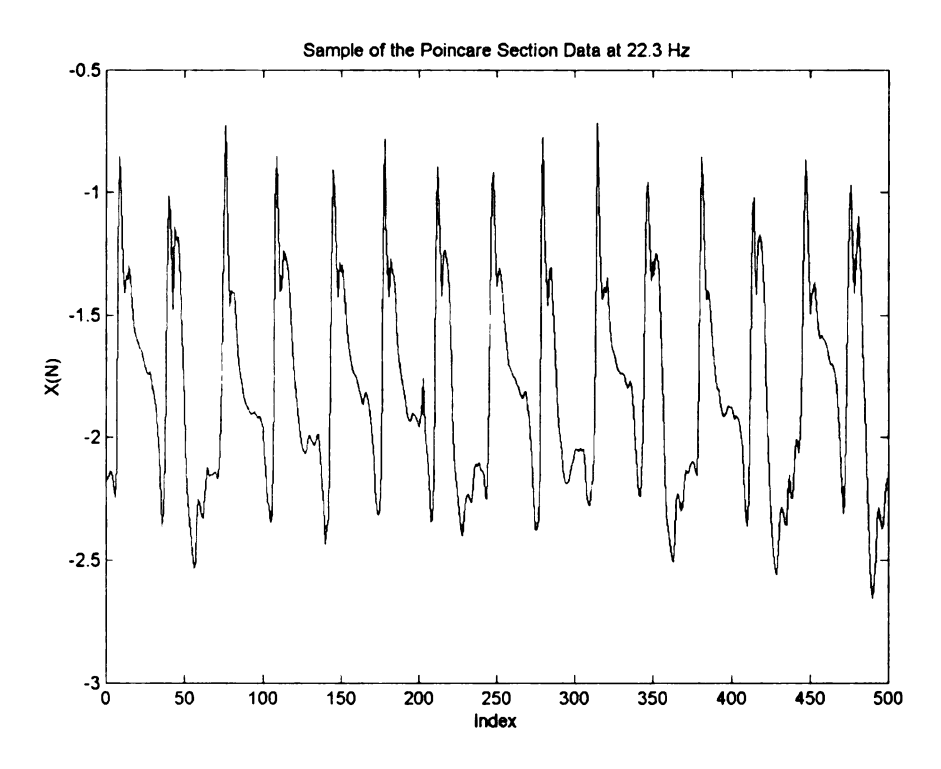


Figure 4.18: Sample of the Poincaré section data at 22.3 Hz plotted against its index.

For of 21.9, 22.1, and 22.3 Hz, the FNN and correlation dimension programs were run to gather information about the dimension of the dynamics at these frequencies. Table 4.2 contains the FNN information. Refer to the Appendix, Figure A.5, to examine the correlation dimension information which yields a correlation dimension of 2.4439 at 29.1 Hz, 3.3973 at 22.1 Hz, and 3.1805 at 22.3 Hz.

	21.9 Hz		22.1 Hz		22.3 Hz	
Dimension	FFN	Percent	FFN	Percent	FNN	Percent
First	19640	99.43%	26458	99.67%	26611	99.21%
Second	11526	58.35%	18125	68.28%	15293	57.02%
Third	2244	11.36%	4919	18.53%	3399	12.67%
Fourth	411	2.08%	750	2.83%	689	2.57%
Fifth	83	0.42%	99	0.37%	191	0.71%
Sixth	27	0.14%	18	0.07%	58	0.22%
Seventh	8	0.04%	3	0.01%	15	0.06%
Eighth	0	0.00%	0	0.00%	0	0.00%
Ninth	0	0.00%	0	0.00%	0	0.00%

Table 4.2: FNN data of 21.9, 22.1, and 22.3 Hz.

Figure 4.19, Figure 4.20, and Figure 4.21 show the FFT and the Poincaré-section FFT of 21.9, 22.1, and 22.3 Hz respectively. Figure 4.19 highlights some very interesting frequencies. There are two pairs of frequency peaks on either side of the driving frequency of 21.9 Hz. These paired frequencies have distances of 0.4 and 4.27 Hz from the driving frequency. These distances match up with the first two peaks in the FFT, which have frequencies of 0.4 and 4.27 Hz respectively. Taking these frequencies and dividing them by the driving frequency produces (probably) irrational numbers. If 0.4/21.9 and 4.27/21.9 were truly representing rational ratios, then we would know we have some sort of period doubling going on, which is similar to what was taking place in the pervious section with 8 and 9.8 Hz. But here the fraction is (seemingly) irrational, which means these frequencies arise on their own, and are independent of the driving frequency. This means there are three frequencies that are affecting the dynamic behavior of the cantilever beam. The slightly elevated spectrum near the frequency peaks suggests a narrow-band chaos. As such were classified this as chaos with 3-frequency quasi-periodicity [30].

The order of the subharmonic is 21.9/0.4 as well as 21.9/4.27 giving subharmonic orders of 54.75 and 5.129 respectively, which are similar to the subharmonic orders of region II in chapter 3.

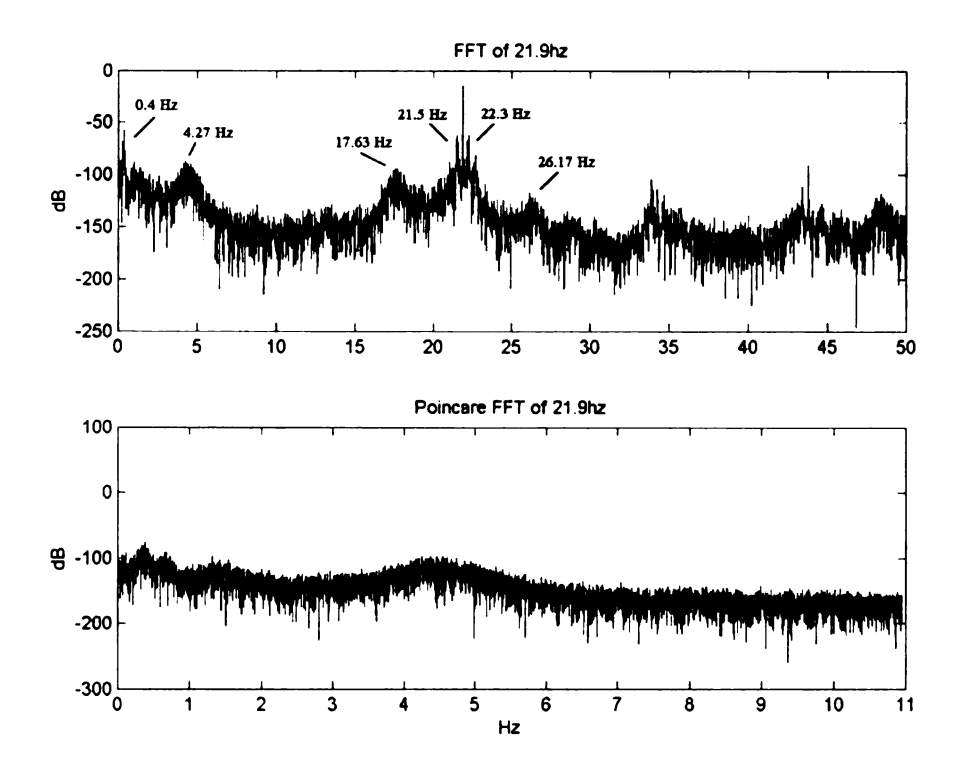


Figure 4.19: FFT and the Poincaré FFT of 21.9 Hz.

In Figure 4.20 there are several frequency peaks but only three of these peaks have a convincing affect on the driving frequency. It seems likely that the behavior that was noticed with 21.9 Hz is also appearing here. Figure 4.20 has a pair of frequencies that accompany the driving frequency on either side. These frequencies have distances from the driving frequency of 5.05 Hz in the first sub region and 4.83 in the second sub region. Once again the first peak on each FFT has a frequency that matches this difference. And similarly this frequency divided by the driving frequency yields an irrational number. The small peak to the right of 22.1 Hz occurs at a distance of 22.1

minus 2(10.5). The FFT is slightly raised. Adding the 10.5 Hz peak, we conclude that the dynamics is either very narrow-band chaotic or quasi-periodic with 3-frequencies, and that this structure occurs in both the sub intervals 1 and 2. Therefore we concluded that the behavior of the cantilever beam at 22.1 Hz can be classified as quasi-periodic or narrow band chaos with 3-frequency quasi-periodicity.

Highlighted in Figure 4.21 for the 27.3 Hz case are the frequencies that are paired to the driving frequency and their governing response frequency of 0.68 Hz. This subharmonic order is approximately 33. There is a broadband of the spectrum elevated above the noise level, suggesting chaos or stochasticity. Again the response frequency divided by the driving frequency yields (probably) an irrational number and we can conclude that the behavior of the cantilever beam at 22.3 Hz can be classified as chaos with 2-frequency quasi-periodicity and intermittency.

In summary, in Region *II* we see chaotic and quasi-periodic dynamics associated with either 3-frequency quasi-periodicity or 2-frequency quasi-periodicity with torus wrinkling and intermittency.

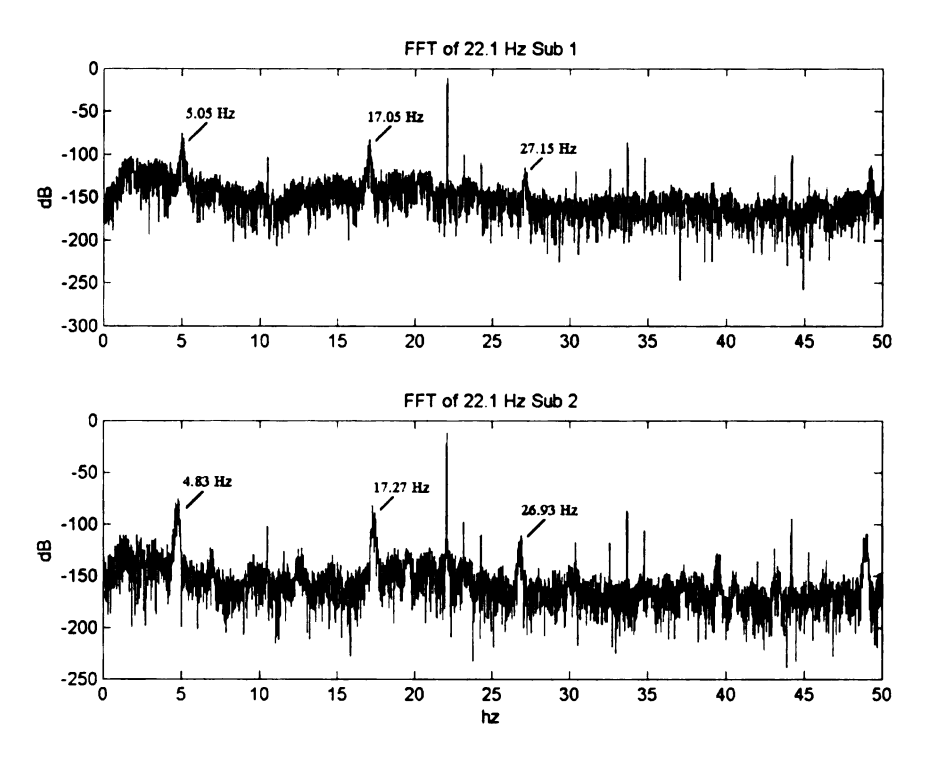


Figure 4.20: FFT of 22.1 Hz segments 1 & 2.

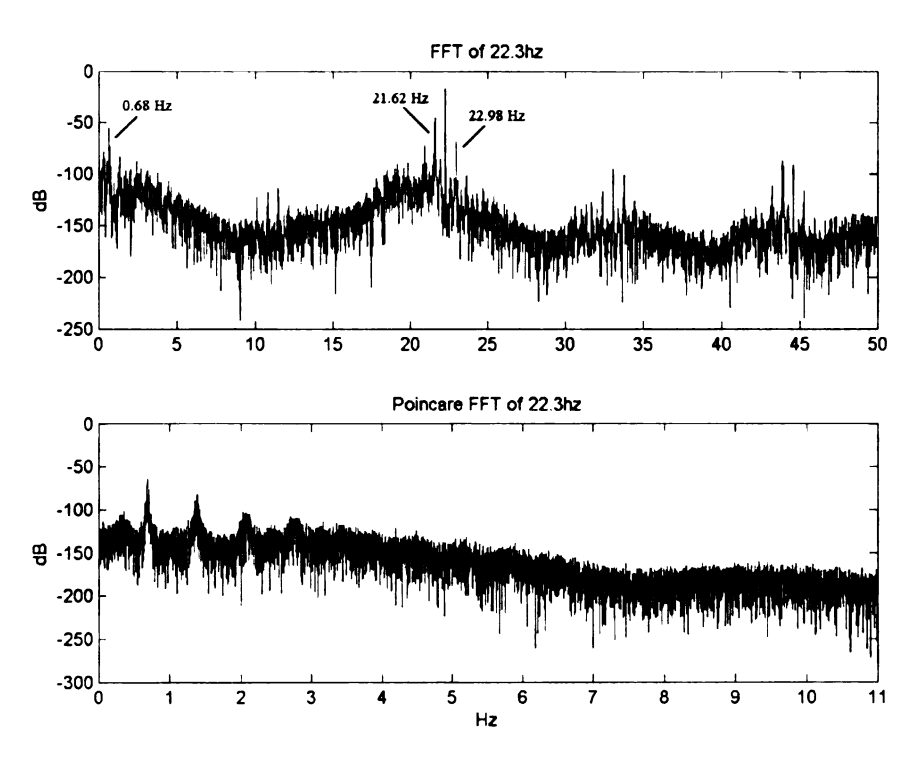


Figure 4.21: FFT and the Poincaré FFT of 22.3 Hz.

4.1.3 Region III & Hybrid (25.7 Hz)

Figure 4.22 displays the six graphs that show Poincaré section of the Poincaré section, in both delay and index from, at a frequency of 25.7 Hz and its sub divided regions which were picked form the obvious change in the response signal.

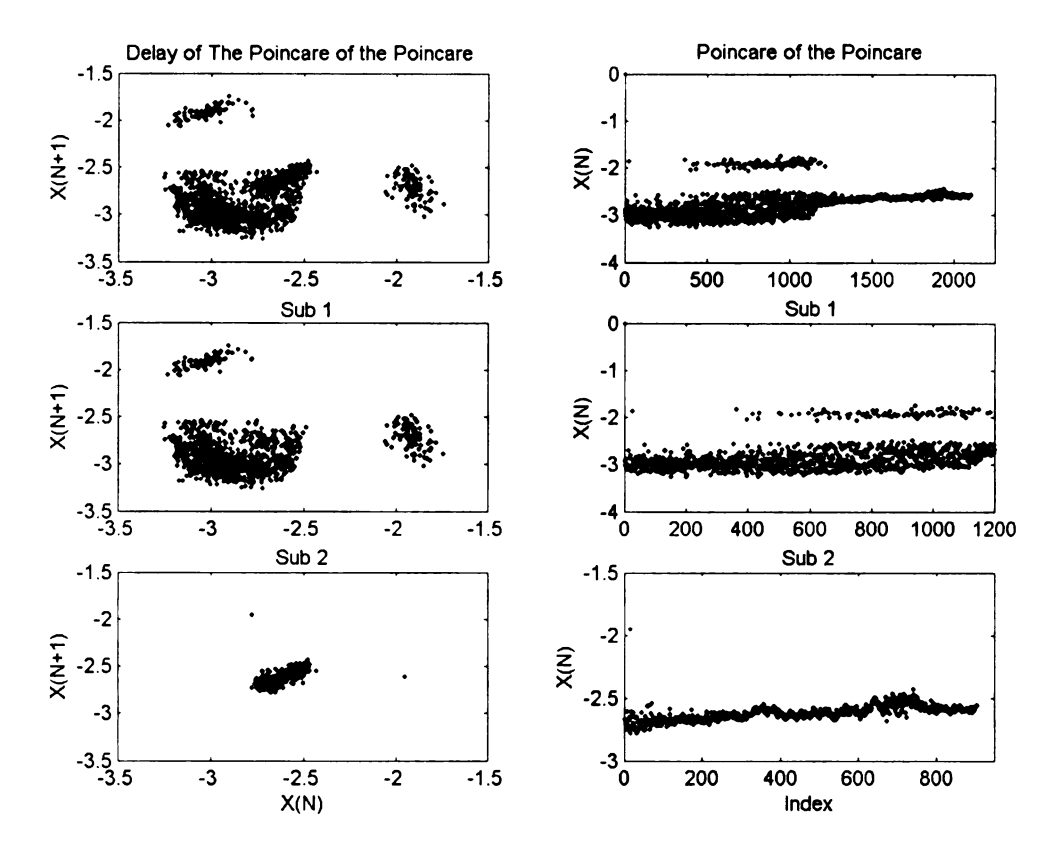


Figure 4.22: Poincaré section of the Poincaré section for 25.7 Hz and its two sub regions.

These graphs give valuable insight in to the behavior the cantilever beam. We can clearly see that there are two distinct responses going on in the first sub region. If we were to plot the Poincaré section in a delay map of just this region it would appear to be just a thick torus, that is presented in Figure 4.23, but after analyzing data from 45.6 Hz we can conclude that what is going on at 25.7 Hz is a fat torus shrinking to a thinner torus

		1
		ņ

as the dynamics changes. Section 4.2 will focus on this phenomena, is also showing the delay map of the 25.7 Hz Poincaré section.

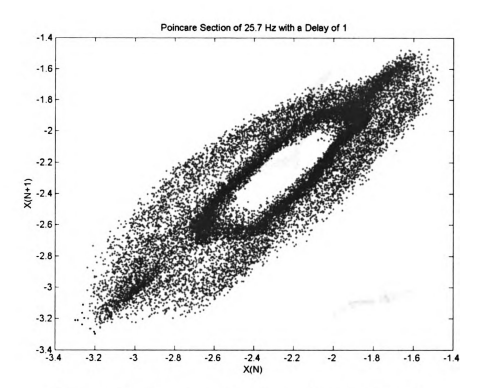


Figure 4.23: Delay map of the Poincaré section of 25.7 Hz.

The θ dynamics was taking with respect to each sub segment, which both have a common center, the x-bar is -2.3 and the y-bar is -2.3 on the Poincaré section delay map. The winding number was calculated to be -0.52297 rads/cyc (-0.0832 cyc/cyc) for the first segment and -0.55395 rads/cyc (-0.0882 cyc/cyc) for the second segment. Figure 4.24 and Figure 4.25 present the delayed θ dynamics plot and we can conform that the plot is in fact a torus governed by circle map dynamics. There is no strong indication of torus winkling (negative slope regions on the circle map), and hence the dynamics look quasi-periodic. However, the segment 1 plot has a "kink" in it, so maybe there is a very narrow banded chaos involved, maybe related to the fatness of torus. Once again if you

consider the diagonal line in the plots there are near tangencies at -2, -2 and 1,1. The near tangency of the torus angle return map to the diagonal indicated that intermittency plays a role in the quasi-periodic dynamics.

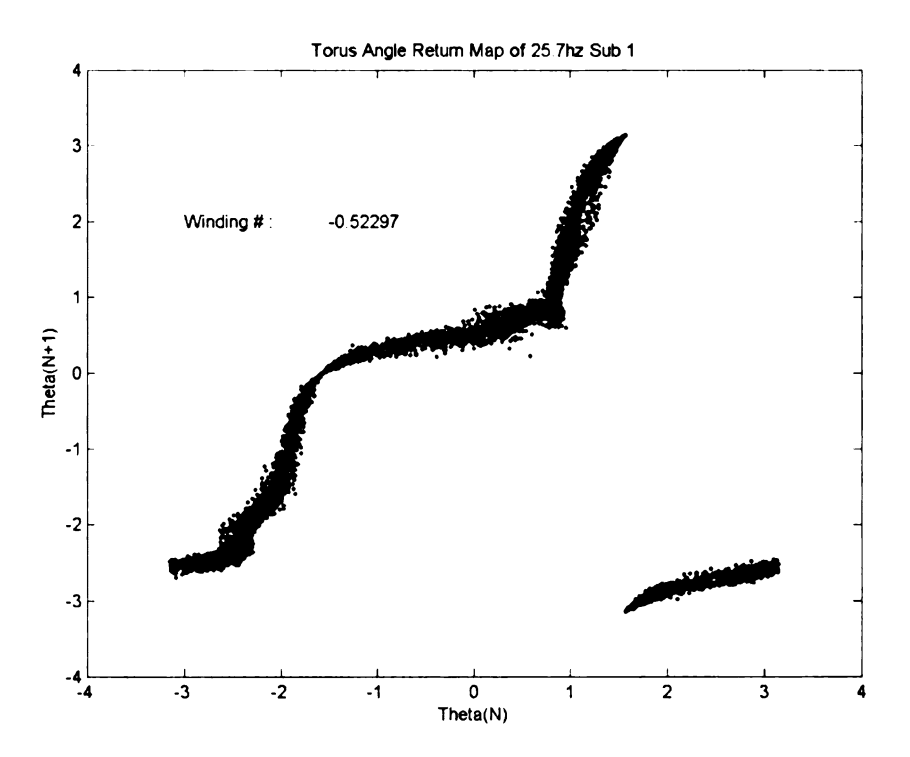


Figure 4.24: Torus angle dynamics at 25.7 Hz of sub 1.

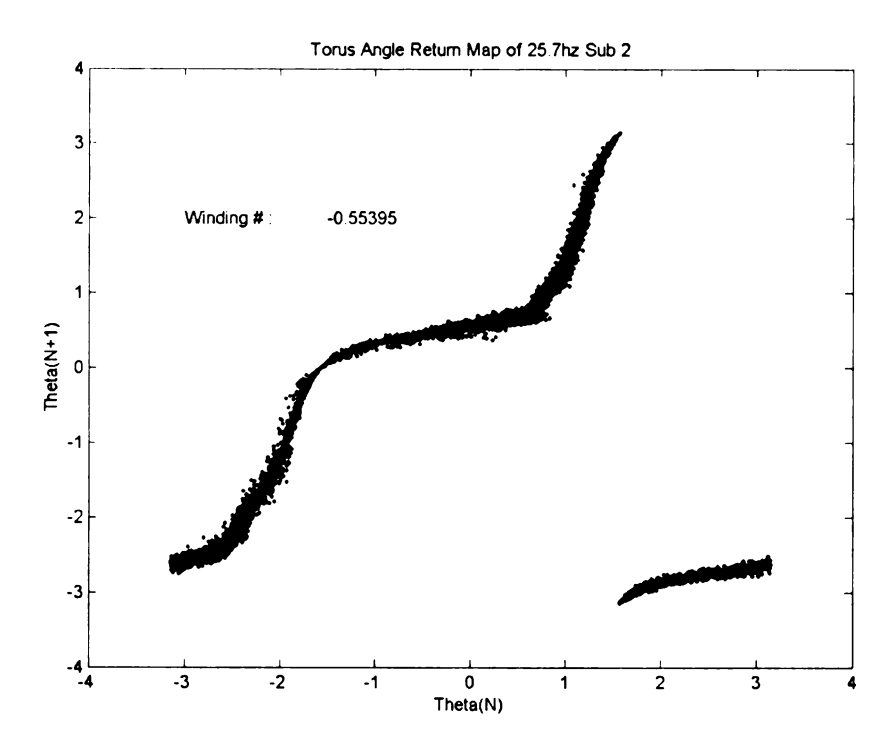


Figure 4.25: Torus angle dynamics at 25.7 Hz of sub 2.

To get an idea of the dimensionality at 25.7 Hz, the FNN and correlation dimension programs where run. Table 4.3 contains the FNN information. Refer to the Appendix, Figure A.6, to examine the correlation dimension information, which yields a correlation dimension of 2.4579.

	25.7 Hz		
Dimension	FFN	Percent	
First	23056	99.59%	
Second	11572	49.98%	
Third	1673	7.23%	
Fourth	89	0.38%	
Fifth	6	0.03%	
Sixth	0	0.00%	
Seventh	0	0.00%	
Eighth	0	0.00%	
Ninth	0	0.00%	

Table 2.3: FNN data of 25.7 Hz.

Figure 4.26 highlights the FFT frequencies that are paired to the driving frequency and the subharmonic response frequencies of 2.08 Hz in the first data segment and 2.37 Hz in the second data segment. In the second region the subharmonic frequency minus the driving frequency does not match up with the spike highlighted in the figure but is only off by 0.01 so this maybe because of frequency resolution effects and thus is treated as if it was at 23.33 Hz. Again the frequency divided by the driving frequency yields an irrational number and we can conclude that the behavior of the cantilever beam at 25.7 Hz can be classified as dominantly 2-frequency quasi-periodicity. Using the winding numbers given in the torus angle figures for both segments to estimate the subharmonic frequencies of each segment yields values of 2.139 Hz for the first segment and 2.266 Hz for the second segment. From the FFT it appears that these frequencies are the torus frequencies. These subharmonic frequencies yield a similar subharmonic order for region III of Chapter 3. Looking at the peak that is to the right of the driving frequency in Figure 4.27 it is interesting to note that the frequency is close to half the fundamental normal frequency of 47 Hz. Therefore the normal degree-of-freedom resonance that was noticed could have come about through this relationship.

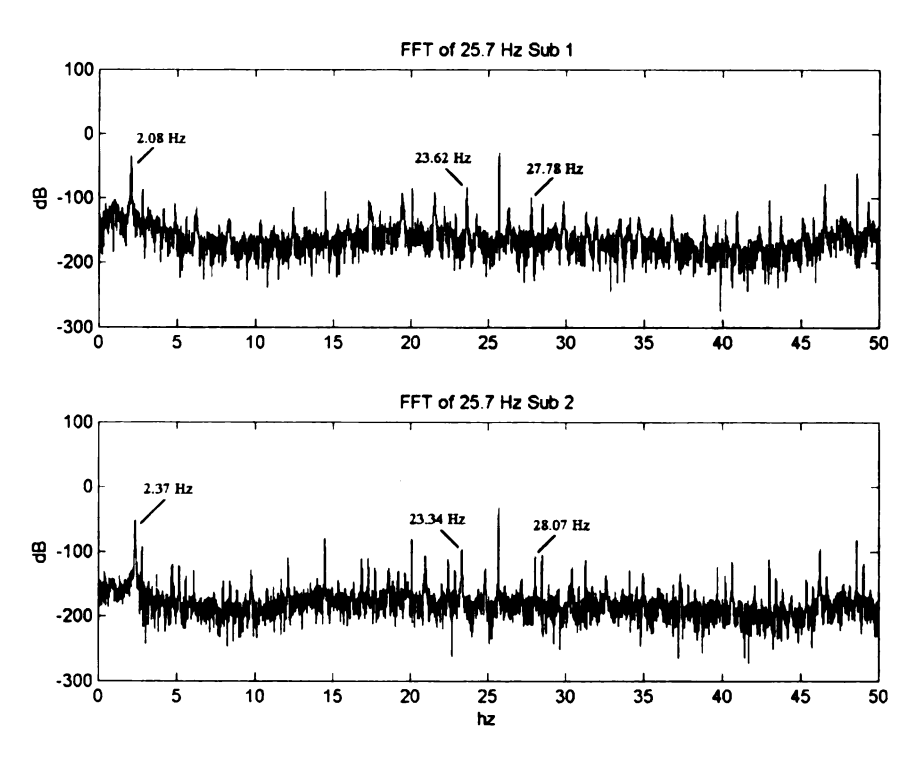


Figure 4.26: FFT of 22.1 Hz Sub 1 & Sub 2.

4.1.4 Region VI (43.8, 44.4, 45.2 & 45.6)

43.8, 44.4, 45.2 and 45.6 Hz were the forcing frequencies selected from region VI. The cantilever beam was then forced at the given frequency for an extended amount of time to allow it to settle into a steady state, after which the collection of data was started. Data was collected for 15 minutes at 45.2 Hz, for 30 minutes at 45.6 Hz, and for 40 minutes at 43.8 and 44.4 Hz. This time trace data was then imported into Matlab and the Poincaré section was taken. Unfortunately the data that was taken at 43.8 Hz was corrupted and was rendered useless. But the other frequencies of region VI revealed some of the most interesting dynamics yet.

Figure 4.27 shows the delay map of the Poincaré section at 44.4 Hz, which displays a very nicely defined torus. The Poincaré section of the Poincaré section was

not performed on this data because no new information could be gathered. Figure 4.28 shows the delay map of the Poincaré section at 45.2 Hz, which displays an unusually shaped torus. A delay of 5 was used to see this torus in its "optimal" form. Again the Poincaré section of the Poincaré section was not used because no new information could be obtained. Figure 4.29 shows the delay map of the Poincaré section at 45.6 Hz, which displays what appears to be some sort of doubled torus. A delay of 3 was use to see this torus in its optimal form. For this case the Poincaré section of the Poincaré section could come in handy to see the torus size variation in this response data. Refer to Section 4.2 for more on this phenomenon.

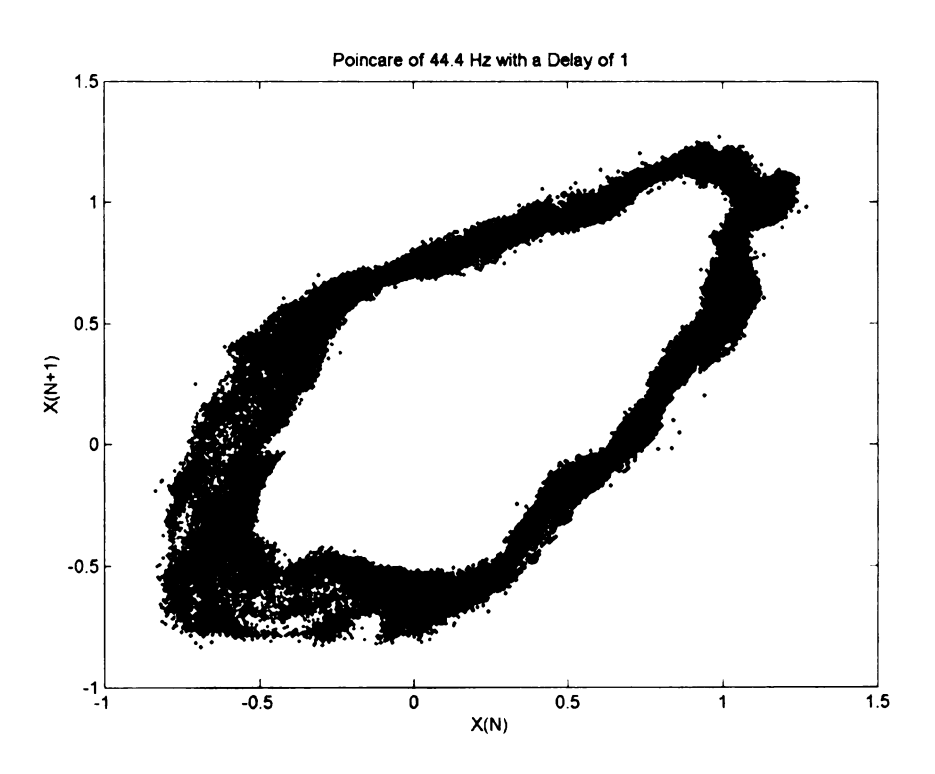


Figure 4.27: Poincaré section of 44.4 Hz with a delay of 1.

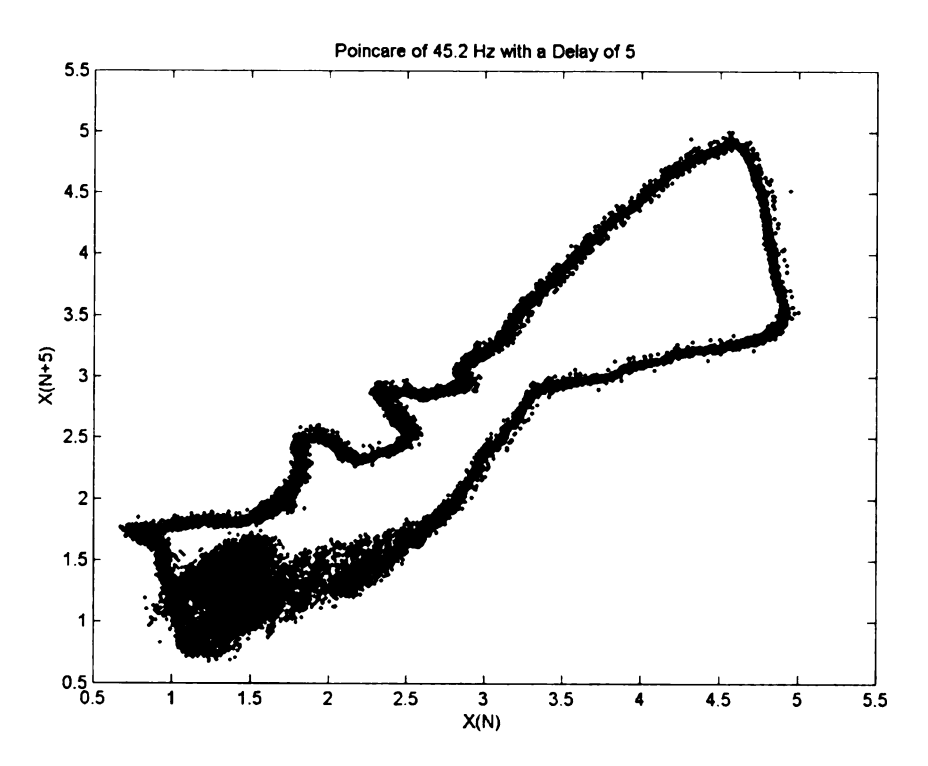


Figure 4.28: Poincaré section of 45.2 Hz with a delay of 5.

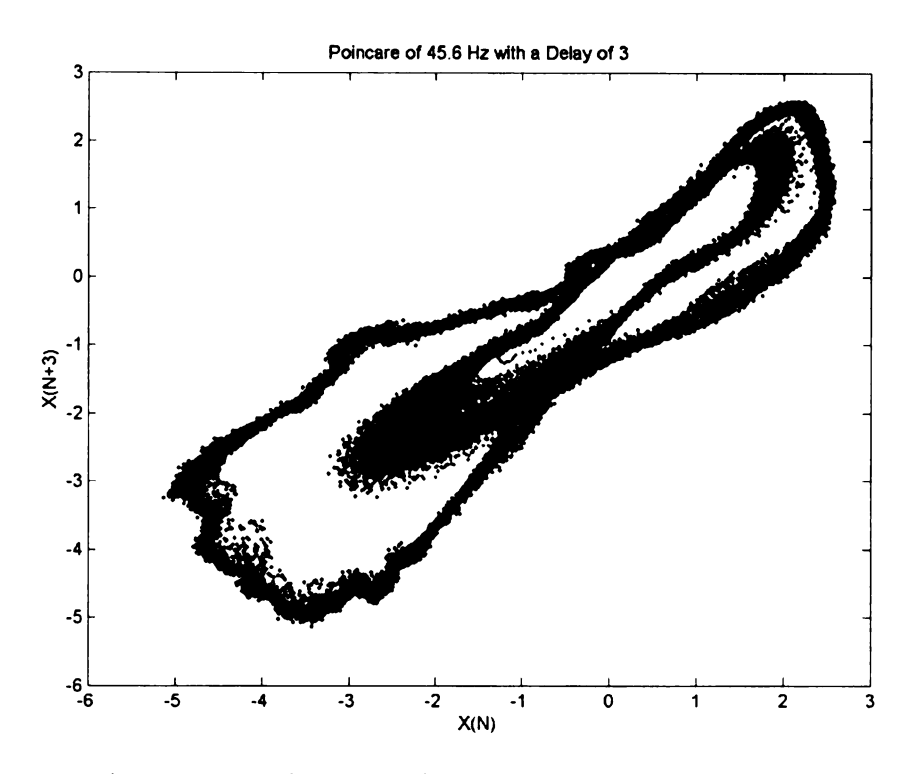


Figure 4.29: Poincaré section of 45.6 Hz with a delay of 3.

The torus angle return plots of 44.4, 45.2, and 45.6 Hz are Figure 4.30, Figure 4.31, and Figure 4.32 respectively, and give some insight into the structure of the tori. The winding numbers were -0.76796 rads/cyc (-0.1222 cyc/cyc) at 44.4 Hz, -0.10303 rads/cyc (-0.0164 cyc/cyc) at 45.2 Hz, and -0.090993 rads/cyc (-0.0145 cyc/cyc) at 45.6 Hz. No wrinkling is evident in the circle map at 44.4 Hz and hence the dynamics are dominantly quasi-periodic. The circle maps for 45.2 Hz and 45.6 Hz lie close to the diagonal, corresponding to the small winding numbers. If there is any wrinkling, as might be suspected from Figure 4.28, it is only on a very small scale in θ. Hence, the dynamics are dominantly quasi-periodic. Intermittency may play a role in the dynamics that take place at 44.4 Hz, but it is unlikely that intermittency is involved with the dynamics that take place at 45.2 and 45.6 Hz because in this case the torus return maps place the dynamic response along the diagonal for the entire time.

The doubled torus at 45.6 Hz is clear in the double circle map on θ . A single-valued circle map could be obtained by redefining the angle to cover two loops (4π radians) around the torus. A question may arise as to whether the data from 45.2 and 45.6 Hz surround a torus doubling bifurcation. This is addressed later. If torus doubling has occurred, it is accompanied by the doubling of the circle map in a higher dimensional manifold.

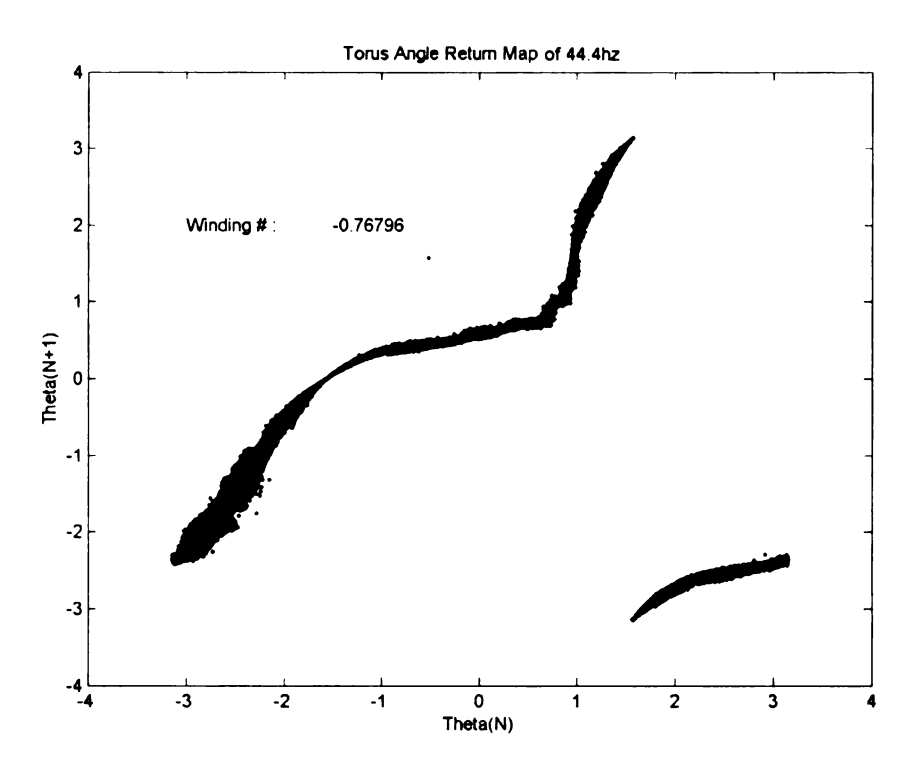


Figure 4.30: Torus angle dynamics of 44.4 Hz.

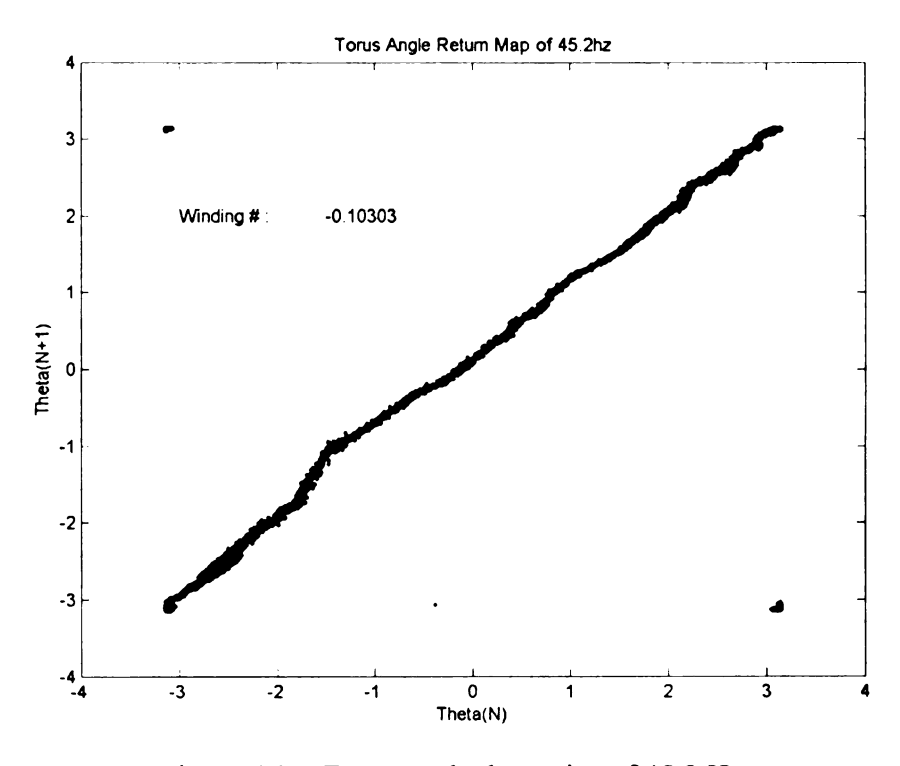


Figure 4.31: Torus angle dynamics of 45.2 Hz.

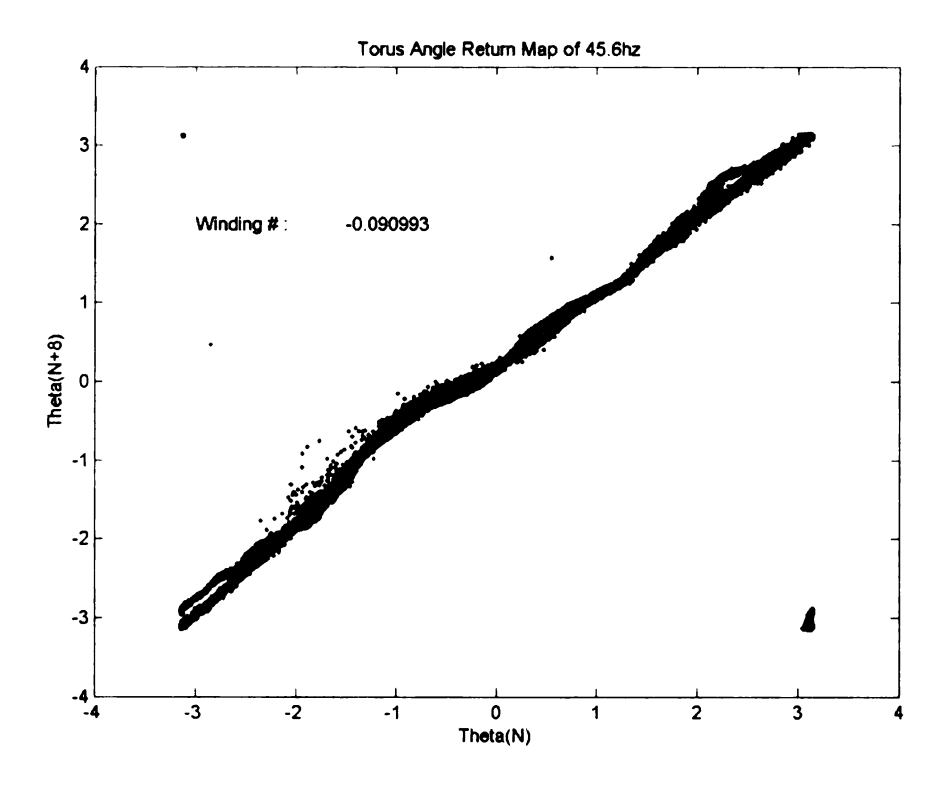


Figure 4.32: Torus angle dynamics of 45.6 Hz.

To get an idea of the dimensions of dynamics at 44.4, 45.2, and 45.6 Hz, the FNN and correlation dimension programs where run. Table 4.3 contains the FNN information. Refer to the Appendix, Figure A.6, to examine the correlation dimension information. The correlation dimensions are 3.5714 at 44.4 Hz, 2.8328 at 45.2 Hz, and 2.9595 at 45.6 Hz.

	44.4 Hz		45.2 Hz		45.6 Hz	
Dimension	FFN	Percent	FFN	Percent	FNN	Percent
First	107159	99.54%	40139	98.58%	109221	99.57%
Second	68768	63.88%	16755	41.15%	45828	41.78%
Third	14677	13.63%	2725	6.69%	6974	6.36%
Fourth	1848	1.72%	402	0.99%	977	0.89%
Fifth	180	0.17%	85	0.21%	213	0.19%
Sixth	9	0.01%	23	0.06%	48	0.04%
Seventh	0	0.00%	6	0.01%	22	0.02%
Eighth	0	0.00%	0	0.00%	0	0.00%
Ninth	0	0.00%	0	0.00%	0	0.00%

Table 4.4: FNN data of 44.4, 45.2, and 45.6 Hz.

The FNNs yield information about how many delay cords are needed to describe the *data*, not the bifurcation. A torus doubling bifurcation requires at least a four-dimensional phase space.

Figure 4.33 to Figure 4.35 give the FFT and the FFT of the Poincaré section at 44.4, 45.2, and 45.6 respectively. The FFT of 44.4 Hz displays a similar reponse to the frequencies in region *II*. In this case the subharmonic frequency is 5.32 Hz, which complements the driving frequency at 39.08 and 49.72 Hz. This informs us that once again we are dealing with 2-frequency quasi-periodicity. We were unable to find a correlation between the other spikes, which can be seen in the FFT, and the driving frequency. But these are of relatively low order, and are likely to be associated with the torus being slightly fat. By multiplying the winding number in cycles per cycles by the driving frequency of 44.4 Hz the result is 5.423 Hz is close to the subharmonic frequency spike at 5.32 Hz and thus the yields that the torus frequency. (If examined closely one will notice a peak right up against the Y-axis, at a frequency of 0.4 Hz. Notice that there are similar peaks on either side of the driving frequency peak. If these were judged as significant, we could classify the response behavior to be 3-frequency quasi-periodic). The subharmonic order of 8.3 matches well with Chapter 3.

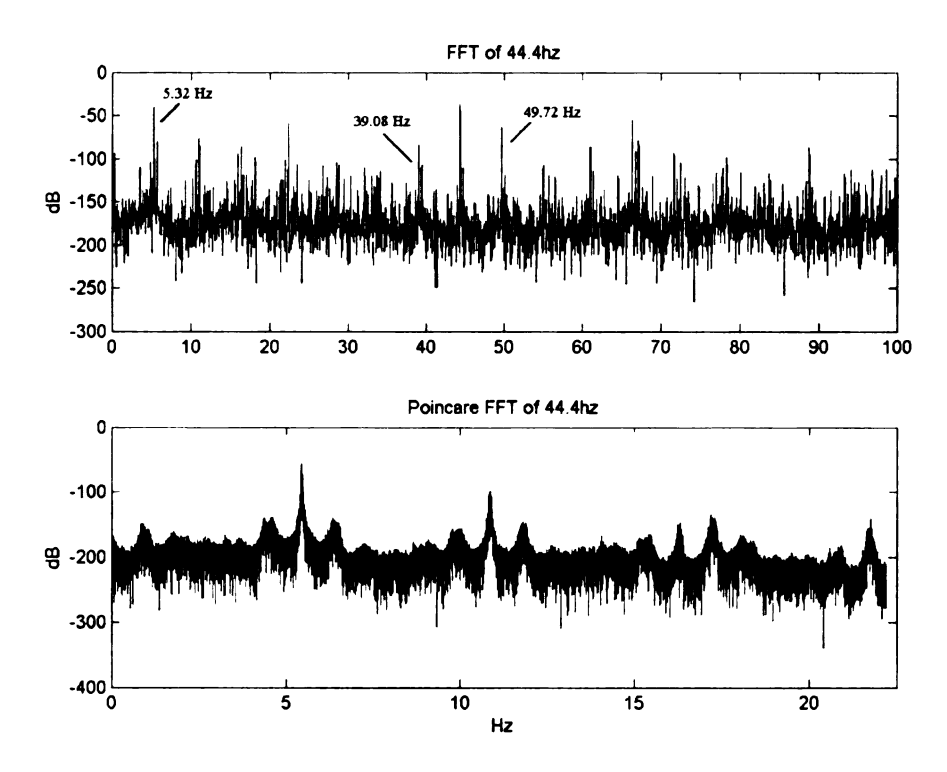


Figure 4.33: FFT and the Poincaré FFT of 44.4 Hz.

The FFT of 45.2 Hz held some very interesting subharmonics. The many spikes that can be see Figure 4.34 possess a pattern that that follows: 0.44, 0.9, 1.34, 1.8, 2.24, 2.68, 3.14, 3.58, 4.04, 4.48, 4.92,..., etc. It may be easier to see the pattern like this: 0, 1, 0, 1, 0, 0, 1, 0, 1, 0, 0, 1, ..., etc. where 0 represents an addition of 0.44 Hz to the pervious frequency and 1 represents adding 0.46 Hz to the previous frequency. This pattern continues though out the entire FFT; 0, 1, 0, 1, 0 back to 0, 1, 0, 1, 0 and again, and again, and again. The combination of these frequencies eventually adds up to the driving frequency of 45.2 Hz. This interesting pattern is probably due to the frequency resolution, which is mentioned in Chapter 3. So, this behavior appears to be a case where there are two predominant frequencies with the subharmonic occurring on the order of about 100. This order matches with region VI in Chapter 3. The dynamics corresponds to 2-frequency quasi-periodicity.

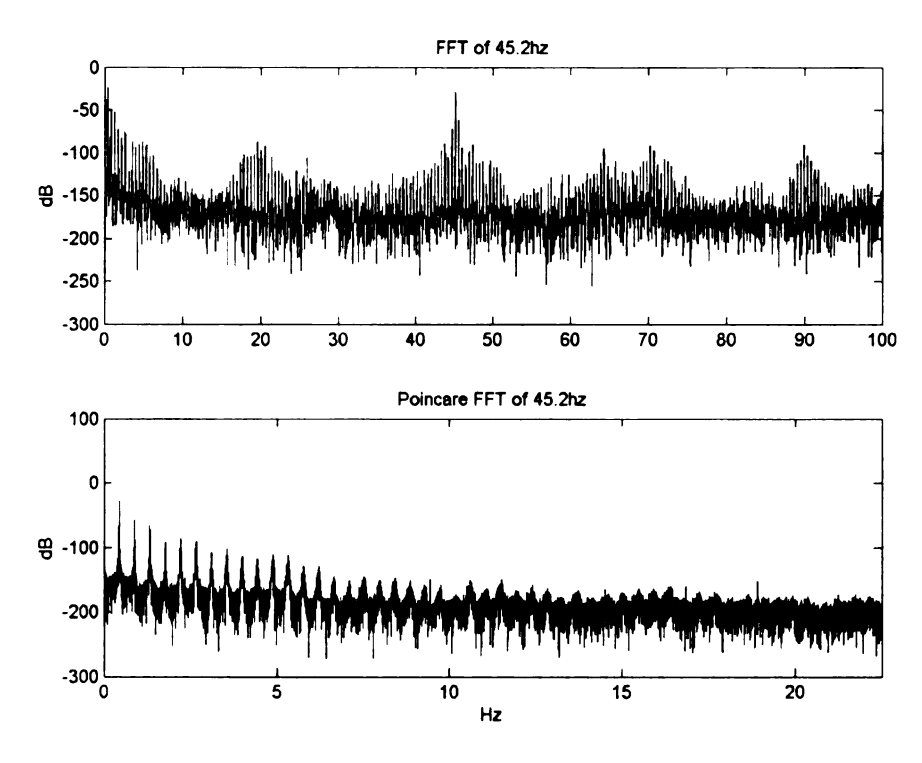


Figure 4.34: FFT and the Poincaré FFT of 45.2 Hz.

The FFT of 45.6 Hz, displayed in Figure 4.35, has a similar behavior to the 45.2 Hz case, in that the subharmonic is extremely dominant. In this case, the subharmonic frequency of 0.6 Hz is associated with the main torus, and the winding number. The 0.3 Hz is then a subharmonic resonance of the 0.6 Hz component, associated with torus doubling. This subharmonic is at an order of 152 with respect to the excitation! The dynamics are classified as 2-frequency quasi-periodic with torus doubling. The winding number of -0.0145 cyc/cyc matches well with the subharmonic of order 76, which corresponds to the main (undoubled) torus.

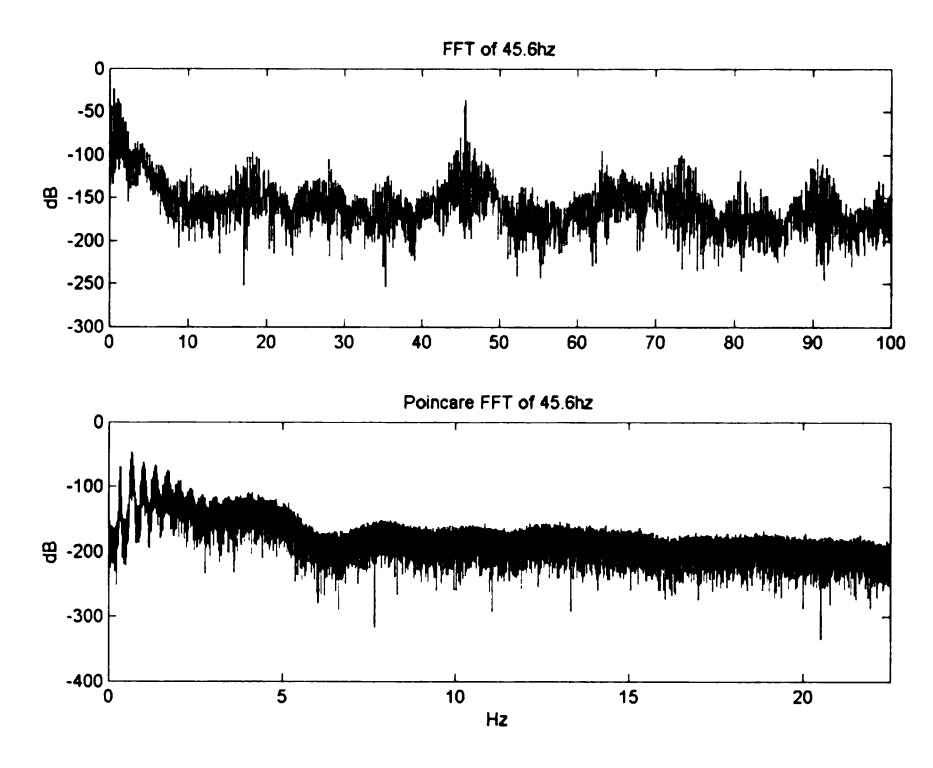


Figure 4.35: FFT and the Poincaré FFT of 45.6 Hz.

4.1.5 Analysis of **37.9** Hz

The behavior of the cantilever beam when it was forced at 37.9 Hz was unlike anything that has been presented thus far. In fact the beam did not really "do" anything; the cantilever was stationary and it appeared that nothing was going on. What caught our attention was that during the frequency sweeps it was noticed that the response strain gage signal became what appeared to be a triangle wave accompanied by an audible ring coming from the beam. Figure 4.36 presents the FFT and a sample of the time trace response signal. The first peak is the driving frequency; this peak is followed by a peak at double the driving frequency and then a peak at triple the drive frequency and so forth and so on; even the 10th and 11th harmonics are significant. This would then be a superharmonic resonance. The response of the cantilever beam in Matlab does not really

appear do be a triangle wave. This may be do to the way the GxView and TEAC interpretation of the response data, or the response could be a bit different than during the frequency sweeps.

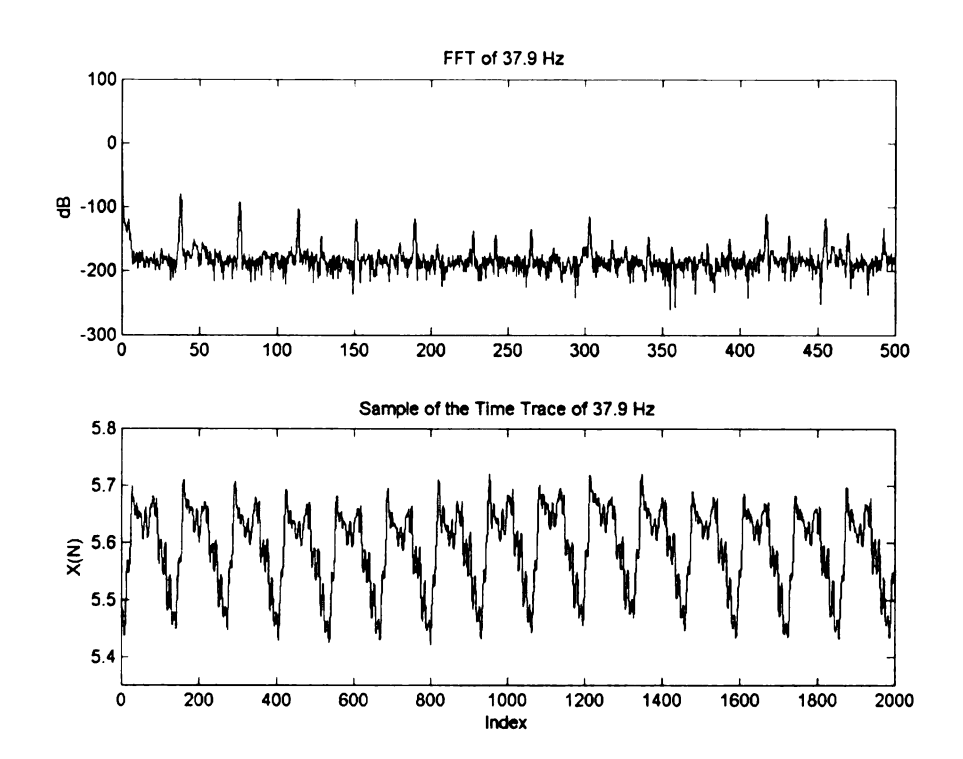


Figure 4.36: The FFT and sample time trace of 37.9 Hz.

4.2 Torus Doubling

Figure 4.37 shows the Poincaré section of the Poincaré section plotted against its index of 45.6 Hz, and present what appears to be four torus cycles. Indeed the top two infrequent toroidal crossings are due to a warping of the torus in higher dimensions, and are not indicative of data circumnavigating the torus. But viewing the torus doubling in Figure 4.26 we can see that there is definitely a double torus involved in the behavior of the cantilever beam's response.

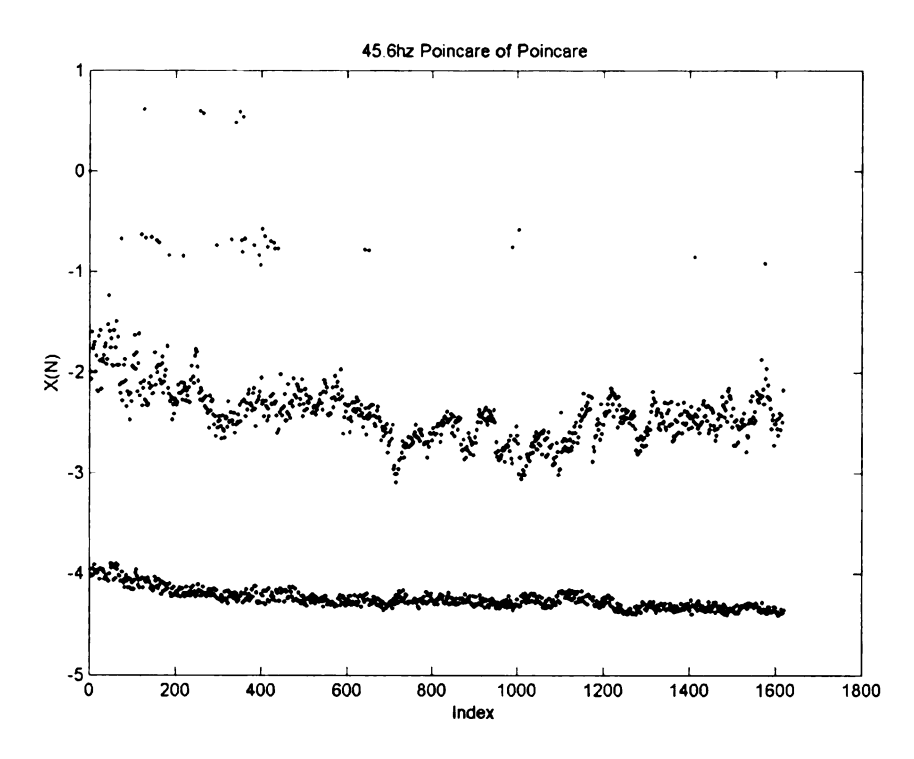


Figure 4.37: Poincaré section of the Poincaré section of 45.6 Hz plotted against its index.

This torus warping phenomenon has appeared in two of our cases, at 25.7 and 45.6 Hz. The case at 25.7 Hz was a little weird because the torus was not really visible, but after viewing the Poincaré section of the Poincaré section in both the delay maps and against its index (Figure 4.22), what at first glimpse looks like torus doubling turned out to really be torus warping. In Figure 4.38 we present samples of short data records at various frequencies in Poincaré section delay maps. This data was taken in the given order: starting at 46 Hz we swept down slowly to 45.84 Hz where the torus doubling phenomena began. Notice that there are two cases at 45.84 Hz. In the first one case there is no indication of a torus doubling, while a little will later data was taken at that same frequency and the torus doubling had become active and as the frequency was increased again, the doubled torus disappeared. Figure 4.38 is interesting to see because it gives a visual idea of how torus doubling becomes active as well as how it becomes dormant.

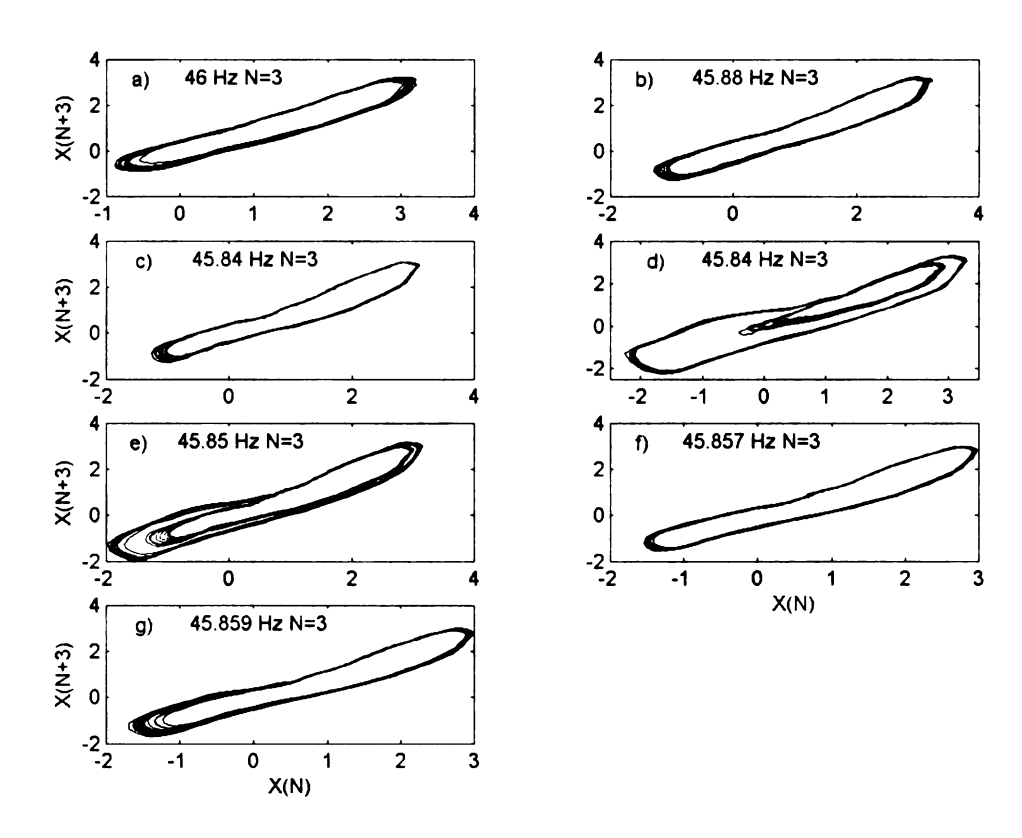


Figure 4.38: Example of torus doubling with increasing excitation frequency.

Chapter 5

Conclusion

This thesis has given a better understanding into the dynamic behavior of a cantilever beam undergoing friction forced excitation at its tip. From the frequency sweep stand point we were able to see regions in which active dynamics were taking place. Dynamics in these regions were then investigated more closely by examining the cantilever beam behavior at specified frequencies.

In region *I*, the two frequencies chosen were 8 and 9.8 Hz. These frequencies induced the beam to behave with the desired dynamics. Upon examination it was found that the subharmonic frequencies of 8 and 9.8 Hz approximately matched the subharmonic order of region *I*. It was also determined that the cantilever beam was probably behaving due to the effects of period doubling.

In region *II*, three frequencies were chosen to inspect the characteristics of the cantilever beam. These frequencies were 21.9, 22.1, and 22.3 Hz. Each one of these frequencies presented its unique behavior. In the case of 21.9 Hz, the inspection of the strain gage data yielded a system which behaved something like coupled tori, with one of the tori fat and the other skinny. As it turned out, at a driving frequency of 21.9 Hz the system had two independent subharmonic frequencies, which meant there were three frequencies that affected the dynamic behavior of the cantilever beam. This behavior was classified as chaos arising from 3-frequency quasi-periodicity. Also the subharmonic order approximately matched the subharmonic order of region *II* in chapter 3. The lowest frequency was 54.75 times smaller than the driving frequency.

In the case of 22.1 Hz, the examination indicated that there were two different dynamic time segments. How this change in the dynamics took place can only be speculated, but it most likely came about because of small changes in the parameters. By splitting up the dynamic segment we were able to see the different types of dynamic response that arose. The main difference between the two segments was that the second segment produced a better-defined torus; the first segment appeared to be a cloud like torus with one edge relatively well defined and the other scattered. The subharmonic frequency of the system excited at 22.1 Hz in both segments yielded the same basic response, which was classified as quasi-periodic or narrow band chaos with 3-frequency quasi-periodicity. Once again the subharmonic frequency gave way to a subharmonic order the resembled that of region *II* in chapter 3.

In the final case in region *II*, the driving frequency of 22.3 Hz produced a dynamic response that appeared to be on the brink of chaos by torus wrinkling. This was interpreted from the fact that the torus angle return map, Figure 4.16, had a nearly zero-slope region. The FFT in Figure 4.19 implies that the dynamic behavior had the same basic type of response as the 22.1 Hz case and thus was classified as chaos with 2-frequency quasi-periodicity. Plus, the subharmonic frequency yielded a subharmonic order of about 33, which was equivalent to that of region *II* in chapter 3.

Region III and the Hybrid region shared the next frequency of interest of 25.7 Hz.

Once again the strain gage data was divided into two segments after it was noticed that the response changed significantly. In the first segment it appeared that the dynamic response was due to a fat torus shrinking into a thinner torus. The subharmonic frequencies for both segments allowed us to classify the systems behavior as dominantly

2-frequency quasi-periodicity. These subharmonic frequencies gave way to a subharmonic order (around 12 for the first segment of data) that resembled those in region *III* of chapter 3.

In region VI, four frequencies were selected to investigate the dynamic properties of the cantilever beam they were: 43.8, 44.4, 45.2, and 45.6 Hz. The data taken at 43.8 Hz was corrupted and was rendered useless. But data from the other frequencies data revealed some of the most interesting results. In the case of 44.4 Hz, the dynamics were determined to be dominantly quasi-periodic.

In the case of 45.2 Hz, the small winding number and proximity to the diagonal in the torus angle return map, suggested that there might be some torus wrinkling, but it was only on a very small scale in the torus angle, and thus the dynamics were considered to be dominantly quasi-periodic. The subharmonic order in this case was on the order of about 100, which resembled the subharmonic order seen in the sweeps of region VI sub 2.

In the case of 45.6 Hz, there was what would appear to be a perfect example of torus doubling. By examining the FFT of the strain gage response and the winding number a connection between the two became apparent. The main torus was associated the winding number with a subharmonic order of 75, and the other subharmonic frequency (order of 150) was associated with the torus doubling.

The normal fundamental frequency became a factor in the response of region VI.

The pattern that the response created was similar to that of the hybrid region but involved a larger response order. It was deduced that the hybrid region response was because of the affect of superharmonic resonance of order 2. The fundamental normal frequency was a 47 Hz, the hybrid region lies close to 47/2 Hz.

The last frequency that was examined was not part of any regions that were defined in chapter 3. The frequency was 37.9 Hz and it was interesting because the response signal appeared to be a triangle wave and an audible ring came from the beam. The FFT yield information that showed that the superharmonic resonances are an important part of the behavior of the beam.

The extremely low-frequency responses (observed with subharmonic orders of 33, 54, 100, and even 150) were note worthy. They tended to occur in the range of 0.4 to 0.7 Hz. These frequencies are well below the 2.5 Hz fundamental frequency of the beam. As such, this beam phenomenon differs from the high-to-low frequency modal energy cascade documented in the literature. In two parameter regimes, the extreme subharmonic order was seen to vary continuously, typically incommensurately with the excitation frequency, yielding quasi-periodic behavior on tori. This differs from frequency demultiplication, observed by Van der Pol and Van der Mark [13], which occurs at fixed, pure subharmonics, and then bifurcates. The low frequencies are not the result of beating as the FFTs indicate the low frequency spikes to be independent ones.

Although is project was not directly tied to any specific engineering problem, it does have valuable information about the response behaviors of a system that is undergoing non-linear friction forced excitation. Two of the fundamental frequencies (2.5 Hz unload and 13.5 Hz load) did not even have an effect the cantilever beam. And cases where linear modeling would say that nothing should happen; chaos and or quasiperiodic responses became apparent. This reaffirms the idea that non-linearities can not be taken lightly and are extremely important if one is to fully understand and appreciate the dynamics of a given system.

Some future work can be done to mathematically model the dynamic response of this system. I would suggest finding the equations of motion for the cantilever beam using Newtonian and Lagrangian methods; it might also be helpful to use finite element method as well. The normal degree of freedom was seen to be active in some of the responses. It might be necessary to include contact compliance in the friction law, as it was observed in earlier friction measurements [1]. The experiment has a displacement-dependent normal load, due to the tilt in the beam fixture, influencing the friction. As the FNN studies indicated four to six delay coordinates needed in the reconstructed Poincaré sections, a low order model may need two transverse (bending) beam modes, plus the normal degree of freedom. Using the reduced equations of motion, a simulation that mimics the parameters in the experiment can be run, and the simulation response data can be compared with the experimental data.

Appendix

This appendix contains figures that deal with the fixed frequency examination. These figures are of interest, but were not placed in Chapter 4 to allow for an easier read.

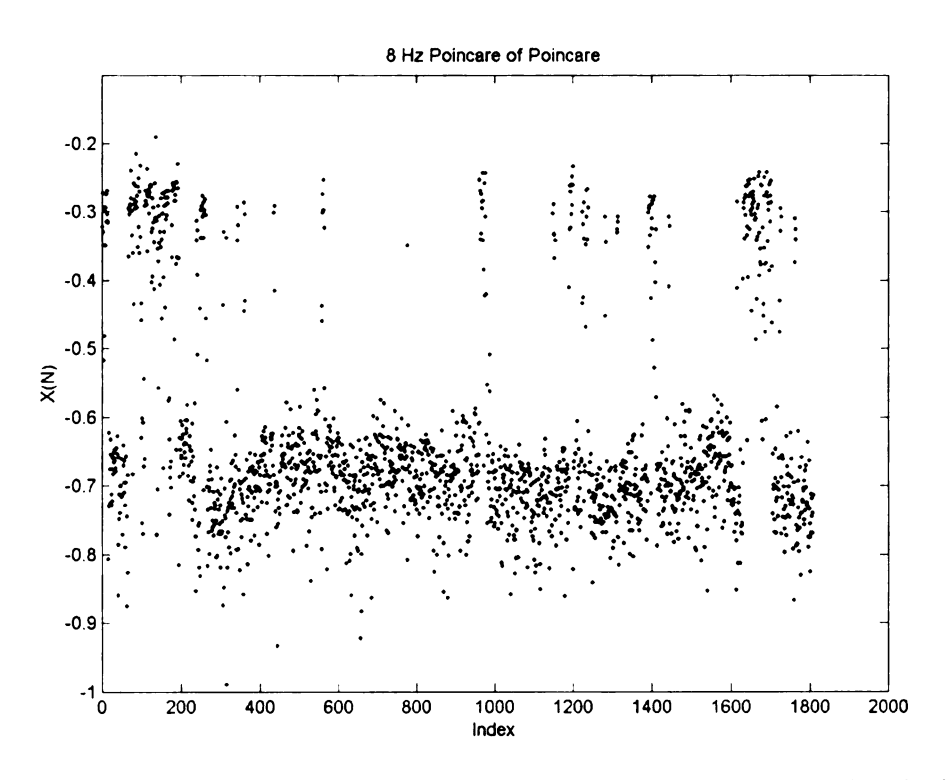


Figure A.1: Poincaré section of the Poincaré section of 8 Hz plotted against its index.

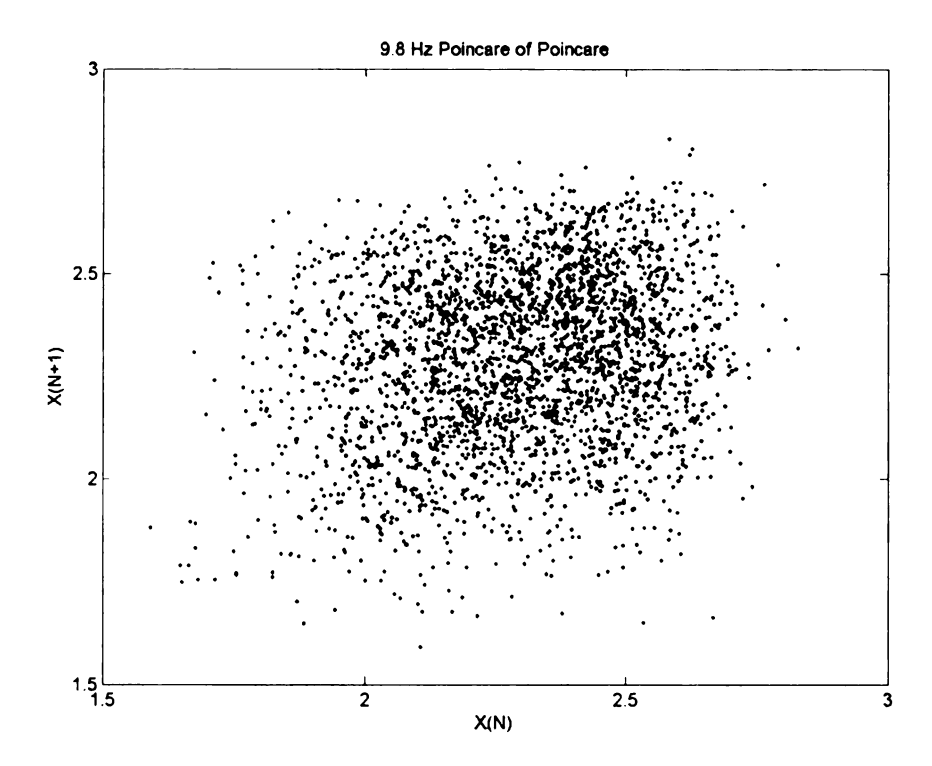


Figure A.2: Poincaré section of the Poincaré section delay map of 9.8 Hz.

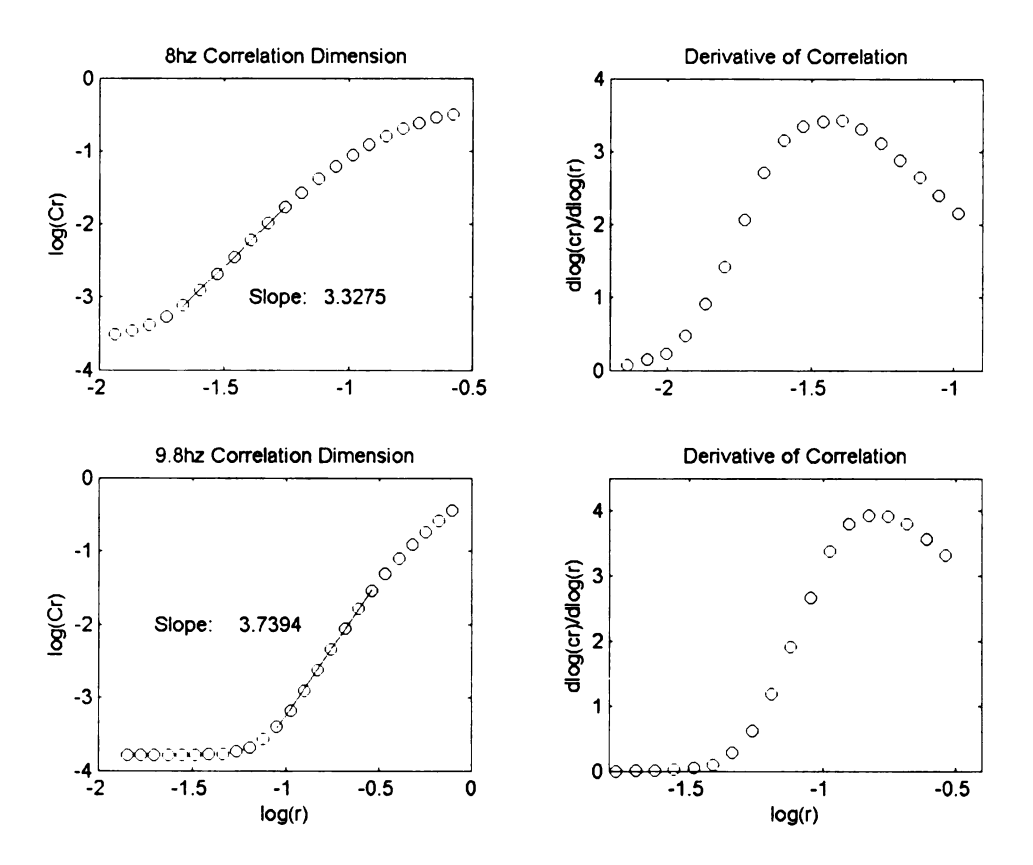


Figure A.3: Correlation dimension and derivative of 8 and 9.8 Hz.

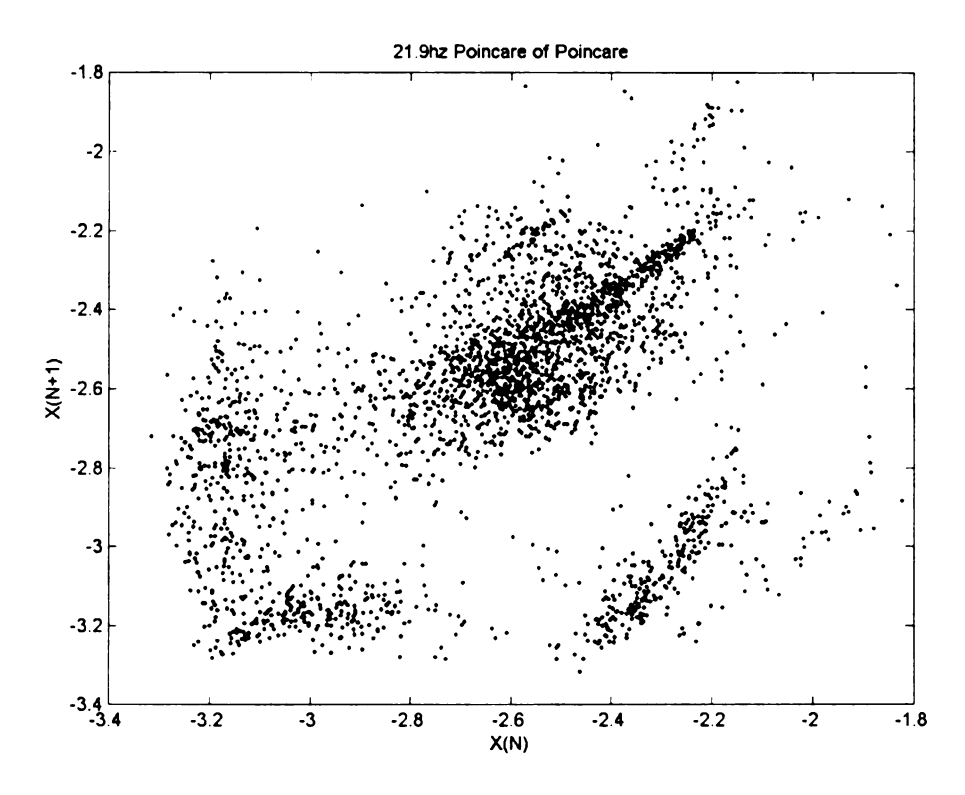


Figure A.4: Delay Map of the Poincaré section of the Poincaré section of 21.9 Hz with Delay of 1.

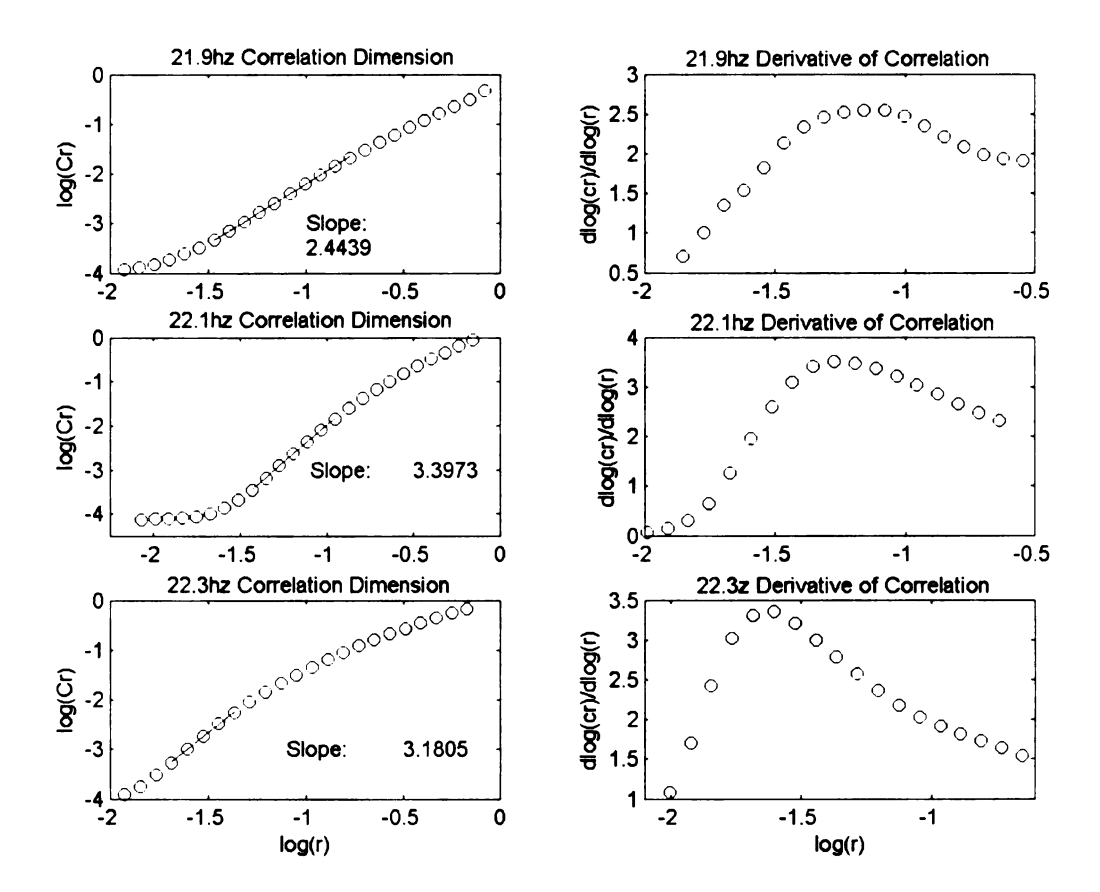


Figure A.5: Correlation number and their derivatives vs. log(r) for 21.9, 22.1 and 22.3 Hz.

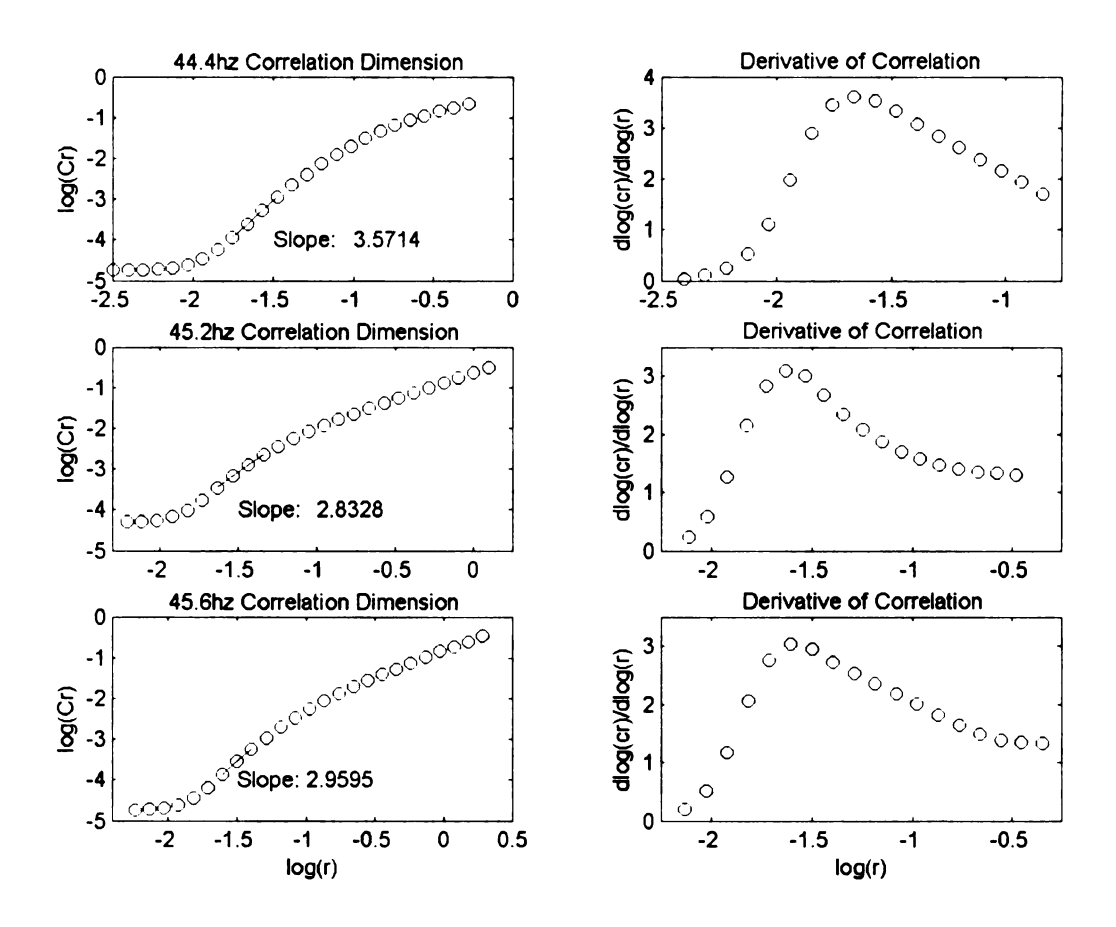


Figure A.6: Correlation number and their derivative vs. log(r) for 44.4, 45.2 and 45.6 Hz.

BIBLIOGRAPHY

- [1] Ramana Kappagantu V. An "Optimal" Modal Reduction of Systems with Frictional Excitation. Ph.D. thesis, Mechanical Engineering, Michigan State University, 1997.
- [2] A. G. Haddow and S. M. Hasan. Nonlinear Oscillation of a Flexible Cantilever: Experimental Results. Abstract from Non-Linear Vibrations, Stability, and Dynamics of Structures and Mechanisms Conference. Blacksburg, VA June 1-3, 1988.
- [3] S. A. Nayfeh and A. H. Nayfeh. Nonlinear Interactions Between Two Widely Spaced Modes External Excitation. *International Journal of Bifurcation and Chaos*. 3(2): 417-427, 1993.
- [4] S. A. Nayfeh and A. H. Nayfeh. Energy-Transfer from High-Frequency to Low-Frequency Modes in a Flexible Structure via Modulation. *Journal of Vibration and Acoustics*. 116(2): 203-207, 1994.
- [5] A. H. Nayfeh and D. T. Mook. Energy-Transfer from High-Frequency to Low-Frequency Modes in Structures. *Journal of Mechanical design*. 117:186-195 Sp. Iss. B, 1995.
- [6] Ali H. Nayfeh and Char-Ming Chin. Nonlinear Interaction in a Parametrically Excited System with Widely Spaced Frequencies. *Nonlinear Dynamics*, 7:195-216, 1995.
- [7] K. Oh and Ali H. Nayfeh. Nonlinear Combination Resonances in Cantilever Composite Plates. *Nonlinear Dynamics*, 11:143-169, 1996.
- [8] K. Oh and A. H. Nayfeh. High- to low-frequency modal interactions in a cantilever composite plate. *Journal of Vibration and Acoustics*, 120(2): 579-587, 1998.
- [9] T. J. Anderson, A. H. Nayfeh, and B. Balachandran. Coupling between High-Frequency Modes and a Low-frequency Mode: Theory and Experiment. *Nonlinear Dynamics*, 11:17-36, 1996.
- [10] A. H. Nayfeh and D. T. Mook. *Nonlinear Oscillations*. John Wiley, New York, 1979.

- [11] M. Qriouet and C. Mira. Fractional Harmonic Synchronization in the Duffing-Rayleigh Differential Equation. *International Journal of Bifurcation and Chaos in Applied Sciences and Engineering*, 4(2):411-426, 1994.
- [12] K. Yagasaki. Higher-Order Averaging and Ultra-Subharmonics in Forced Oscillators. *Journal of Sound and Vibration*, 210(4):529-553, 1998.
- [13] Balth. Van Der Pol and J. Van Der Mark. Frequency Demultiplication. *Nature*, 120: 363-364, 1927.
- [14] N. N. Minorsky. *Nonlinear Oscillations*. Princeton, NJ: Van Nostrand, chapter 24, 1962.
- [15] J. J. Stoker. Nonlinear Vibrations in Mechanical and Electrical Systems. New York: Interscience Publishers, 1950.
- [16] G. Zames and N. A. Schneydor. *Dither in Nonlinear Systems*. IEEE Transaction on Automatic Control. 21: 660-667, 1976.
- [17] B.F. Feeny and F.C. Moon. Quenching Stick-Slip chaos with Dither. *Journal of Sound and Vibration*, 237(1): 173-180, 2000.
- [18] E. C. Miranda and J. J. Thomsen. Vibration Induced Sliding: Theory and Experiment for a Beam with a Spring-Loaded Mass. *Nonlinear Dynamics*, 16:167-186, 1998
- [19] Z. L. Zhang and Q. T. Tao. Experimental Study of Non-Linear Vibrations in a Loudspeaker Cone. *Journal of Sound and Vibration*, 248(1):1-8, 2001.
- [20] B. Feeny. Nonlinear Dynamics of Stick-Slip Oscillators. Aerospace Stuctures: Nonlinear Dynamics and System Response. AD-Vol. 33, 23-33, 1993.
- [21] S.W. Shaw. On the Dynamic Response of a System with Dry Friction. *Journal of Sound and Vibration*. 108(2): 305-325, 1986.
- [22] A. Guran, F. Pfeiffer, and K. Popp. Dynamics with Friction Modeling, Analysis and Experiment Part I. World Scientific Publishing Co Pte Ltd, Singapore, 1996.
- [23] R. A. Ibrahim. Friction-Induced Vibration, Chatter, Squeal, and Chaos: Part I & II

 Mechanics of Friction. In *Friction-Induced Vibration, Chatter, Squeal and Chaos*, volume DE-49, 107-138, 1992.
- [24] B. Armstrong-Hélouvry, P. Dupont, and C. Canudas de Wit. A Survey of Models, Analysis Tools and Compensation Methods for the Control of Machines with Friction. *Automatica*, 30(7):1083-1138, 1994.

- [25] B. Feeny, A. Guran, N. Hinrichs and K. Popp. A Historical Review on Dry Friction and Stick-Slip Phenomoena. *Applied Mechanics Reviews*. 51(5), May 1998.
- [26] http://www.exploratorium.edu/complexity/CompLexicon/poincare.html (Forth of June 2003).
- [27] A. Raman, A. Bajaj, P. Davies. On the Slow Transition Across Instabilities in Non-Linear Dissipative Systems. *Journal of Sound and Vibration*, 192 (4): 835-865 May 16, 1996.
- [28] M. Kennel, R. Brown and, H. Abarbanel. Determining Embedding Dimension for Phase-Space Reconstruction Using a Geometrical Construction. *Physical Review*, A. 45 (6): 3403-3411 Mar. 15 1992.
- [29] P. Grassberger and I. Procaccia. Measuring the Strangeness of Strange Attractors. *Physica* 9D (1-2): 189-208, 1983.
- [30] P. Berge, Y. Pomeau, C. Vidal. Order within Chaos: Towards a Deterministic Approach to Turbulence. Wiley-Interscience, 1987.
- [31] M. J. Feigenbaum. Quantitative Universality For A Class of Non-Linear Transformations. Journal of Statistical Physics. 19 (1): 25-52, 1978.

